METRICS TO EVALUATE COMPRESSION ALGORITHMS FOR RAW SAR DATA

by

Chané Pieterse

Submitted in partial fulfilment of the requirements for the degree
Master of Engineering (Electronic Engineering)

in the

Department of Electrical, Electronic and Computer Engineering
Faculty of Engineering, Built Environment and Information Technology

UNIVERSITY OF PRETORIA

April 2019

SUMMARY

METRICS TO EVALUATE COMPRESSION ALGORITHMS FOR RAW SAR DATA

by

Chané Pieterse

Supervisor:	Prof. W.P. du Plessis
Co-supervisor:	Dr R.W. Focke (CSIR)
Department:	Electrical, Electronic and Computer Engineering
University:	University of Pretoria
Degree:	Master of Engineering (Electronic Engineering)
Keywords:	Synthetic Aperture Radar (SAR), Data Compression, Performance Evaluation, Metrics

Modern synthetic aperture radar (SAR) systems have size, weight, power and cost (SWAP-C) limitations since platforms are becoming smaller, while SAR operating modes are becoming more complex. Due to the computational complexity of the SAR processing required for modern SAR systems, performing the processing on board the platform is not a feasible option. Thus, SAR systems are producing an ever-increasing volume of data that needs to be transmitted to a ground station for processing.

Compression algorithms are utilised to reduce the data volume of the raw data. However, these algorithms can cause degradation and losses that may degrade the effectiveness of the SAR mission. This study addresses the lack of standardised quantitative performance metrics to objectively quantify the performance of SAR data-compression algorithms. Therefore, metrics were established in two different domains, namely the data domain and the image domain. The data-domain metrics are used to determine the performance of the quantisation and the associated losses or errors it induces in the raw data samples. The image-domain metrics evaluate the quality of the SAR image after SAR processing has been performed.

In this study three well-known SAR compression algorithms were implemented and applied to three real SAR data sets that were obtained from a prototype airborne SAR system. The performance of these algorithms were evaluated using the proposed metrics. Important metrics in the data domain were found to be the compression ratio, the entropy, statistical parameters like the skewness and kurtosis to measure the deviation from the original distributions of the uncompressed data, and the dynamic range. The data histograms are an

important visual representation of the effects of the compression algorithm on the data. An important error measure in the data domain is the signal-to-quantisation-noise ratio (SQNR), and the phase error for applications where phase information is required to produce the output. Important metrics in the image domain include the dynamic range, the impulse response function, the image contrast, as well as the error measure, signal-to-distortion-noise ratio (SDNR).

The metrics suggested that all three algorithms performed well and are thus well suited for the compression of raw SAR data. The fast Fourier transform block adaptive quantiser (FFT-BAQ) algorithm had the overall best performance, but the analysis of the computational complexity of its compression steps, indicated that it is has the highest level of complexity compared to the other two algorithms.

Since different levels of degradation are acceptable for different SAR applications, a trade-off can be made between the data reduction and the degradation caused by the algorithm. Due to SWAP-C limitations, there also remains a trade-off between the performance and the computational complexity of the compression algorithm.

ACKNOWLEDGEMENTS

I would like to thank the following people for their support.

My two supervisors, Warren P. du Plessis and Richard W. Focke: for the guidance, support and sharing of your extensive knowledge during my studies. I also want to thank you for your valuable inputs when marking or reviewing my reports and paper. I learned so much from you both. Thank you for always being available and willing to help.

Jani Steyn: for teaching me about SAR and also going through immense trouble to get the SAR data in the correct format for me to use. Also, thank you for providing the SAR processing code I required to complete my studies. Thank you for always being available and willing to share your SAR knowledge.

Charmaine Horn for the language editing and **Ciara Blaauw** for reviewing the technical content.

Casper van Zyl and the CSIR: for supporting and funding my research. Thank you Casper for your support with managing my studies and ensuring that I always had the resources I required to complete the work.

My husband, Jean/Luke Pieterse: for your support and ambition in life. Thank you for working hard with me to achieve our goals.

My parents and sister: for their love and support throughout my studies. Thank you for always setting an example of hard work and perseverance.

My saviour and rock, my God, Jesus Christ: for giving me the opportunities and abilities to achieve my goals, and for carrying me in times of hardship. Your love is unfailing.

LIST OF ABBREVIATIONS

A/D	Analogue to Digital
ADC	Analogue to Digital Converter
ALS	Audio Lossless Coding
AREND	Aircraft for Rhino and Environmental Defense
ATR	Automatic Target Recognition
BALVQ	Block Adaptive Lattice Vector Quantiser/Quantisation
BAQ	Block Adaptive Quantiser/Quantisation
BATSVQ	Block Adaptive Tree-Structured Vector Quantiser/Quantisation
BAVQ	Block Adaptive Vector Quantiser/Quantisation
BMPQ	Block Adaptive Magnitude Phase Quantiser/Quantisation
CR	Compression Ratio
CS	Compressive Sensing
CSA	Canadian Space Agency
CSAR	Circular SAR
CSIR	Council for Scientific and Industrial Research
CWT	Complex Wavelet Transform
DAC	Digital to Analogue Converter
DBS	Doppler Beam Sharpening
DCT	Discrete Cosine Transform
DEM	Digital Elevation Model
DST	Department of Science and Technology
DT-CWT	Dual Tree CWT
ECBAQ	Entropy-Constrained Block Adaptive Quantiser/Quantisation
ESA	European Space Agency
FBAQ	Flexible Block Adaptive Quantiser/Quantisation
FFT	Fast Fourier Transform
FFT-BAQ	Fast Fourier Transform Block Adaptive Quantiser/Quantisation
FLAC	Free Lossless Audio Codec
FMCW	Frequency-Modulated Continuous-Wave
G3	Gulfstream-III
GCF	Global Contrast Factor
GIF	Graphics Interchange Format
GPS	Global Positioning System
HEVC	High Efficiency Video Coding
HH	horizontal transmitting, horizontal receiving
I	In-phase
IC	Image Contrast
IED	Improvised Explosive Device
IET	Institution of Engineering and Technology
InSAR	Interferometric SAR
IRF	Impulse Response Function
IRW	Impulse Response Width
ISR	Intelligence, Surveillance and Reconnaissance
JAXA	Japanese Aerospace Exploration Agency

JPEG	Joint Photographic Experts Group
JPEG-LS	Lossless JPEG
JPL	Jet Propulsion Laboratory
KLT	Karhunen-Loève Transform
LBG	Linde Buzo Gray
LVQ	Lattice Vector Quantiser/Quantisation
LZW	Lempel-Ziv-Welsh
MPE	Mean Phase Error
MPEG	Moving Picture Experts Group
MSE	Mean Square Error
NASA	National Aeronautics and Space Administration
NRA	No Return Area
NSSC	Natick Soldier System Center
PDF	Probability Density Function
PNG	Portable Network Graphics
PolSAR	Polarimetric SAR
PSF	Point Spread Function
PSLR	Peak-to-Side Lobe Ratio
Q	Quadrature
RSN	Radar, Sonar and Navigation
SAR	Synthetic Aperture Radar
SDNR	Signal-to-Distortion Noise Ratio
SLC	Single-Look Complex
SNR	Siganl-to-Noise Ratio
SQ	Scalar Quantiser/Quantisation
SQNR	Signal-to-Quantisation Noise Ratio
SR	Spatial Resolution
SWAP-C	Size, Weight, Power and Cost
TCQ	Trellis-Coded Quantiser/Quantisation
TCVQ	Trellis-Coded Vector Quantiser/Quantisation
TD-BPQ	Transform-Domain Block Predictive Quantiser/Quantisation
TD-BPTCQ	Transform-Domain Block Predictive Trellis-Coded Quantisation
TDC	Time Domain Correlation
TSVQ	Tree-structured Vector Quantiser/Quantisation
UAV	Unmanned Aerial Vehicle
UWB	Ultra-wideband
VarTCQ	Variable rate Trellis-Coded Quantiser/Quantisation
VarTCVQ	Variable rate Trellis-Coded Vector Quantiser/Quantisation
VarVQ	Variable rate Vector Quantiser/Quantisation
VIR	Visible-Infrared
VQ	Vector Quantiser/Quantisation
WHT	Walsh-Hadamard Transform
WT	Wavelet Transform

TABLE OF CONTENTS

CHAPTER 1 INTRODUCTION

1.1 PROBLEM STATEMENT

Modern synthetic aperture radar (SAR) systems have size, weight, power and cost (SWAP-C) limitations since platforms are becoming smaller while SAR operating modes are becoming more complex. Thus, these systems are producing an ever-increasing volume of data that needs to be transmitted to a ground station for near real-time processing and stored on board for post-processing. A compression algorithm seeks to reduce the data volume of the raw data without causing degradation and losses, which may degrade the effectiveness of the SAR mission. This work addresses the lack of standardised quantitative performance metrics, which can be utilised to objectively quantify the performance of SAR data-compression algorithms.

1.1.1 Context of the problem

SAR is the only long range remote sensing sensor that can provide high-resolution images of wide areas in all weather conditions, during the day or night [1], [2]. Another advantage of SAR is that it provides information that is complementary to optical images. Furthermore, certain frequencies have penetration capabilities, which allow for much more information to be extracted from a scene. Subsequently, SAR has been used for various military, commercial and earth observation applications for the past three decades [1], [2].

Military applications include intelligence gathering, remote sensing, reconnaissance, and gathering of target information for military operations [1], [3]. An example of an airborne SAR technology with a long endurance, wide-area surveillance capability, is Lockheed Martin’s lightweight TRACER system [4]. This system can be used on manned or unmanned

platforms. The TRACER has a higher stationary and mobile target detection rate than its predecessors. It can also detect objects that are buried, camouflaged or concealed under dense foliage and is used to support disaster relief, counter-terrorism and humanitarian aid missions. TRACER is a good example of how the advantages of SAR can be exploited in real-world applications.

SAR is also well-known for its earth observation applications which include agriculture and earth resource monitoring, climate science, flood mapping, oceanography, oil spill detection, geomorphology, subsidence monitoring, landscape mapping, derivation of elevation models after natural disasters, and human geography [2], [3]. For these applications SAR sensors are usually implemented on satellites. Examples of spaceborne SAR sensors that are currently operational include Sentinel-1, Radarsat-2 and TerraSAR-X.

The first civilian SAR satellite, SEASAT, was launched in 1978, had a resolution of 25 m × 25 m and only had a single polarisation [2]. Sentinel-1, a C-band imaging radar launched in 2014, has a resolution of up to 5 m × 5 m, can operate in four modes and is dual polarised [5]. The improvement in the spatial resolution of airborne SAR sensors from the 1950s to the 21st Century is depicted in [6]. Over the years there have been SAR sensors that operated over multiple frequency bands and were fully polarised, for example the SIR-C system [7]. Sandia National Laboratories, a subsidiary of Lockheed Martin, developed the Mini-RF SAR on board the LRO spacecraft, which was launched in 2009 to orbit the moon [8]. It operates at two frequencies (S-band and X-band), two resolutions (150 m and 30 m), has interferometric and communications functionality, while only weighing 16 kg. Compared to systems developed in the same time period, modest data rates were achieved. While existing spacecraft are capable of much higher data rates, the platforms are heavier and not capable of multi-frequency, multimode operation for the same budget as that of the Mini-RF SAR [8]. This technology demonstrated that a trade-off exists between the data rate and the platform's size and cost.

A very popular research topic and industry tendency is unmanned aerial vehicles (UAVs). The advantages of a UAV system include lower risk in terms of human fatigue, lower cost, and long endurance missions. A local project showing these and other advantages of a UAV system is the Aircraft for Rhino and ENvironmental Defence (AREND) project [9]. The AREND project entails the design of a UAV by a group of South African as well as international students, to address the problem of poaching in the Kruger National Park. The system covers a 30 km search range, can remain airborne for more than 90 minutes, has a very low noise output to ensure that it remains undetected by poachers, and sends sensor data or images to a ground station. These objectives could be met by using a small, lightweight, unmanned aircraft as the platform.

Other major international companies that also research, design, and develop UAVs include Lockheed Martin, IMSAR and the National Aeronautics and Space Administration (NASA). Not only do they focus on UAVs, but they have also integrated UAVs and SAR systems. A recent UAVSAR technology is the NanoSAR systems. In 2014 IMSAR was contracted to develop small, lightweight SAR systems for small UAVs that have to be launched near the front lines [10]. The contract was signed to support the Natick Soldier System Center (NSSC) whose goal is to develop technologies that protect soldiers and increase their combat effectiveness. The NanoSAR B system produces high-quality radar images at a rate of 6.5 Mbps while the system only weighs 3.5 lbs (1.6 kg) and transmits 1 W of power [10]. The real-time SAR data are compressed by onboard firmware before transmission to the ground station. Sandia National Laboratories implemented a SAR sensor on two Class III UAVs, namely the Sky Spirit Mini UAV, used for long duration surveillance missions, and the TigerShark UAV, used to detect improvised explosive devices (IED) and for intelligence, surveillance and reconnaissance (ISR) operations [11]. Sandia's goal for the past twenty years has been to improve radar performance while decreasing the size of sensors in order to deliver smaller, lighter and less expensive systems to be implemented on lightweight UAVs for tactical missions [11]. Yet, Sandia and NASA's Jet Propulsion Laboratory (JPL) are still implementing SAR systems on large platforms since these platforms provide more processing power and bandwidth, which optimise the radar's performance [11]. Examples

include Sandia's RQ-4 Global Hawk UAV system used for long endurance ISR missions [12] and JPL's UAVSAR, implemented on a Gulfstream-III (G3) jet, for earth observation missions around the world [13].

In the case of military applications, SAR technology is increasingly being used on small UAV platforms [4], [10]-[18], whereas for earth observation applications, satellites are being equipped with higher resolution SARs while the platforms are becoming smaller and lighter [8], [19]. In both cases, SWAP-C plays an important role in the system design. Not only are platforms becoming smaller, but SAR technology is also moving towards being multi-band, multi-polarized, having very high resolution, and also having multiple operating modes [5], [8], [17]. All of these factors contribute to the ever-increasing volume of data that modern SAR systems are producing, while the sensor size is limited by the SWAP-C constraints of modern platforms.

Another important characteristic of most modern SAR systems is that the SAR system has to be split up into an onboard section and a ground-based section, where the SAR processing is performed at the ground-based section. Thus, the acquired data are only processed on board when on-line mode of operation is required for the application, for example when situational awareness during the flight is necessary for tactical response [18], [20]. For most other SAR applications the raw data are transmitted to a ground station for near real-time digital processing (also referred to as quick-look processing) while the data are also being stored on board for high quality off-line processing after the SAR mission [14]-[18], [21]. The reason for this configuration is that performing the SAR processing on board is resource and power expensive, and it also increases the physical size and thus weight of the platform, which are critical requirements for long endurance missions [14], [22].

Since it is necessary to transmit the raw SAR data to a ground station at a remote location, the effect of spectrum congestion needs to be considered. For successful SAR processing and mission data analysis, the global positioning system (GPS) data, motion sensor information, and sensor status information, all need to be transmitted to the ground station

[14], [15]. Depending on the application, bi-directional communication may also be required since commands from the ground station to the platform also need to be transmitted [18]. Not only is the system bandwidth for raw SAR data transmission limited by the transmission of other system information from the platform, but spectrum congestion poses another challenge for modern SAR systems. The spectrum congestion that SAR systems face is due to military and commercial communications that are using more bandwidth in the higher frequency bands, previously only used by radar systems [23], [24]. So despite technological advances, the downlink bandwidth of the platform remains a limiting factor [5], [8], [25].

Thus, the main constraints for the throughput design of these SAR systems are the unavailability of a downlink with a high data rate and the immense storage capacity required [5], [26], [27]. These constraints can be addressed by implementing a compression algorithm on board the platform that reduces the data rate before storing and/or transmitting the data to the ground station [14], [21].

1.1.2 Research gap

A compression algorithm seeks to reduce the data volume to solve the problem of transmitting and/or storing the raw data. However, any degradation and loss that the algorithm causes should also be determined, as a low quality SAR image may degrade the effectiveness of the SAR mission. Therefore, the compression algorithm must be evaluated to determine whether it is effective in reducing the data volume, as well as how significant the associated image-quality losses that occurred are.

Despite the importance of being able to quantify the performance of SAR data-compression algorithms, there does not appear to be a widely-accepted set of metrics for this purpose. The problem is compounded by the fact that different publications on SAR-data compression often propose new metrics to emphasise the unique benefits of the proposed algorithms (e.g. [29] and [30]). In [28] the topic of measuring the quality of compressed SAR data was identified as future work. This lack of standardised quantitative performance metrics means that the performance of SAR-data compression algorithms cannot be objectively quantified.

1.2 RESEARCH OBJECTIVE AND QUESTIONS

The main objective of this study is to determine which metrics can be used to evaluate the performance of a compression algorithm for raw SAR data. These metrics consider how significantly the data rate is reduced, the loss of information, and the computational complexity required for the compression. In order to achieve the research objective, the following research questions must be addressed:

1. Which algorithms are efficient, low complexity solutions for compressing raw SAR data?
2. How can the effectiveness of a compression algorithm for a specific application be evaluated objectively?
   2.1. How effective is the algorithm in compressing the raw SAR data?
   2.2. What is the effect of the compression algorithm on the quality of the SAR image?
   2.3. What is the computational complexity associated with the compression algorithm?

Different compression algorithms are investigated to determine which algorithms are suitable to compress raw SAR data. Raw SAR data are the data received from the analogue-to-digital converters (ADCs), before any SAR processing is performed. To establish what algorithms are suitable for raw SAR data, the characteristics of raw SAR data must be known. In this way an algorithm can be chosen so that it exploits the unique characteristics of raw SAR data. This will ensure that the compression algorithm is a generic solution to compressing raw SAR data.

Another objective is to implement a compression algorithm of which the advantages greatly outweigh the disadvantages associated with it. This implies that the algorithm must efficiently compress the data before any SAR processing is performed, without causing detrimental effects that may affect the output of the SAR system. In order to determine whether the algorithm is efficient, quantitative metrics to evaluate the efficiency of a compression algorithm must be established.

Another objective is to determine the effect that the compression algorithm has on the quality and reliability of the final SAR image. This implies that the metrics to quantitatively evaluate the quality of a SAR image must be established. These metrics should not only consider metrics on the visual quality of the intensity image formed, but also those that relate to the complex SAR image formed after processing.

The last objective is to compute the computational complexity of the compression algorithm. This metric will ensure that the algorithm is a feasible solution to implement on a practical, generic SAR system with its associated constraints.

The established metrics can be used to prove that the implemented compression algorithm is indeed significantly advantageous. This is clear from the effectiveness in reducing the data volume, while the algorithm yields cost and resource savings due to the low complexity of the implementation, all without having detrimental effects on the quality of the SAR image.

1.3 APPROACH

A typical characteristic of most modern SAR systems is that the system is divided into an onboard section, with the onboard hardware consisting of the transmitting and receiving unit, ADCs and a data downlink, while the ground-based section consists of the SAR image processing unit [21], [27]. In [31] a SAR system is described as comprising of three subsystems: the SAR sensor, the platform and data downlink, and the ground signal processor. The downlink as shown in Figure 1.1, can be set up in two different configurations: either the platform's onboard storage unit will be accessed for high-quality post-processing at the ground station (known as off-line operation), or as a second option the raw SAR data are transmitted to the ground station for near real-time processing (known as on-line operation). Therefore, the compression algorithm is implemented on the platform as part of the payload in order to reduce the data volume before the data is sent to the onboard storage unit and before the data is transmitted to the ground station. The stage at which a

compression algorithm will be implemented can be seen in Figure 1.1. It is implemented at the output of the ADCs, before any SAR processing, subsequently raw received SAR data are the input to the compression algorithm unit. The implementation of a compression algorithm at the mentioned stage of the receive chain, means that the storage and downlink bandwidth limitations of a modern SAR system are addressed.

In order to addresses the lack of standardised quantitative performance metrics to objectively quantify the performance of SAR data-compression algorithms, three compression algorithms will be implemented. After the decompression, SAR processing can be performed to yield the desired output of the SAR system. For each algorithm the established metrics will be evaluated in order to compare the efficiency and suitability for the application. Using the results of the evaluation metrics, the best suited compression algorithm can be chosen to be implemented on board the SAR platform.

In order to find a solution to the research problem, the following method will be followed:

1. Determine the unique characteristics of raw SAR data.
2. Determine the metrics to quantitatively evaluate the effectiveness of a compression algorithm.
3. Establish what metrics can be used to quantitatively evaluate the quality of a SAR image.
4. Compute the computational complexity of each algorithm.
5. Perform an extended theoretical study on previously published research.
6. Implement three compression algorithms from the literature.
7. Perform a verification experiment, using real SAR data, to determine whether the established metrics can be used to objectively quantify the performance of SAR-data compression algorithms.

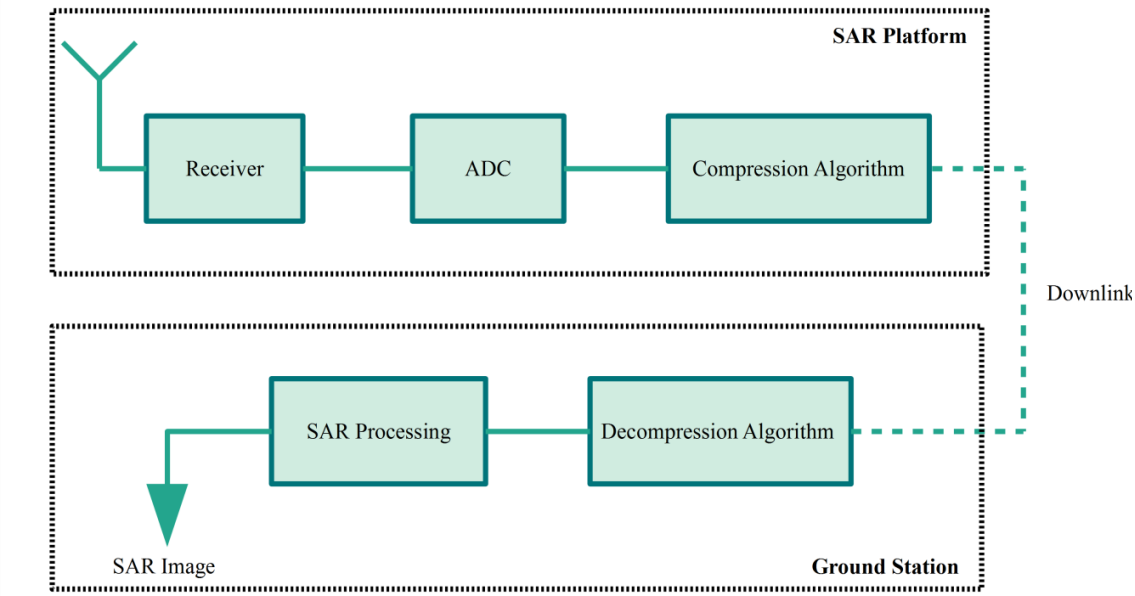

Figure 1.1 Block diagram of a modern SAR system receive chain – showing at what stage the compression algorithm is implemented.

1.4 RESEARCH GOALS

The goal of this work is to determine whether the established metrics can be used to objectively quantify the performance of SAR-data compression algorithms. Therefore, metrics have to be established in two different domains, i.e. before and after SAR processing is performed. The effects of the algorithm on the raw data, as well as on the output of the SAR system, must be quantitatively evaluated to establish whether the algorithm is a viable solution. Thereafter, the computational complexity of each algorithm should also be computed. The chosen compression algorithms should be low cost, low complexity solutions for SAR platforms with SWAP-C constraints. The algorithms should also be suitable solutions for general SAR technologies and applications.

1.5 RESEARCH CONTRIBUTION

A critical evaluation of a number of SAR-data compression performance metrics from literature is performed. A few new metrics were also established to address certain limitations in the current performance evaluation metrics of SAR-data compression algorithms. The definitions and importance of each metric were discussed.

The metrics are also divided into two domains to test the algorithms at two stages within the SAR system. Evaluating the algorithm at two stages means one can distinguish between the data volume reduction capability of the algorithm and the image degradation caused by the algorithm. The computational complexity of the algorithm is also investigated to determine the relation to the volume of data that the algorithm operates on.

The metrics in the different domains are a valuable aid when a trade-off is required between the data reduction capability of the algorithm and the degradation caused by the algorithm. The performance vs. the complexity of the algorithm is another trade-off consideration, depending on the SAR application.

1.6 RESEARCH OUTPUTS

A paper was accepted for publication in the Institution of Engineering and Technology (IET) Radar, Sonar and Navigation (RSN) journal on 5 October 2018. The paper is titled: “Metrics to Evaluate Compression Algorithms for Raw SAR Data” [32].

1.7 DISSERTATION OVERVIEW

The structure of the dissertation and the content of each chapter are summarised in this section.

Chapter 2 provides an introduction to SAR systems. The history of SAR is explored as well as the operation of SAR systems. Thereafter, a brief introduction to the well-known SAR technologies and applications is given, while the chapter concludes by investigating the characteristics of raw SAR data.

In Chapter 3, a literature study on compression algorithms that would be suitable for raw SAR data, was performed. The main topics under investigation are general compression algorithms, compressive sensing, as well as lossy and lossless SAR compression algorithms. It was found that when exploiting the characteristics of raw SAR data, a suitable algorithm can be implemented.

In Chapter 4, the research design, research instruments, data used, and analysis techniques are discussed. This includes the scope of the study and the method of evaluating the performance of the chosen compression algorithms. The evaluation method is implemented in two stages, at different places in the SAR process.

In Chapter 5, the quantitative performance metrics, to be used when comparing different compression algorithms for raw SAR data, are established. The proposed metrics are divided into two sets, namely data-domain metrics and image-domain metrics, and correspond with the first two domains when producing SAR outputs. The metrics of importance for different SAR technologies and applications are also summarised.

Chapter 6 provides the steps followed to implement each of the three compression algorithms. The real SAR data sets are statistically analysed in order to confirm the characteristics of raw SAR data as found in literature. Thereafter, the encoding and decoding steps, as well as the computational complexity of each algorithm are discussed. The three algorithms include the block adaptive quantiser (BAQ), the fast Fourier transform (FFT) BAQ (FFT-BAQ), and the flexible dynamic BAQ (FDBAQ).

In Chapter 7, the results of evaluating the metrics after applying the compression algorithms to the real SAR data sets, are provided and discussed. The chapter starts with providing Google Earth and SAR images of the scenes. Thereafter, the three compression algorithms are evaluated by computing the metrics at two stages in the SAR process.

Chapter 8 presents concluding remarks on the study and its achievements. Future work and improvements are also briefly discussed.

CHAPTER 2 SAR SYSTEMS

2.1 CHAPTER OVERVIEW

In this chapter a brief introduction to synthetic aperture radar (SAR) theory and operations is given. In Section 2.2, the history of SAR and the inception of civilian SAR systems are discussed. The operation of a SAR system is explained in Section 2.3, as well as the artefacts found in SAR images. A brief discussion on well-known SAR technologies and their applications is given in Section 2.4. In Section 2.5, the unique characteristics of raw SAR data are investigated, as they differ from the characteristics of other types of radars.

2.2 SAR HISTORY

SAR was invented in 1951 by Carl A. Wiley, a mathematician at Goodyear Aircraft Company in Litchfield Park, Arizona [6], [33]. He discovered that the radar returns from individual objects, in a passing radar beam, had minuscule Doppler shifts relative to the antenna. Wiley analysed the exact frequency of the return signal and realised that one could create a very detailed radar image of the scene. He achieved this with an antenna that was a hundred times smaller than the required conventional antenna to analyse the same scene size. Wiley applied to patent his discovery in 1954 and named it Doppler Beam Sharpening. This is however called SAR in the time domain and can be seen as the first SAR patent [33]. The same concept of synthetic aperture was developed independently by the University of Illinois and the University of Michigan shortly after Wiley had discovered it, but was explored in a more practical sense [6]. The first SAR images were created in 1953 by a Goodyear system called DOUSER, which was deployed on a C-47 aircraft [6], [33]. The system could only correctly identify objects or features that were at least 152 m across [6], while the latest SAR

system from Lockheed Martin, the TRACER, can detect vehicles, buildings, and metallic objects in broad swaths of dense foliage with a resolution measured in inches [4].

Initial SAR research and developments were for military applications like reconnaissance and man-made target detection. During the 1970s, the advantages of using SAR for civilian applications became apparent, and consequently led to a rapid increase in the use of SAR for earth observation missions [7], [19], [34]. New capabilities were demonstrated by the abundance of spaceborne missions that started with the launch of the Seasat in 1978 by the USA. In the 1990s, Europe, Japan and Canada followed with the ERS, J-ERS-1, and the Radarsat-1 satellites, respectively [3], [7], [34]. Further milestones in the 1980s and 1990s include SAR techniques like polarimetry, interferometry and differential interferometry. In 2007 the first bi-static SAR satellite, TerraSAR-X, was launched and introduced a new class of SAR satellites, which now had resolutions of up to a metre and was classified as very high resolution [7], [19], [34]. These new class satellites include TanDEM-X, the COSMO-SkyMed satellite constellation as well as Radarsat-2 [7], [34]. The number of near-polar orbiting, land imaging civilian satellites operational as of August 1972 to 2013 is depicted in [19].

It is clear that the development of SAR systems is driven by the need for higher information content in the SAR output. This can be achieved by multi-channel operation, multi-frequency and multi-polarisation capabilities, increased resolution, time series operation as well as by using multiple observation angles [7]. All of these advanced capabilities contribute to the high data volumes generated by modern SAR systems.

2.3 THEORY OF OPERATION

Since SAR is a system using radar, it is an active sensor, which means it provides its own illumination to form an image of the scene [1], [35]. Illumination of the scene is in the form of radio waves. This means SAR can be operated in all weather conditions, during the day or night; whereas optical systems are dependent on ambient light and are affected by

inclement weather. SAR has additional advantages over optical systems, which include that more information can be gathered from a scene as both phase and amplitude components are measured for coherent imaging systems. Optical systems are incoherent and only measure light-intensity values [1], [35]. At certain frequencies, SAR systems can penetrate dense foliage to detect objects of interest as well as penetrate the ground surface to reveal objects buried underground [1], [7].

A SAR system consists of an antenna mounted on a moving platform, which transmits a signal in a side-looking direction relative to the direction of motion, and measures the radar backscatter, σ_0 [7]. The radar backscatter is caused by scatterers in the scene. Scatterers are objects in the scene that reflect the transmitted radio waves back in the direction of the SAR receiver [1]. Thus, an illuminated scene consists of many scatterers with varying levels of reflectivity or backscatter, depending on various factors including their dielectric and physical properties [7], [36]. Different terrain types have different levels of backscatter, for example, man-made objects produce very high backscatter, while smooth surfaces or calm water has a low level of backscatter [7]. As the platform moves, pulses are transmitted at distinct positions and returns are collected from the same swath. SAR uses the Doppler shift of consecutive radar returns, generated by the motion of the platform, to synthesise a large antenna which allows high azimuth resolution despite a physically small antenna [1], [35]. The synthesised large antenna has an aperture the length of the flight path. The operation of a typical SAR system is depicted in Figure 2.1[1].

Spatial resolution is measured in units of distance (metres) and is defined as the minimum distance at which two adjacent point scatterers can be accurately distinguished. Consequently, for a fine or high resolution SAR system, closely spaced scatterers separated by this minimum distance will be visible as individual targets in the SAR image. Since SAR images are two-dimensional, the resolution is specified for both the azimuth and range dimensions. The azimuth resolution for SAR systems is independent of the platform altitude

[1] The author would like to thank Dr Jaco de Witt from the CSIR for the drawing of the figure.

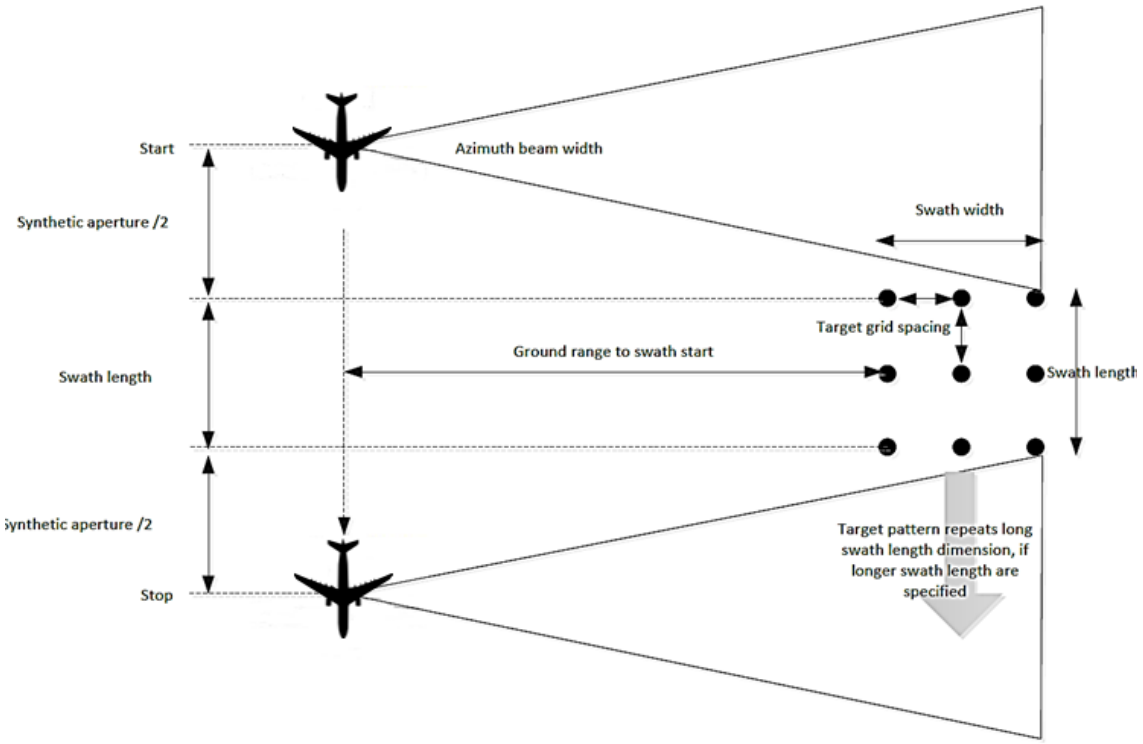

Figure 2.1 Operation of SAR system (Top view).

and wavelength, since the Doppler effect is utilised by the moving platform, which creates a Doppler frequency shift [7]. The azimuth resolution, δ_a, is equal to half the antenna length and is defined as

$$\delta_a = \frac{d_a}{2}, \tag{2.1}$$

where d_a is the antenna length [1], [7]. Fine range resolution is achieved by using wideband waveforms and pulse compression for the transmit pulse of the SAR system. Two-way propagation is a characteristic of a monostatic radar system, consequently a factor-of-two gain in range resolution is obtained. The range resolution, δ_r, is given as

$$\delta_r = \frac{c_0}{2B}, \tag{2.2}$$

where c_0 is the speed of light and B is the system bandwidth [1], [7].

A few examples of established SAR operating modes include [1], [7], [35]:

- Stripmap
  The full transmit distance is used to image a large, continuous strip of terrain. This is the most widely used mode of operation.
- ScanSAR
  An area of terrain is illuminated with a mechanically or electronically steered antenna beam. This mode can be used to image a larger swath width, but at the price of achieving lower resolution than achievable with the stripmap mode.
- Spotlight
  The scene is imaged with finer azimuth resolution and at multiple viewing angles in one flight. This mode is well suited for imaging multiple smaller scenes of interest along the flight path.
- Circular SAR (CSAR)
  In CSAR a circular trajectory is followed to image the scene. This means a very high resolution, as well as a 360° integration angle (the angle over which the SAR system gathers returns from the scene), is obtained. CSAR also have three-dimensional imaging capabilities.

Every pixel of a complex SAR image consists of a real and an imaginary part, consequently it is a phasor and contains amplitude and phase information [7]. The output of any basic SAR system is a high-resolution, two-dimensional, intensity image of the illuminated scene. SAR images represent an estimate of the radar backscatter for that scene. Bright features imply that a large amount of the radar energy was reflected back, which represent high backscatter, while dark features imply that very little energy was reflected back and represent low backscatter [1], [2]. The two dimensions of a SAR image correspond to the along-track dimension, known as cross-range (or slow time) in radar imaging, and the cross-track dimension, known as down-range (or fast time) [1], [7].

The complex values measured for each radar return are combined through SAR signal processing to form the SAR image [2]. The goal of SAR processing is to establish the range and cross-range coordinates of all the targets within the scene by compressing the distributed energy of the targets. The two main steps in SAR processing are range and azimuth compression and can be seen as two separate matched filter operations along the two respective dimensions [7]. In both steps a reference function for that dimension is generated to be used in the matched filtering operation, which is performed as convoluting the signal in the applicable dimension with the corresponding reference function [2], [37]. Many image formation algorithms exist, each with associated advantages and disadvantages. Doppler beam sharpening (DBS) is the oldest and most fundamental SAR image formation technique [1]. Currently, the most general methods for SAR processing are the Two-dimension algorithm and the Range Doppler Processing algorithm [38]. The Two-dimension algorithm processes the range and azimuth data simultaneously, while the Range Doppler Processing algorithm implements range compression and azimuth compression separately as two one-dimensional matched filter operations [1], [38]. Other well-known algorithms include the chirp scaling algorithm, the backprojection algorithm, and the frequency-wavenumber algorithm [1], [37], [39].

Certain artefacts exist in SAR images after basic SAR processing has been performed. The most serious phenomenon occurring in SAR images, as SAR is a coherent sensor, is speckle noise [35], [36]. This means that the magnitude of each pixel is the sum of the complex returns by scatters in the coherent system. Another phenomenon related to SAR images is geometric distortion since SAR measures the distance to a target [36]. The effect of geometric distortion is greater on taller objects and causes foreshortening, shadowing, and layover. Another artefact is the presence of phase errors due to the non-linear motion of the aircraft or errors made in the velocity measurement [35]. When an aircraft is moving along a flight path to illuminate the swath, it is assumed that the platform travels along a straight line with a constant velocity and altitude. These assumptions are however incorrect, as the platform slightly deviates from the ideal flight path during operation. Another discrepancy

is the phase shifts caused by moving targets in the scene [35]. Since SAR operation relies on the assumption that the targets in the scene are stationary, while the platform is moving, these phase shifts defocus the SAR image and lead to the displacement of the moving targets and thus cause quality degradation.

In order to form a well-focused, high-quality SAR image, additional processing steps may also need to be performed, depending on the artefacts present in the SAR image. These processing steps may include: motion compensation and autofocus, Doppler centroid estimation, range migration correction, phase correction or phase calibration, multi-look processing and/or speckle filtering or segmentation, and geocoding [35], [37], [40]. It is therefore evident that performing high-quality SAR processing on board the platform is resource expensive. This is why it is advantageous to implement the SAR processing at the ground-based section of the modern SAR system.

2.4 SAR TECHNOLOGIES AND APPLICATIONS

The output or products of a SAR system can be used for various applications and each SAR technology renders different information. Although more than one SAR technology can be used for some of the applications, only a few of the well-known SAR technologies, with their primary applications, are discussed below.

2.4.1 Single frequency, single polarisation basic SAR systems

Conventional SAR systems are used to create high resolution, two-dimensional images of the Earth's surface. Operation includes only a single pass over the scene using a single polarisation transmit/receive unit. The basic output is a single-look complex (SLC) image, for which the phase information is discarded [35]. Further processing can be performed to add radiometric and geometric corrections and/or speckle noise reduction to the image [31]. After more advanced processing, geophysical information, like the surface roughness or moisture content of soil, can also be derived [31]. The most important applications of conventional, simple SAR systems are discussed.

- Image classification

Image classification is identifying the different features within an image by distinguishing different levels of radar backscatter, e.g. high radar backscatter areas from medium, low or no return areas (NRAs). NRAs include shadows, paved areas like roads or parking lots, dry lake beds and sandy terrain, as well as water surfaces [1], [2]. The different levels of return are used to identify groups of pixels with similar statistical properties and thus the image is divided in homogeneity categories [41]. The output is a detailed map of an entire region with its distinct features. For wide-area surveillance, automatic target recognition (ATR), also known as unsupervised algorithms, is increasingly being used as it is a time-consuming process for a human operator to search through all the data [42]. Important applications of SAR image classification, where wide areas are being surveyed, are the mapping of land use (important for forestry and agriculture), assessment of the affected areas in disaster relief operations, and illegal or accidental oil spill detection [3].

- Detection of man-made targets

When investigating the different levels of backscatter in a SAR image, man-made returns are highlighted since these objects provide a very high radar backscatter [1], [2]. The high levels of backscatter can be attributed to the characteristics of man-made objects which make them highly radar reflective [1]. For example, the electrically conductive materials that the objects are made of, the large, flat surfaces of these objects, and the retro-reflective properties that exist due to the surfaces forming right-angle junctions or corners. Although the detection of man-made targets is a very important military application, it is also required for earth observation applications. In military applications, SAR is used to identify adversary facilities and points of interest on the land and ocean, where counter-piracy and maritime law enforcement are important examples [43]. For civilian applications, SAR images are not only used to detect ships in coastal regions, which aids in the monitoring of illegal fishing activities and vessel traffic, but they are also used to track urban and rural development over time [1], [3].

- Global monitoring (Change detection)

Many changes occur on land due to human activity and climate change over time. SAR is used for earth observation applications like ice monitoring and the study of climate change, where the global carbon cycle, the global energy/water cycle, and other human activities are monitored [3], [44]. The SAR system needs to be sensitive to small changes when monitoring a global cycle, consequently the radiometric resolution of the SAR system is an important factor [44]. The radiometric resolution of an imaging system is the system's ability to detect miniscule differences in the reflected energy. In order to preserve the radiometric resolution of a system, frequent calibrations are required [44]. A high signal-to-noise ratio (SNR) indicates that the signal level is greater than the noise level and therefore the noise does not mask any of the small changes that may appear in a scene.

2.4.2 Ultra-wideband (UWB) SAR systems

UWB SAR has a very large bandwidth compared to conventional SAR systems [45]. The system uses short pulses with a rapid change in modulation, to produce a large bandwidth in the frequency domain. A very short pulse enables high resolution since the distances are measured more accurately [45]. The main advantages of UWB operation are improved resolution and more information about the reflectivity of the targets in the scene [45], [46]. UWB SAR has applications in remote sensing and medical imaging since the technology is well-suited for the detection of concealed objects [47]. UWB SAR operates in lower frequency bands than conventional radar systems, usually the very high frequency (VHF) and ultra-high frequency (UHF) bands. The corresponding antennas can transmit the required short waveforms for UWB operation and the penetration capabilities are greater at these frequencies.

- Imaging through unconventional mediums

The applications of UWB SAR include uses in the military and civilian domains. In the military domain UWB radar is used for foliage penetration, ground penetration, and through-wall detection [47], [48]. The ground penetration capabilities of UWB SAR make it highly affective for the detection of landmines [46]. Popular civilian applications include the

monitoring of oil reservoirs [49], by imaging the perforations or fractures in the well, and medical imaging, like the detection of tumours [50].

2.4.3 Interferometric SAR (InSAR)

InSAR uses the phase difference between two complex SAR images by exploiting the speckle inherent to coherent imaging systems [7], [35], [42]. The SAR images for InSAR operation are acquired in one of two configurations [7], [51]. Either from mutually displaced flight tracks, known as across-track interferometry, most often used to measure the surface topography, or from along-track or differential interferometry. The measurements of the latter are taken at two distinct times during a second pass on the scene. With InSAR data it is possible to detect and measure miniscule path length differences or velocities in the order of several metres per second down to a few millimetres per year [7]. Measurements of this accuracy are possible since the phase of each pixel can be used to obtain range information that is accurate to a fraction of the radar wavelength [7].

- Surface topography

Topographic maps or three-dimensional models, known as digital elevation models (DEMs), can be constructed using InSAR since the height variations can accurately be measured [35]. These maps are used to analyse the surface parameters, for modelling and simulation in various fields, and to create accurate maps, to mention only a few uses.

- Measurement of displacements

InSAR is typically used for various remote sensing applications like the measurement of displacements. These include the detection of moving objects (for example cars or ships), and geophysical applications like monitoring earthquakes, landslides, glaciers, and volcanoes [2], [3], [51]. The changes in the surface are detected by comparing two InSAR topographic maps produced before and after a natural event occurred [35].

2.4.4 Polarimetric SAR (PolSAR)

PolSAR is an advanced imaging technique where the radar transmits and receives multiple polarisations (VV, HV, HH, and VH), and produces four SAR images of the same scene [35]. Thus, each scatterer is characterised by a complex 2 by 2 scattering matrix [2], [52]. Since the full scattering matrix is measured, the system is sensitive to the shape, orientation, and dielectric properties of the scatterers, which means much more information is obtained than with conventional, single polarisation SAR systems [7], [35].

- Change detection and feature tracking

PolSAR has many applications including agriculture (soil moisture estimation and crop assessment), oceanography, forestry (forest monitoring, classification, and tree height estimation), and disaster monitoring (oil spill detection, disaster assessment) [7], [35], [52].

2.4.5 Image fusion

Image fusion is defined as “the combination of two or more different images to form a new image by using a certain algorithm” [53]. A lot of times the information provided by one sensor is not sufficient [53]. Different sensors operate in different bands of the electromagnetic spectrum and therefore the images of different sensors vary in spectral, spatial and temporal resolution. By combining the data from different sensors, complementary information is produced. In this way, the advantages of each sensor type can be exploited to produce unique information and improve interpretation of the scene. Image fusion has applications in topographic mapping, land use mapping, flood monitoring, ice- and snow monitoring as well as other geological applications [53].

- Fusion of Visible-Infrared (VIR) sensor data and SAR images

Optical systems are affected by cloud cover given that it is a passive sensor, which is a disadvantage when mapping regions with frequent cloud cover [53]. Since SAR is an active sensor, it is unaffected by cloud cover and thus complements optical systems. VIR provides the reflective and emissive characteristics of the surface, while SAR provides the structural

and dielectric characteristics of the surface [53]. The accuracy of land-use mapping can be improved by combining the characteristics of the two sensors [54], [55].

- Fusion of multi-frequency or multi-temporal SAR images

A great number of SAR systems are currently operational for remote sensing applications and will be in the future as SAR became the sensor of choice [56]. These systems have different operating frequencies, polarisations, wave modes, and incident angles [57]. Therefore, the information produced by each sensor is also different. This means that the information from different SAR systems, with variable spatial resolutions or acquisition at different times, can be combined to produce complementary information and improve the quality of the SAR information [57]. This approach is highly favoured for land-use mapping, urban area classification, and building recognition [56], [57].

2.5 CHARACTERISTICS OF RAW SAR DATA

As mentioned in Chapter 1, the characteristics of the data to be compressed have to be known to aid in choosing a suitable compression algorithm. The characteristics of raw SAR data, before any processing, are investigated in this subsection.

For SAR, the value of each resolution cell is the superposition of a large number of scatterers (each with random phase) [7] and leads to a signal with Gaussian statistics [58]. Since raw SAR data are obtained through a coherent recording process of a very large number of independent random variables, it follows from the Central Limit Theorem that the raw data can be accurately modelled as zero-mean Gaussian noise [59], [60]. The Central Limit Theorem states that the behaviour of a complex system may be characterised by a Gaussian distribution if the sample is obtained through the sum of a large number of independent observations, randomly generated, and not too heavily correlated [36], [61]. In a typical SAR system, the analogue to digital converters (ADCs) sample the in-phase (I) and quadrature (Q) components of the baseband signal. Thus, the distributions of the I (real) and Q (imaginary) components are characterised as standard Gaussian distributions with equal

standard deviation and slowly changing variance in the range and azimuth directions [22], [25], [60], [62], [63]. Since the I and Q components are Gaussian distributions, the magnitude component is assumed to follow a Rayleigh distribution [64], while the phase is uniformly distributed between $-\pi$ and π [60], [65]. Another characteristic is that the I and Q components, as well as the magnitude and phase components are statistically independent of each other [60], [65]. Since the measured signal is noise, raw SAR data typically have a low SNR [62]. Raw SAR data are also nonstationary, which means the data correlation cannot be accurately modelled. Typically, adjacent samples of SAR data are uncorrelated and have the same expected power [26], [60], [63], [65]. This is true for both dimensions. It is also known that the SAR return data have a high dynamic range [25].

The I and Q components can be accurately modelled as zero-mean Gaussian distributions. However, there are some data sets for which the components slightly deviate from a standard Gaussian distribution [25]. The deviation could be caused by features of the scene, e.g. very few scatterers in the scene, or even by the hardware in the system, e.g. the ADC [25]. The ADC causes a truncation error when performing the analogue to digital (A/D) quantization due to the high dynamic range of the SAR return signal [25]. The statistical properties of SAR data also depend on the clutter environment that was illuminated, since different terrains present different backscatter. Clutter for land, sea, and rain all have different reflectivity values and return characteristics [66]-[69]. Man-made objects can produce large, discrete returns, which can cause heavier tails for the distribution [70], while natural terrain typically consists of small scatterers whose returns are characterised by an average backscatter coefficient [34].

The amplitude characteristics of clutter depend on several basic factors [34], [58]:

- The dielectric properties of the surface material.
- The roughness of the surface relative to the radar wavelength.
- The orientation of certain types of scatterers relative to the polarization of the transmit signal.
- The incidence angle at the surface.

The return of clutter does not only depend on the radar parameters, but it also depends on the scattering mechanisms. For example, the backscatter of ground clutter can depend on the vegetation type, current moisture content, and even the season [34], [68], while the backscatter from ocean surfaces can vary with the wind speed or wave height [34], [58], [69].

2.6 CHAPTER SUMMARY

In Section 2.2, the history of SAR and SAR sensors on satellites are explained. In Section 2.3, the operation of SAR systems is explained briefly as well as some SAR processing techniques. It was seen that SAR is a highly advantageous radar imaging system with both military and civilian applications. The most important advantages include the high resolution of a wide swath that can be obtained with a moving platform and a physically small antenna. The basic measurement by a SAR sensor, which is a coherent imaging system, is complex pixel values. Thus, magnitude and phase information are obtained.

Due to artefacts in SAR images, the most common being speckle noise, ancillary processing steps may also need to be performed to produce a well-focused, high-quality SAR image – all of which require complex computations and thus more resources. It is thus evident that it is highly advantageous for modern SAR systems to have the SAR processing unit at the ground-based section of the SAR system.

In Section 2.4, well-known SAR technologies and applications developed during the past few decades are discussed. Basic SAR systems, using a single frequency and a single polarisation, produce an intensity image, with or without further corrections, as the output. UWB SAR has applications in medical imaging and the detection of concealed objects due to its high resolution and low operating frequencies. Since the phase of a single SAR image is not exploitable, InSAR and PolSAR use the phase difference between multiple images for various advanced SAR applications. Image fusion is a means of gaining complementary information by either combining data from different imaging systems or by combining data

from SAR systems with different operating characteristics. In this way, the advantages of each imaging system are exploited to produce unique information and improve interpretation.

The characteristics of raw SAR data are investigated in Section 2.5. From the literature it is evident that the I and Q components of raw SAR data can be accurately modelled as zero-mean Gaussian distributions in most cases. However, there are some data sets for which the components slightly deviate from a standard Gaussian distribution due to specific features of the scene, or due to the hardware in the system. Depending on the terrain type, different levels of radar backscatter will be returned, which can also have an effect on the shape of the distribution of the raw SAR data.

CHAPTER 3 COMPRESSION OF RAW SAR DATA

3.1 CHAPTER OVERVIEW

In the previous chapter the characteristics of raw SAR data were investigated. In this chapter, the compression algorithms known in the literature as well as the state of the art in the compression of raw SAR data are summarised. In Section 3.2 the origin and applications of general compression algorithms are discussed. This discussion includes lossless and lossy compression, an overview of quantisation, and a brief introduction to compressive sensing. Thereafter, in Section 3.3, well-known algorithms in the field of compressing raw SAR data are summarised so that an informed choice could be made about the algorithms to be compared in this study.

3.2 GENERAL COMPRESSION ALGORITHMS

In Section 1.1 it was mentioned that data compression is a requirement due to the high data volumes being generated by modern technology, and the limited storage and transmission capacity. Nowadays, data are also mostly in digital form, which means the data are represented by bytes [71]. Some data types require a large number of bytes to represent the data. An example of the immense data volume generated by modern systems is given in [71]. Various space agencies including the European Space Agency (ESA), the National Aeronautics and Space Administration (NASA), the Canadian Space Agency (CSA), and the Japanese Aerospace Exploration Agency (JAXA) are collaborating on a programme to monitor global change. The system generates half a terabyte of data per day that needs to be

transmitted and stored for analysis. It has become evident that the volume of produced data increase more rapidly than the development of storage and transmission capabilities [72].

The goal of data compression is to reduce the number of bits required to represent a data set by removing redundancy in the data and representing the data in a more compact form [71], [73]. One of the first examples of data compression is Morse code, invented in 1838 for use in telegraphy [71], [72]. Morse code is based on using shorter code words for letters that occur more frequently in a language. Information theory was introduced in the 1940s through work done by Shannon and Fano [72]. In 1951 an optimal method for using shorter codes for frequently occurring characters was found by David Huffman [71], [72]. Early data compression was typically implemented in hardware, but in the late 1970s the development of software compression programmes began [72]. These initial software programmes were all predominantly based on adaptive Huffman coding. In the mid-1980s the Lempel-Ziv-Welch (LZW) algorithm became the method of choice for most general-purpose compression algorithms [72].

When compressing, the structure in the data or the level of randomness can be exploited. An example could be the statistical structure in data, however many other types of structure exist in the data depending on the data type [71]. The vocoder (voice coder) is an example of where the structure of speech is being exploited to compress the data [71]. Not only can the structure in the data be exploited when compressing, but also the perceptual characteristics of the users of the data. Therefore, a lot of compression algorithms make use of the visual or auditory perceptual limitations of humans to discard information that cannot be perceived [71], [72], for example audio, video and image compression algorithms.

Data compression can be lossless or lossy [71], [73]. Lossless compression algorithms reduce the number of bits by identifying and eliminating statistical redundancy. Since no information is lost after decompression, the data are fully recoverable. Lossy compression algorithms permanently eliminate bits of data that are redundant, unimportant or undetectable, thus some loss of information does occur.

3.2.1 Lossless compression

Lossless compression is based on Shannon's entropy theorem, where the data are encoded with the number of bits equal to the entropy of the data. Entropy is the information content of the data and is also a measure of the maximum compression that is possible without any loss of information [74]. Thus, only redundant information is removed to achieve the best possible lossless compression ratio. Lossless compression is important for applications where large differences between the original and reconstructed data cannot be tolerated since the reliability of the data is of critical importance [71]. Text compression, for example, is an application that requires lossless compression since small errors can change the meaning of the message being communicated. Other applications include certain computer files, bank statements and medical results [71]. Lossless algorithms found in early information theory literature include Huffman coding, arithmetic coding, LZW algorithms and run-length encoding [72], [74].

The process of lossless compression can be summarised in two steps: the decorrelation step and the entropy coding step. Linear prediction is used to achieve decorrelation by removing some of the structure in the data. The difference between the original and predicted sample is called the residual. Lossless entropy coding methods like LZW, Huffman or arithmetic coding are used to encode the residuals [71]. Adjacent speech samples of a speech segment are highly correlated [73]. This implies that the previous samples can be used to predict the value of the current sample with only a small random error. It is also known that adjacent pixels in an image are highly correlated and can thus be used to predict pixel values [71]. Therefore, lossless compression can be obtained by exploiting these properties and encoding and transmitting the residuals [71], [73]. Modern compression standards include free lossless audio codec (FLAC) and Moving Picture Experts Group (MPEG)-4 audio lossless coding (ALS) for digital audio, and portable network graphics (PNG), graphics interchange format (GIF) or Lossless Joint Photographic Experts Group (JPEG-LS) for images.

It was seen in Chapter 2 that the complex I and Q components are noise like, following a Gaussian distribution. This implies that conventional, lossless data compression standards are ill-suited to compress raw SAR data since these algorithms generally exploit correlations and redundancies in the data [34], which are not present in raw SAR data [65]. It is also confirmed in [75], where lossless audio encoders, FLAC and MPEG-4 ALS, were used in an attempt to compress raw radar data. These methods use predictive coding which is not suited for data with a large random component. It was found that these methods could not compress the radar data at all.

In [75], Huffman coding, which does not assume correlation between the samples, was also used to compress raw radar data of different types of radar systems. However, the Huffman decoder needs a dictionary (that differs for each vector) to map prefix codes to previous values and thus produce the original vector. Attaching the corresponding dictionary to each compressed vector significantly reduced the compression ratio that was achieved, from 2.6 to 1.9 on average. Other general lossless compression algorithms from the 7-zip file archiver were also used to compress the raw radar data, also achieving a poor compression ratio of 1.7 on average.

3.2.2 Lossy compression

For lossy compression methods the data cannot be exactly reconstructed due to loss of information. However, this loss of information means that much higher compression ratios can be obtained than for lossless compression [71]. Lossy compression is based on Shannon's rate-distortion theorem which states that the bit-rate can be reduced by allowing an acceptable amount of distortion of the signal [71], [74]. Lossy compression is implemented in applications where the lack of fully recovered data does not present a problem. Since the data can still be interpreted without error or ambiguities, the loss of information can be tolerated. In the late 1800s the concept of lossy compression for sound was already being applied in early telephony and sound recording by discarding high- and low frequency components [72]. Examples of where lossy compression are applied include speech, audio, images and video. Lossy compression can be applied in these applications

since the data display little randomness, but are mostly represented by limited values, and many fine details cannot be perceived by the human visual or auditory systems [72].

Lossy compression consists of a transform to separate important data from unimportant data, followed by lossless compression of the important data and discarding the unimportant data [72], [73]. JPEG is currently the most popular compression standard for colour and grayscale still images due to its small file sizes, colour detail and compatibility in all operating systems [76], [77]. Video approximates continuously moving images by playing still images in a sequence, called frames. Therefore, JPEG is also used for fast coding and decoding of still images in the MPEG standard for video compression [76], [77]. H.264 has been the state-of-the-art in video compression since 2003, but High Efficiency Video Coding (HEVC) is a new video compression standard developed to surpass the coding efficiency of H.264 [76].

3.2.3 Quantisation

Quantisation is widely used in lossy compression methods since it is a simple process [71]. Quantisation is the process of representing a large set of values with a discrete, smaller set of values [71], [73]. A historical example of quantisation is rounding off [78]. The quantisation process consists of an encoder and a decoder [71]. The encoder divides the entire range of values occupied by the original data set into intervals, each with an associated codeword. The decoder then generates a reconstruction value for every codeword. This reconstruction value differs from the original input value which can lie anywhere within the interval. Therefore, the operation is irreversible as it removes irrelevant data by reducing the size of the alphabet required to represent the data set [71], [73]. Quantisation is well-known for the process of converting analogue signals to digital signals, known as analogue-to-digital conversion (ADC) as well as for the inverse process of digital-to-analogue conversion (DAC) [71].

The goal of quantisation is to find the best possible representation of the data set for a specific data rate [74], [78]. However, since loss of information occurs; errors are introduced by the process. The error is the difference between the original and the reconstructed data. The

errors introduced by the quantisation process are non-linear and signal dependent, and is known as quantization noise or quantisation distortion [73]. The quality of a quantiser can be determined by measuring the distortion resulting from reproducing the original values from the encoded values. The most common distortion measure is the squared error, also represented as the signal-to-quantisation-noise ratio (SQNR) [74], [78]. It is important to note that a trade-off exists between the two primary performance measures: the achievable rate and the distortion produced [78].

The most general quantisation schemes are uniform quantisation, non-uniform quantisation, and vector quantisation [71], [73]. A uniform quantiser is the simplest scheme, since the decision intervals are of equal length and can be represented by a constant called the quantisation step size [71], [73]. The reconstruction values are also the midpoints of each interval. A non-uniform quantiser takes the probability density function (pdf) of the input into account when choosing the intervals [71], [73]. Thus, to decrease the distortion, the intervals are smaller in regions of high probability versus regions of lower probability of occurrence. A uniform or non-uniform quantiser is called a scalar quantiser (SQ) if the input is quantised one sample at a time [71]. A vector quantiser (VQ) groups consecutive samples or blocks of samples to form the code vectors [71], [73]. The list of code vectors forms the codebook of the VQ. Therefore, a VQ requires a complex encoder to search through all the vectors in the codebook and to choose the best representation of the input. The decoder, however, only uses a table lookup process and therefore the VQ is an attractive solution to problems where the decoding resources are limited compared to the resources available for encoding [71]. A VQ usually outperforms an SQ, however, it has higher computational complexity [73]. It is important to note that VQ can be used as a lossy compression method, even if adjacent samples are uncorrelated, although correlation would improve the performance [73].

3.2.4 Compressive sensing

The well-known Nyquist-Shannon sampling theorem states that a digitised signal needs to be sampled at a rate of twice the signal bandwidth in order to fully recover the original signal.

However, the relatively new field of compressive sensing (CS) states that far fewer samples can be acquired based on the rate of information of a signal, and not the signal bandwidth, since redundancy exists in the samples [79].

CS exploits the fact that a lot of signals are intrinsically sparse in some domain [79]. Sparsity means the information content is thinly distributed and many coefficients are zero, while the non-zero coefficients are sufficient to fully reconstruct the original signal [80]. If a signal is sparse in one domain, it implies the signal has redundancy in another [79]. It is generally known that each media type is sparse in a specific domain and this information is exploited in the compression of multi media [79]. For compressive sensing it is important that the domain in which sampling takes place is not sparse, but that sparsity exits in some domain incoherent to the sampling domain. To ensure that the sampling domain is non-sparse, the signal can be transformed to an intermediate domain that is incoherent with the sparsifying domain [79]. It was found that any random domain is highly likely to be incoherent with any other domain [80]. Therefore, in some cases, random sensing matrices are chosen as transform matrices to ensure that the incoherence requirement between the sampling domain and the sparsifying domain is met.

CS is in essence using an underdetermined system to fully recover the original signal, while making the assumption that the signal is sparse in some, incoherent domain [79]. CS reduces the sampling rate of a system without prior knowledge of the signal and is therefore a beneficial method in the field of digital signal processing. CS has applications in data compression, channel coding, inverse problems and data acquisition [80]. The advantages of CS, as well as the sparse nature of some radar applications, also make this technique useful for applications in the electromagnetic field, which include: pulse compression, antenna arrays, direction of arrival estimation, inverse scattering and radar imaging [81], [82]. Some of these applications of CS have been demonstrated using real data [82].

If one deviates from the Nyquist sampling theorem and apply underdetermined sampling to a signal, loss of information is inevitable. However, it is the philosophy of CS that this

information loss will be tolerable if sparsity of the signal in some domain can be assumed [82]. This method eliminates the need for a high sampling rate, which is generally a requirement for digital signal processing, although most general compression algorithms end up eliminating the redundancy in the data after Nyquist sampling. CS increases the algorithm efficiency due to the lower sampling rate requirement and the reduced computational complexity [81].

3.3 COMPRESSION ALGORITHMS FOR RAW SAR DATA

An overview of well-known algorithms for raw SAR-data compression is presented in this section. Since lossless compression of raw SAR data is not customary, the discussed algorithms are all lossy compression methods. The algorithms have been categorised as scalar quantisation methods, vector quantisation methods, transform coding methods, compressive sensing applied to raw SAR data, and compression after range focusing the raw data. Some well-known fusion methods in the literature are also briefly discussed.

3.3.1 Lossless algorithms

In literature it has been concluded that due to the high entropy of raw SAR data, lossless compression algorithms are not suited for the compression thereof [31], [83]. In [31], it was found that the raw SAR data from the NASA DC-8 airborne SAR had an entropy value of 6-7 bits/sample. Therefore, for the general 8-bit quantization from the ADC on board a platform, a compression ratio of less than 20 % would be achievable. Not only is lossless compression ill-suited due to the high entropy of SAR data, but it has also been found that lossless compression algorithms cause the data to be more susceptible to errors caused by transmission [31].

It was mentioned in Subsection 3.2.1 that lossless compression algorithms, which utilise predictive coding, are ill-suited for the compression raw SAR data since these methods take advantage of sample to sample correlation. Since conventional lossy compression techniques utilise transform coding, which also exploits the correlation between samples, they are also

rendered ill-suited for the compression of raw SAR data [65], [84]. The characteristics of raw SAR data and the abovementioned factors imply that quantisation is a suited method for the compression for raw SAR data [84].

3.3.2 Scalar quantisation

One data compression method that has successfully been used on board spaceborne platforms when the system is data rate limited, is block adaptive quantisation (BAQ) [34], [60], [85]. An adaptive quantiser estimates the statistics of the data and then changes the quantiser characteristics to try and match the observed statistics [60]. Therefore, to design an optimal quantiser, the statistics of the data must be known. Although raw SAR data are known to have a high entropy, and are thus not highly compressible, a reduction in the number of bits is possible for the BAQ method, since the dynamic range for a block of data is much less than that of the entire data set [83]. BAQ has been designed to compress raw SAR data, since a Gaussian statistic signal, with slowly varying power, forms the basis of the BAQ design [31], [34], [60]. Since the I and Q components of the data are assumed to be Gaussian with zero mean, the distribution can be described by a single parameter, the standard deviation.

It receives the uniformly quantised data from the ADCs and then splits the data into smaller blocks. The block size is chosen such that each block has Gaussian statistics, while also ensuring that the variance of the samples within each block is small relative to the variance across all blocks in the data set [34], [60], [83]. The optimum quantiser used in BAQ is known as a Lloyd-Max quantiser [31], [86], [87], and outputs a fixed bit rate. The objective of the quantiser is to minimise the distortion by quantising the values within each block non-uniformly. For two-bit encoding, one bit is the sign bit, while the other bit indicates the signal level, thus whether the sample is above or below the threshold [60]. The threshold is the transition point that is optimally placed in an ensemble of data with a Gaussian distribution, such that the distortion in the reconstructed data is minimised. The reconstructed values are the centroid of the area between zero and the threshold and the centroid of the area between the threshold and infinity, on the positive and negative sides of zero. It is important to note

that the standard deviation is transmitted with the encoded data for use in the reconstruction process performed at the ground station. The results in [60] show that the BAQ achieved the required data volume reduction, while also satisfying the hardware constraints of modern, spaceborne SAR systems, since it is of low complexity [85]. Although this method was originally designed for only two bits of encoding, it can be extended to provide greater compression accuracy by increasing the number of thresholds and consequently the number of encoding bits [62].

Encoding the I and Q components is known as the Cartesian format of the BAQ method. However, different variations of the BAQ have also been investigated in literature [26], [62], [88], [89]. For the block adaptive magnitude phase quantisation (BMPQ) variation, the raw complex data are represented by the magnitude and phase components. This is known as the polar format of the BAQ method. Again, the quantiser and reconstruction process are designed to minimise the mean square error for the respective distributions. As mentioned in Section 2.5, the magnitude component follows a Rayleigh distribution while the phase is uniformly distributed. The number of bits allocated to each component is varied to find the best compression solution for the application. For example, if the application requires reliable phase data, the phase component can be encoded with more bits than the magnitude component to better preserve the phase information. BAQ outperforms BMPQ in terms of the SNR in the image domain, although BMPQ has significantly better performance in the data domain. This is due to the accuracy of the phase component since it is encoded with more bits than for conventional BAQ. However, encoding the magnitude component with fewer bits causes the I and Q components to contain less information compared to the information content of these components in the BAQ case. It was also concluded that the distribution of the magnitude component is not well suited for compression, while the phase component cannot be compressed at low bit rates due to its zero order entropy [85].

Another variation of the BAQ is the entropy-constrained BAQ (ECBAQ) [90]-[92]. ECBAQ features non-integer rate programmability, which is an important feature for the onboard compression of SAR data in modern applications. ECBAQ can be described as an optimum

quantiser, a uniform block adaptive quantiser in this case, followed by an entropy coder like Huffman coding or the adaptive arithmetic coder. This method aims to outperform the BAQ, while retaining the low complexity of the BAQ.

It has been found that using a fixed encoding bit rate for the entire scene, that is independent of the signal power, is not optimal [5], [92]. Since the SNR varies with the power levels of the received signal, a fixed encoding bit rate degrades the SNR, and therefore, varying the encoding bit rate can outperform the BAQ. The Flexible Dynamic Block Adaptive Quantization (FDBAQ) is the latest extension of the conventional BAQ method by adaptively selecting the encoding bitrate according to the local SNR [21], [92], [93]. In essence this means that blocks that contain bright scatterers, are encoded with a higher number of bits to preserve the information. It has been observed that for purely homogeneous scenes, the FDBAQ does not provide any improvements over the BAQ. However, for heterogeneous scenes FDBAQ provides significant improvements. The main difference between the FDBAQ and the ECBAQ is that the FDBAQ adapts the bit rate for every block of data, while the bit rate is fixed for the operation of the ECBAQ [92]. The optimum quantiser for the FDBAQ can be a uniform or non-uniform block adaptive quantiser followed by an entropy encoder, which produces a variable bit rate that is generally a non-integer value [5], [92]. FDBAQ is well suited for SAR missions that produce a high data rate and large dynamic range. It retains the highly advantageous, low complexity of the BAQ method while also producing results comparable to the BAQ method. The ability to vary the encoding bit rate enables SAR systems to have multiple operating modes.

BAQ was designed for the compression of raw SAR data by the Jet Propulsion Laboratory (JPL) and was first implemented on the Magellan spacecraft used to image Venus [60]. Thereafter, it was also implemented on board the SIR-C spacecraft which was used to obtain multi-frequency and multi-polarisation radar images from a low earth orbit [94]. Thereafter, the BAQ algorithm was extended to have a varying compression ratio (options being 4, 3, or 2 bits/sample) chosen by the mission controller based on the operating mode [27]. This algorithm, known as flexible block adaptive quantiser (FBAQ) was implemented on board

the ENVISAT satellite to enable wave mode operation, used to measure directional wave spectra of the ocean. Most recently an extension of the FBAQ method, known as the flexible dynamic block adaptive quantiser (FDBAQ) algorithm has been implemented on board the Sentinel-1 satellite. After evaluating the algorithm using real Sentinel-1 data, it was concluded that FDBAQ achieves an average bit rate comparable to that of a BAQ with an output bit rate of 3 bits, but with the added benefit of improved SNR in the high-reflectivity areas in the scene, while also not degrading the quality of the low-reflectivity areas [5]. It must be noted that the added flexibility of the bit rate per block is important for modern SAR systems, since different operating modes and applications have different image quality and data volume requirements [5], [63].

3.3.3 Vector quantisation

Vector quantisation (VQ) is an extension of SQ, the difference being that it quantises groups of samples called vectors [85]. This conceptual difference causes VQ to outperform SQ due to the following reasons [88], [95]:

- the space-filling advantage, ascribed to adding another dimension when using vectors,
- the shape advantage which depends on the distribution of the input data, and
- the ability to exploit statistical dependencies among the data, called the memory advantage.

The operation of VQ [29], [85], [88], [95], [96] includes grouping the data into vectors and generating a codebook. For each input vector, the encoder searches for the code word which aims to minimise the mean square error between the data and their assigned code words. Each vector is assigned a code word and only the index of the best suited code word is transmitted along with the encoded data. The decoder consists of a look-up table that outputs the code word that matches the address it received. As the vector size increases, the performance also increases [88], [96]. However, an increased vector size requires more computations and memory.

VQ-based methods group samples together to form vectors and assign code words to each vector. The types of VQ methods generally applied to compress raw SAR data include full search VQ using a codebook, tree-structured VQ, and lattice VQ [29], [85], [95].

- Full search VQ using a codebook (LBG-VQ) [29], [85]

The full search VQ uses a codebook generated by the Linde, Buzo, Gray (LBG) algorithm, and code words are chosen in such a way to minimise the distortion. This method achieves improved performance when compared to the SQ methods discussed in the previous subsection. When applying this type of coder, the performance is improved even more when the components of the vector are correlated (see Subsection 3.3.6).

- Tree-structured VQ (TSVQ) [95]

TSVQ does not perform as well as the LBG-VQ method when compressing data, but it is a very computational efficient method. It is a variable rate method and has progressive transmission properties, which makes it highly suited for practical implementations.

- Lattice VQ (LVQ) [85], [95]

LVQ is usually applied when the data follow a well-known pdf, with zero mean. Often times, when the data do not adhere to this condition, a transform is applied to the data. Since the I and Q components of raw SAR data can be assumed to follow a Gaussian distribution, as seen in Section 2.5, the LVQ method is well suited for the compression of raw SAR data. LVQ is a fast algorithm and aims to preserve the performance capabilities of the LBG-VQ method. The lattice is chosen depending on the distortion measure between the data and the assigned code words. The codebook is then adapted to the distribution type of the data by using a truncated version of the lattice. Spherical, pyramidal or elliptical codebook versions are used for Gaussian, Laplacian or Elliptical sources, respectively. By choosing an optimal lattice suited for the distribution of the data to be compressed, the computational complexity is reduced compared to that of the LBG-VQ method.

In [85] full search VQ (LBG-VQ) and LVQ are proposed to compress the raw SAR data. The results using simulated data, show that VQ-based algorithms outperform BAQ, especially at low bit rates. LVQ is well-suited for SAR-data compression since it has low computational complexity compared to LBG-VQ and achieves good results for the simulated

data. In [29] LBG-VQ, Kohonen feature maps, and lattice techniques are applied to SARAPE data. LBG-VQ achieves better performance than the other two methods, while the Kohonen feature maps method has lower computational complexity. It can be concluded that VQ-based techniques perform better when the components of the vector are correlated.

It can be concluded that VQ-based methods outperform BAQ at low bit rates [29], [85], [95], since it is known that VQ naturally outperforms SQ [73]. It was shown that by exploiting the correlation achieved by grouping the data into vectors, better performance could be achieved [96]. VQ-based techniques reduce the data rate at the price of higher complexity [29], [85], [95]. Consequently, SQ remains the method of choice for practical implementation since the complexity of VQ is a major disadvantage [96].

Trellis-coded quantisation (TCQ) is a special case of VQ where the code words are restricted to be paths on a trellis [97]. The rate-distortion performance of TCQ is superior to that of SQ, while it is also an improvement on VQ since it is much more computationally efficient [98]. In contrast with full search VQ, the computational complexity for TCQ is independent of vector length, therefore, very long vectors can be processed [97], [98]. In [98], the TCQ and trellis-coded vector quantization (TCVQ) methods performed well and showed low bit-error sensitivity. These techniques are also compared with BAQ and VQ and the results show that they outperform these two methods in terms of the SNR. The cost of improved performance is the computational complexity of the TCQ method that greatly exceeds that of the BAQ, but is comparable to that of VQ at the same rate.

3.3.4 Transform coding

The compression algorithms discussed in the previous subsections describe the implementation of algorithms in the time domain. It is important to note that these algorithms can also be applied to data in the transform domain. The condition that must be met, is that the values in the transformed domain must have the same data statistics as in the time domain, namely zero-mean Gaussian distributed [83]. Due to the phase coherence that raw

SAR data exhibit, this condition is true for large block sizes. Consequently, the BAQ is used extensively in the transform domain as well.

Transform coding has been successfully implemented for the compression of images and forms the basis of the JPEG2000 standard [97]. Transform coding causes energy compaction in the new domain which can be exploited when compression is required; a characteristic that is not present in the time domain [22]. The aim of compression in the transform domain is to use a transform that represents the important information content of the data with the fewest number of coefficients [83]. The coefficients that contain less information, can be discarded, or coded with fewer bits, without detrimentally affecting the image quality.

When the coefficients are Gaussian, the Karhunen-Loève transform (KLT) is the optimal basis [83]. Unfortunately, the implementation thereof is impractical since it requires the computation and inversion of a very large autocorrelation matrix. It was found that the discrete cosine transform (DCT) achieves results that are comparable with the performance of the KLT [83]. Raw SAR data are frequency modulated in both range and cross-range directions [83]. In the range direction, the modulation is due to the transmitted pulse, while in the azimuth direction it is modulated by the movement of the SAR platform (Doppler effect). Therefore, by combining frequency-domain methods with BAQ, the compression performance can be improved at the cost of increased encoding complexity [22].

A popular frequency domain algorithm is the fast Fourier transform BAQ (FFT-BAQ) [83], [99]. The data are transformed by performing a two-dimensional FFT of the raw SAR data, after which the average envelope of the transformed data is known. The main objective of the FFT-BAQ operation is to match the compression scheme to the energy variation of the frequency envelope. Therefore, the region with higher energy is quantised with more bits, while the coefficients which carry less energy are quantized using fewer bits. The coefficients which will be neglected by low pass filtering are not encoded, but discarded. Therefore, FFT-BAQ has the added advantage of onboard, digital filtering [22]. FFT-BAQ outperforms the BAQ as well as all other frequency domain approaches. However, the

increase in computational complexity is significant [83], [99]. Instead of the FFT, the DCT or the Walsh-Hadamard transform (WHT) can be used with the BAQ for compression in frequency domain. DCT-BAQ achieves similar performance to that of the FFT-BAQ, while the WHT-BAQ requires a less complex hardware implementation, at the price of decreased performance [83]. In [22] the DCT is implemented followed by arithmetic coding. The DCT exposes the structure in the data, while arithmetic coding exploits that structure when compressing the data.

A newer transform coding method for raw SAR data is the use of wavelets and wavelet packets [100], [101]. Transform coding consists of decomposing the signal in an orthonormal basis. The wavelet coefficients are computed and thereafter the coefficients have to be quantised. The quantiser is designed to ensure that the the entropy of the quantised coefficients is minimized for a given distortion rate. In general image compression applications, the probability density function of the wavelet coefficients is peaked, implying that the number of significant coefficients is very low. In [102] an experiment was performed to determine the four top performing one-dimensional wavelets when applied to raw SAR data. These wavelets were compared to the BAQ method and it was concluded that none of the standard wavelet bases could outperform the BAQ in terms of the SNR.

Due to the characteristics of raw SAR data, a slightly different approach is followed in [100] and [101]. A two-dimensional wavelet transform with two decomposition levels is applied to the raw data frame. The real and imaginary components of the raw data samples are transformed separately. It is also recommended that the wavelet should be derived directly from the raw SAR data to ensure that it is an optimal 2-D wavelet. Redundancy minimization in the transform domain serves as the optimality criterion in the derivation process. The results show that the optimal wavelet outperforms the standard wavelets [101].

Overall, some wavelet methods have produced results that are comparable to the performance of the BAQ, while also being implemented on low complexity hardware [22], [102]. However, none of the methods have surpassed the performance of the BAQ. This is

because longer transforms increase the performance, but consequently require more storage and more complex computations [22].

3.3.5 Compressive sensing

In the field of CS applied to raw SAR data, problems with the conventional sampling technique are identified [103]-[105]. Firstly, since modern SAR systems produce increasingly higher resolution outputs, which demand wider bandwidth and larger synthetic aperture, a higher sampling rate, according to the Nyquist-Shannon sampling theorem, is required. A higher sampling rate results in longer transmission and sampling times, a larger volume of data, and increased hardware complexity. All of these factors are challenges that modern SAR systems face. Another identified problem is that all the current methods of compressing raw SAR data, compress the data after sampling and therefore it is evident that redundancy exists after sampling at Nyquist rate. It is thus clear why the need for CS of raw SAR data arose.

CS acquisition of signal requires three elements: a basis where the data are assumed sparse, a reconstruction algorithm and a measurement (sampling) method [105]. It is important to note that successful reconstruction of the under-sampled signal is only possible if the data are in fact a sparse representation of the original, uncompressed signal after applying the transform [104]. CS compresses the raw SAR data by sampling the signal below Nyquist rate. CS also generally has the advantage of simple compression steps, while the decompression requires more complex steps [103]-[105]. This setup is beneficial since modern SAR systems require low complexity compression because it is executed on board the platform, where computational resources are limited. The decompression can be more complex since it is executed at a ground station, where SWAP-C are no longer limitations.

The compression of raw SAR data in the CS framework, by using the dual tree complex wavelet transform (DT-CWT) and the real wavelet transform (WT) as sparsifying transforms, is presented in [103] and [104], respectively. The studies are performed using a simulated scene with point targets, as well as measured satellite data. The proposed methods

achieve fast compression by applying a two-dimensional FFT and random sampling, and thus reduce the computational complexity required for onboard compression of raw SAR data. However, neither sparsifying wavelet transforms provided enough sparsity of the SAR signal to yield a compression ratio of higher than 2:1.

In [105] it was observed that when using a Haar wavelet basis, only the high-return objects in the image, which are compressible because they are highly localised, are preserved. Very bright scatterers, generally from man-made objects, are typically sparse in the space domain and slightly sparser in the wavelet domain. Therefore, the SAR image was divided into two components, namely the sparse areas with bright scatterers, and the remaining, non-sparse areas. Additional techniques were also implemented to improve the reconstruction quality of the non-sparse areas of an image. These techniques include standard CS with additional post-processing, and secondly, a hybrid CS technique. It was concluded that modified CS techniques can outperform traditional Nyquist rate sampling techniques for low bitrates, with the added condition that the image contains very bright scatterers, and thus adheres to the sparsity requirement. If the sparsity condition is not met, Nyquist sampling compression techniques achieve a higher compression ratio and better quality SAR images than the standard or modified CS techniques.

It is stated that for radar imaging, the sparsity condition required for CS only holds true if the scene only has a few bright returns [82], [105]. This requirement is usually met for man-made objects, like vehicles or aircraft, in a low reflecting background. Thus, it is evident that CS is an ideal compression method for applications where man-made objects are the targets of interest [82]. The output of the CS method in these cases is also very useful for automatic target recognition (ATR). The clutter returns can also cause the violation of the sparsity condition for CS, which then sets a requirement for pre-processing before CS can be implemented [82]. Suppressing the clutter before performing the CS processing implies that more resources will be required when implementing the compression on board the SAR system. It can thus be seen that CS is highly suited for ISAR applications, rather than for SAR applications where the clutter returns are important for forming an image of the scene.

In the available literature on CS applied to raw SAR data, a lot of the methods are merely theoretical, or applied to simulated data with a known number of ideal point scatterers only, and therefore not necessarily valid for practical SAR applications [82].

3.3.6 Compression after range focusing

Raw SAR data exhibit very little correlation, consequently compressing the raw data is very challenging [28], [96], [106]. It is known that processing the raw SAR data exposes the distinctive features of the scene and increases the correlation. However, performing the entire focusing process on board the platform is resource expensive. The SAR focusing process consists of two steps, as mentioned in Section 2.3. The first step is range focusing (range compression), followed by azimuth focusing (azimuth compression). Azimuth compression is much more resource expensive than the range focusing step.

A possible compression solution has been identified by implementing the range focusing on board the platform, followed by a suitable compression algorithm [28], [96], [106]. Range focusing is obtained by computing the inverse discrete Fourier transform of the data across the range dimension. Range focusing requires only low-complexity computations and has no memory requirements, which makes it ideal for on board implementation. In [28] raw ERS-1 data, before and after range focusing, are shown. Before range focusing the raw data shows no structure, however, after range focusing bright strips appear along the azimuth dimension. The compression algorithms can exploit the increased correlation exhibited after range focusing [28], [96]. This correlation is due to the presence of highly reflective objects in the scene. The returns from these objects are generally stronger than the returns from the surrounding homogeneous areas, and consequently produce SAR scattering that can easily be predicted.

In [28], range focusing is implemented, followed by block-adaptive, variable rate VQ (VarVQ) to compress the raw ERS-1 SAR data. The raw data are compressed with and without the range focusing step. It is shown that implementing the conventional SAR-data

compression algorithms after range focusing, has a clear improvement over compressing the raw data directly. It is also concluded that VarVQ outperforms the other techniques in terms of the SNR, but shows increased computational complexity. However, VQ is not a feasible solution for onboard implementation and therefore, variable rate trellis-coded quantisation (VarTCQ) and variable rate trellis-coded VQ (VarTCVQ) are investigated to compress range-focused SAR data [96]. VQ shows clear improvements over SQ when compressing range-focused data, since it exploits the correlation present in the data. By adding trellis-coding as part of the encoder, VarTCVQ outperforms VarVQ and BAQ at low bit rates and also reduces the computational complexity to suit onboard implementation requirements.

Predictive quantisation techniques for the compression of range-focused data are investigated in [106]. Transform-domain block predictive quantisation (TD-BPQ) and transform-domain block predictive trellis-coded quantisation (TD-BPTCQ) are investigated. The results show that predictive quantisation is a suitable technique for the compression of range-focused data when the scene contains dominant point scatterers. The strong returns from a scatterer, typically a man-made object, forms a characteristic sinusoidal pattern in the range-focused domain, and consequently, the behaviour can be predicted [106]. The algorithms outperform the VarTCVQ technique [96] in terms of SQNR and computational complexity.

It can be concluded that implementing well-known SAR-data compression techniques after range focusing the raw data, improves the performance in terms of the SNR. This is possible since range focusing increases the correlation of the data in the azimuth dimension. The compression algorithms can now exploit the correlation and focused energy in the range-focused SAR image. It was seen that scalar quantisation does not perform well when applied to range-focused data since the limited number of quantisation levels cannot accurately represent the increased dynamic range obtained after range focusing [28], [96]. It is shown that VQ techniques perform well [96], but the computational complexity makes VQ-based techniques impractical [106]. Results show that predictive coding techniques outperform VQ-based techniques due to the predictability that dominant scatterers exhibit after range

focusing. The computational complexity of these techniques is also feasible for onboard implementation.

3.3.7 The fusion of algorithms

In this subsection only a few methods, that are very popular in the literature, are discussed. These techniques combine the advantages of two types of quantisation or the data representation in two different domains to compress the raw SAR data.

The first example is the combination of scalar quantisation and vector quantisation [88], [95]. The raw SAR data are first compressed using the BAQ algorithm. The output of the BAQ, which is a smaller number of bits than the initial bit rate, is now the input to the VQ. The smaller number of bits as input means that the search process can be simplified or even avoided in certain cases. The output of the VQ corresponds to the addresses of the code words. VQ-based techniques like block adaptive vector quantisation (BAVQ), block adaptive tree-structured vector quantisation (BATSVQ), and block adaptive lattice vector quantisation (BALVQ), are compared with the BAQ technique [95]. The BAVQ method outperforms the BAQ method at low bit rates, since the digitisation noise inherent for BAQ is reduced, as well as the computational complexity normally associated with VQ. The proposed BATSVQ and BALVQ algorithms also outperform the BAQ algorithm at low bit rates. Their performance also compares well with that of the BAVQ algorithm, while the reduction in computational complexity makes these methods more advantageous.

Another important example of the combination of algorithms is the combination of time domain methods and transform domain methods. In specific, a lot of literature focus on the fusion of the time and frequency domain, since it had been observed that the best results have been achieved when the BAQ is applied in the frequency domain [99]. WHT-BAQ, DCT-BAQ, and FFT-BAQ have been tested for the compression of raw SAR data [83]. The best results were obtained using the FFT-BAQ. The FFT-BAQ is discussed in Subsection 3.3.4

3.4 CHAPTER SUMMARY

Detailed reviews of the general compression literature and the algorithms specific to the compression of raw SAR data were required to implement the research. In Section 3.2, the algorithms to compress various general data types were discussed. Brief overviews of the principles of quantisation and compressive sensing were also given to understand the algorithms in the following section.

The state of the art in the compression of raw SAR data was briefly summarised in Section 3.3. It was observed that the performance of the compression algorithms highly depends on the statistical properties and the dynamic range of the data to be compressed [29]. Lossless compression algorithms are ill-suited for the compression of raw SAR data due to the high entropy of raw SAR data and the lack of correlation between adjacent samples [31]. From the literature it is clear that the BAQ is the most mature algorithm for the compression of raw SAR data. It has, however, been observed that combining algorithms can lead to improved results at some cost. For example, the BAVQ algorithm produces slightly better image quality compared to the quality obtained using the BAQ, but the additional computations required cannot be justified [99]. Another algorithm receiving a lot of attention, is the FFT-BAQ. It is known to outperform the BAQ, but again leads to increased computational complexity [83].

Each algorithm has advantages and performs well under specific conditions. Although there are many algorithms that have outperformed the BAQ in theoretical studies, BAQ remains the preferred basis algorithm, primarily because it achieves a good trade-off between performance and simplicity [62], [83]. Considering the results from previous studies, as well as the summarised literature in this chapter, the main candidates for raw SAR data compression on board resource constrained platforms, are the standard BAQ, the FFT-BAQ, and the flexible dynamic block adaptive quantiser (FDBAQ) [93], [99].

Until recently, FFT-BAQ was not considered a viable solution due to the high computational requirements, but technological advances in hardware design could see the implementation of FFT-BAQ on board a future SAR platform. Most recently an extension of the FBAQ method, known as the FDBAQ algorithm, has been implemented on board the Sentinel-1 satellite. After evaluating the algorithm using real Sentinel-1 data, it was concluded that FDBAQ achieves an average bit rate that can be compared to a BAQ with an output bit rate of 3 bits, but with the added benefit of improved SNR in the high-reflectivity areas in the scene, while also not degrading the quality of the low-reflectivity areas [5].

CHAPTER 4 APPROACH

4.1 CHAPTER OVERVIEW

This chapter describes the research design of the study. The research design can be described as a comparative analysis with inputs, tasks performed, and outputs. In Section 4.2, the overall approach that was followed to address the research questions, is described. The objective of the research was to establish a set of standardised metrics that can be used in future, to evaluate the performance of a compression algorithm for raw synthetic aperture radar (SAR) data. In Section 4.3, the methods and methodology to prove that the metrics can be used to evaluate the performance of a compression algorithm are explained. This section includes information about the research instruments, data used, the analysis techniques, and the limitations of the method.

4.2 RESEARCH DESIGN

The comparison in this study involves the description of the differences and similarities between the results of the metrics for the three compression algorithms. Comparative research [107] attempts to reach conclusions that are not only valid for a single case, but can explain differences and similarities between objects of analysis in spite of their contextual conditions. When results are compared, theories and hypotheses can be tested, and the scope and significance of phenomena can be evaluated. A weakness of comparative research is that variations in measurement, instruments, sampling, and processing can have detrimental effects on the outcome of the research, and in essence invalidate the conclusion. Therefore, carefully selecting the constants in the study and ensuring that they can indeed be controlled,

are of great importance. Establishing the inputs, tasks and outputs of the research design are also important when designing the research to be performed.

One input to the research process was the SAR system, which consists of the raw SAR data it acquired and the SAR processing algorithm applied to focus the image. The second input to the process was the compression algorithms used to perform the study.

In order to address the research questions in Section 1.2, certain tasks needed to be performed. These high-level tasks included establishing a set of metrics by recognising the metrics currently being used in this field, and also introducing new metrics to address the identified limitations. The definitions and importance of the proposed metrics were also discussed to highlight how they could be used when comparing two SAR-data compression algorithms. Another task performed during the study was to evaluate the proposed metrics for three compression algorithms. In this way, the performance of the algorithms was compared in order to select a better suited solution for the SAR system, and thus proves the validity of the proposed metrics.

The compression algorithms that were chosen to perform the study, were implemented in software and included compression and decompression of the raw SAR data. Decompression is required since it needs to be executed at the ground station before SAR processing can be performed. Compressed data are only required for transmission to the ground station as explained in Section 1.3. Also, to determine how the quantisation errors, caused by the compression algorithm, are propagated into the image domain and thus degrade the quality of the SAR image, decompression is a required step in the process.

The output of the process was the set of proposed metrics to evaluate a compression algorithm for raw SAR data. The metrics were also divided into two domains to test the algorithms at two stages within the SAR system. Evaluating an algorithm at two stages means one can distinguish between the data volume reduction capability of the algorithm and the image degradation caused by the algorithm. In order to choose a better suited

algorithm for the SAR system, the output was used to compare the results of the metrics and make an informed decision. Thus, it can be seen that decision making is required after the process has yielded the output.

For this research it was ensured that certain factors were constrained, with the three algorithms being the only varying factor. The constant factors included that data from the same SAR system were used, implying the same characteristics of the system and the same SAR processing algorithm, as well as a fixed output bit rate for the compression algorithms. The research was conducted using real SAR data of three different scenes. Therefore, the outcome of the study is reliable and repeatable, using other real SAR data sets and compression algorithms. A similar study was conducted where the evaluation metrics results of two compression algorithms were also compared to determine the distortion caused by the encoding of SAR data [108]. The outcome of the research after analysing the output of the research process, is an indication of whether the proposed metrics are useful as performance indicators for raw SAR-data compression algorithms, and in turn addresses the lack of standardised, quantitative performance metrics in this field.

4.3 METHOD

4.3.1 Research instruments

The data used in this study were acquired using the Council for Scientific and Industrial Research (CSIR), South Africa, and the Department of Science and Technology (DST) SAR system. The data sets were provided by the Radar Imaging and Fusion Research Group of the CSIR. The specifications of the SAR system are summarised in Table 4.1.

For the first flight tests, which took place in June 2017, the system operated as a fully polarised, pulsed radar at a single frequency, namely C-band, and a bandwidth of 200 MHz. The specific data sets used in this study were measured on day two of the first flight tests during which only the linear, horizontally transmitting, horizontally receiving (HH)

Table 4.1 CSIR DST SAR system characteristics.

Parameter	**Specification**
Platform	Airborne
Operating mode	Stripmap
Operating Frequency	C-band
RF Bandwidth	200 MHz
Polarisation	HH
Transmission	Pulsed
Quantisation	14-bit I, 14-bit Q
Scenes	Rural, Mine Setting, Peri-urban

polarisation mode was used to image the scenes. In the interim the system has been upgraded to operate as a frequency-modulated continuous-wave (FMCW) radar, with a second bandwidth option of 600 MHz.

The SAR processing algorithm used in this study is a modified, one-dimensional time domain correlation (TDC) algorithm. The modified algorithm was developed in-house by the Radar Imaging and Fusion Research Group of the CSIR. The TDC algorithm traditionally operates by performing matched filtering via a two-dimensional correlation [109]-[111]. For the in-house implementation, the algorithm performs range compression of the data first, followed by an optimised azimuth compression implementation. This modification of the traditional TDC algorithm was implemented to yield faster results since the TDC algorithm is known to be computationally expensive [111]. TDC is a motion compensation SAR processing algorithm, widely used for high range resolution SAR systems due to its accuracy in focusing the images and wide unambiguous extent [110], [111].

All algorithms, processing, evaluation, and analysis discussed in Subsection 4.3.3 were implemented in MATLAB version 8.6 (R2015b), on a Microsoft Windows 10 operating system. The Signal Processing Toolbox (version 7.1) and the Statistics and Machine Learning Toolbox (version 10.1) were also used in this study. It is important to note that all numerical values in this study were represented as double-precision floating-point format, which is MATLAB's default format.

4.3.2 Data

In industry, data of Level 0, Level 1, Level 2, Level 3 and Level 4 are generally produced by SAR systems, depending on the processing and corrections applied to the data [31], [112]. A definition of the product types relevant to this study is given below.

- Level 0 SAR products consist of the raw SAR data before any processing. Level 0 products are divided into four product types which include standard products, calibration products, noise products and annotation products [112].
- Level 1 SAR data are focused data, after performing SAR processing as well as other advanced processing steps, and the output is known as single-look complex (SLC) data [31], [112]. All Level 1 products are geo-referenced and time stamped with zero Doppler time at the centre of the scene. The SAR data are transformed from Level 0 data to Level 1A data by applying a SAR processing algorithm (two-dimensional matched filtering of the data). The data are then transformed to Level 1B data by a processor that corrects the radiometric and geometric errors in the Level 1A output using the Level 0 calibration data products [31]. Level 1 data are the most requested type of data by users and also widely available. Level 1 products are the baseline engineering product from which higher level products are derived [112].

The data sets that were required for this study are of the type: Level 0 standard products, which are the received echoes. Level 0 data were required since the compression of raw SAR data was part of the topic being investigated in this study. Level 1 data were however produced in this study by applying SAR processing to the Level 0 data, as part of the research design.

The Level 0 data sets used include three measured sets of different scene types. The flightpath for the SAR mission covered areas in and around Pretoria, South Africa. Thus, the data represent different terrains which include residential, natural and agricultural areas and can also be classified as low-urban to mid-urban data. The manner in which the level of urbanisation was assigned to each data set, is explained in Chapter 6. Different terrains represent different reflectivity, and in essence, different distributions [67]. This had to be taken into account when the compression algorithms that would be suitable for this SAR system, were chosen.

4.3.3 Analysis techniques

In this research the data were analysed at various stages. From Section 2.5 it is evident that deviations of the raw I and Q components occur in practical data. Thus, the specific data set under investigation needed to be statistically analysed to establish the severity of the deviation from a standard Gaussian distribution. Knowing the distribution of the raw data aided in choosing the compression algorithms that would be suitable for the application of the SAR system, since some of the algorithms are known to exploit the characteristics of the distribution. These algorithms were implemented and then used for the comparative analysis.

The proposed metrics were evaluated in two domains, where different levels of SAR data products are present, called the data domain and the image domain respectively [62], [89], [108]. By evaluating an algorithm at two stages, one can gain insights into the data volume reduction capability of the algorithm, the cause and severity of the digitisation errors introduced, and how these errors are propagated into the image domain; where image degradation might affect the outcome of the SAR mission [62]. The computational complexity of each algorithm was also determined to aid in choosing a low complexity algorithm, suitable for onboard compression.

Certain factors had to be kept constant in order to execute the research in a reliable manner, without varying factors that could cause inconsistencies between the results being compared.

A fixed compression ratio was chosen for both compression algorithms, and the same data sets were used for both algorithms. This was to ensure that the metric results could be compared, and that the only varying factor, being the compression algorithms, may influence the outcome.

After implementing the algorithms, the compression and decompression steps, the first set of proposed metrics was evaluated to determine the effect that each compression algorithm had on the raw data. This evaluation took place in the data domain, before any SAR processing had been performed, and thus, it was Level 0 SAR data being analysed. This stage of evaluation required both the raw, uncompressed data and the decompressed data as input. Thereafter, the uncompressed data and the decompressed data were processed to yield the SAR images to be compared. After SAR processing, the evaluation now took place in the image domain. The SLC products (Level 1 data) of both compression algorithms and the uncompressed data were analysed to evaluate the second set of proposed metrics. These metrics determine the quality degradation of the SAR image of the uncompressed data caused by each compression algorithm. The method that was followed to investigate the validity of the proposed metrics is illustrated in Figure 4.1. The image fusion domain was added to the flow diagram for completeness; however, the fusion domain metrics were not evaluated in this study. This limitation is further discussed in the next subsection.

4.3.4 Limitations and scope

The designed method has limitations, since the study had to be limited to adhere to time and resource constraints. For this study, only measured data from one SAR system were used.

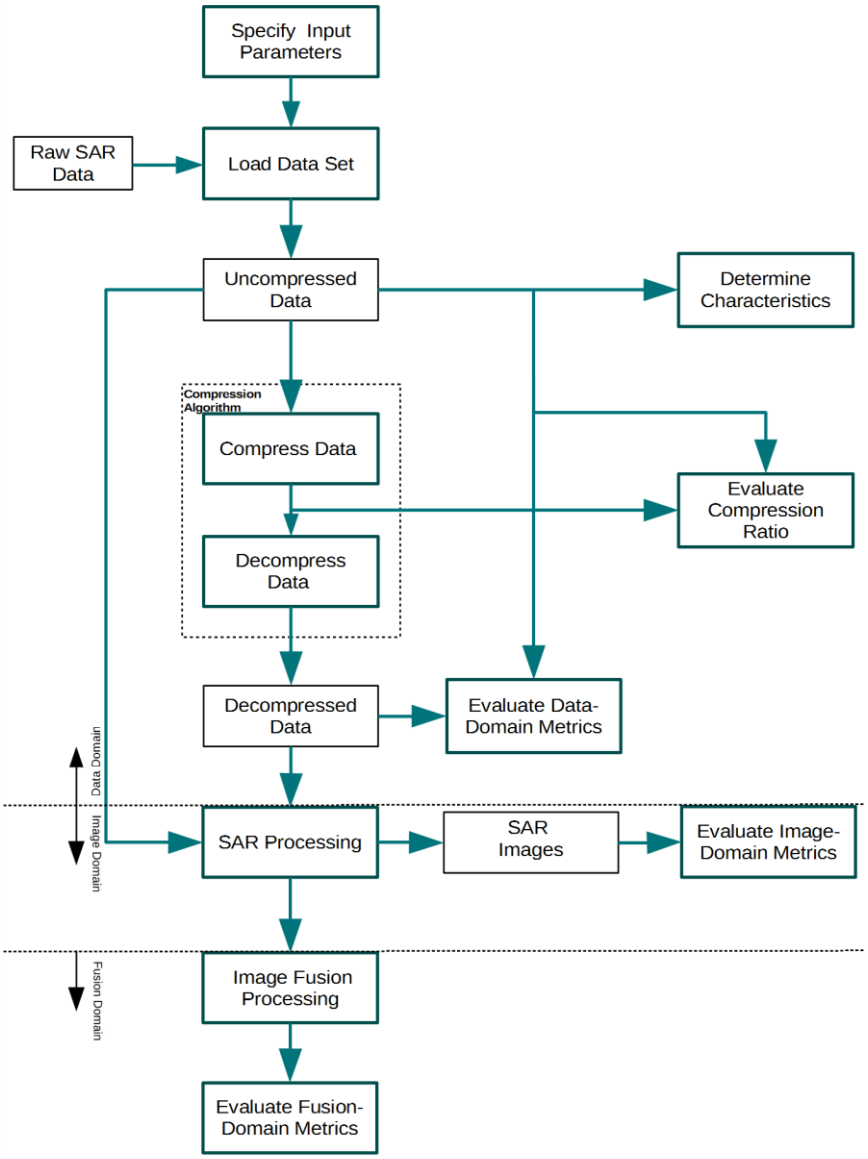

Figure 4.1 Method flow diagram. Adapted from [108].

This SAR system is an airborne system, while most of the literature on the compression of raw SAR data considers spaceborne SAR systems. Since the spatial resolution of a SAR system is independent of platform altitude, the resolution capabilities for airborne and spaceborne platforms do not differ [35], [113]. However, variations in the look/incidence angle, and the look direction, play a major role in the amount of received energy [113]. Generally, these differences can be quite significant between airborne and spaceborne

platforms [113]. However, using appropriate SAR processing algorithms, with features beneficial to the platform type, can render the differences irrelevant to the outcome. These differences do also not invalidate the use of the chosen compression algorithms, since the algorithms can be applied to raw data that follow an assumed distribution, irrespective of the platform type. A simple measure of computational complexity for each algorithm was sufficient in comparing the complexity of the three algorithms.

For the SAR system used in this study, a single image formation process was implemented. Therefore, the effect of different SAR processing algorithms, as well as whether a compression algorithm has an effect on the SAR processing required after compression has been implemented, was not investigated in this study.

The study was limited to the implementation of three compression algorithms, which was sufficient, since a comparison study could be performed as was required to evaluate the validity of the proposed evaluation metrics. All of the algorithms utilise the block adaptive quantiser (BAQ) as the basis, with two algorithms operating in the time domain and the other in the frequency domain. Although this seems like a limiting factor, using the BAQ is beneficial since it remains the basis algorithm for compressing raw SAR data [5], [34]. These algorithms are thus solutions to the generic problem of compressing raw SAR data on board a modern SAR platform. The chosen compression algorithms were not implemented on a real-time embedded platform, since the software implementation was adequate for the purpose of the study. A software implementation produced all the required outputs for this study: the metrics could be evaluated and the results for both algorithms compared to make an informed decision on a better suited solution - without requiring hardware implementation. This also means that the hardware and memory requirements of the algorithms were not investigated in this study, but would definitely be a requirement before implementing an algorithm on board a platform.

Since a lot of compression algorithms for raw SAR data exploit the statistical characteristics of the raw data, the quality of the results may not be repeatable and is associated with the

data sets used in this study. Thus, applying the method to a different data set, of which the statistical characteristics differ immensely from the assumed characteristics in this study, may not render results of the same quality. The characteristics of another data set can differ due to a lot of factors which include: the scene type and the type of clutter returns, the operating frequency of the SAR sensor, platform type, etc. [7], [36], [39]. All of these factors may have an influence on the quality of the results, but in general, the variations can be rectified by carefully selecting a suitable SAR processing algorithm or by adding high-level processing steps [39].

It is also important to note that this study was limited to metrics in the data and image domains only, and does not include metrics for the data fusion domain. Since the output of the used SAR system was only SAR images, it was reasonable to only evaluate metrics for the applicable domains. [1]Since data fusion is an important application receiving a lot of attention in the literature, it is added to the future work.

The scope of this study only considers the compression of raw SAR data, and not the compression of data at any other stage of the SAR system. Since the onboard compression of raw data is required in modern SAR systems, this was a feasible approach. Thus, the compression of SAR images was not investigated in this study, although this approach has also received a lot of attention in the literature.

Although the method has limitations, these limitations do not render the outcome of the study insignificant or irrelevant. The results obtained are reliable and contribute to the scientific community; and further, less delineated research problems can be investigated in future work.

[1] See Chapter 8 for future work.

4.4 CHAPTER SUMMARY

In Section 4.2, the overall design of the research, which was used to evaluate the validity of the proposed metrics for the performance evaluation of compression algorithms for raw SAR data, was discussed. The chosen research design was to perform a comparative analysis to test the proposed metrics. In Section 4.3, the process setup, which includes the analysis techniques and the reliability of the data used, was fully explained. The limitations of the proposed method were also discussed in this section. It can be concluded that although limitations for the study exist, it does not render the outcome of the research insignificant or trivial to the scientific community.

CHAPTER 5 METRICS FOR THE COMPRESSION OF RAW SAR DATA

5.1 CHAPTER OVERVIEW

In this chapter the quantitative performance metrics, to be used when comparing different compression algorithms for raw SAR data, are established. Thereafter, the use of these metrics to determine the performance of a compression algorithm needs to be validated. As explained in Subsection 4.3.3, the proposed metrics are divided into two sets. These sets were evaluated in the first two domains when producing SAR outputs, namely the data and image domains. Therefore, the evaluation metrics for the data and image domains are defined in Section 5.2 and Section 5.3, respectively. It is important to note that the proposed metrics are to be used during the design phase of a SAR system, when a compression algorithm for implementation on board the platform needs to be chosen. Since different SAR applications have different quality and performance requirements, the metrics of importance for some well-known SAR technologies and applications are summarised in Section 5.4. The content covered in this chapter has been accepted for publication in the Institution of Engineering and Technology (IET) Radar, Sonar and Navigation (RSN) journal [32].

5.2 DATA-DOMAIN METRICS

The metrics that can be used to evaluate the efficiency of a compression algorithm in the data domain, are established below. As can be seen in Figure 4.1, these metrics are evaluated after decompressing the compressed data, except for the compression ratio (CR) which is

computed directly after compressing the raw data. These metrics are used to determine the performance of the compression algorithm and the associated losses or errors it induces in the raw data samples. In some of the literature on raw SAR compression algorithms, the only metric used in this domain is the CR (e.g. [22], [83], [88]). Although compression ratio is an important metric, as it determines the data reduction, other metrics that evaluate the losses or errors associated with an algorithm are useful when investigating different compression algorithms. Some studies in the field of raw SAR data compression evaluate the signal-to-quantisation noise ratio (SQNR) in the data domain since it is the most widely used metric to measure the performance of a quantiser [26], [30], [89]. The effects that quantisation has on the image domain results are not considered in the data domain since SAR processing first needs to be performed. The following metrics were suggested to thoroughly evaluate the compression algorithm in the data domain.

5.2.1 Data reduction measure

- Compression Ratio (CR)

The compression ratio, *CR*, is defined as [65]

$$CR = \frac{N_{or}}{N_{com}}, \tag{5.1}$$

where N_{or} is the number of bits of the original data, and N_{com} is the number of bits of the compressed data. The CR indicates how efficiently the compression algorithm has reduced the data volume of the original data.

5.2.2 Statistical parameters

Analysing the statistical parameters of each data set, with and without compression applied, can highlight changes that occurred in the statistical characteristics of the data due to the compression [62], [108]. A significant change in the statistical parameters in this domain means the compression algorithm was not as effective as it ideally could have been, since it corrupted the statistics of the original data.

Note that each metric was evaluated for the uncompressed and decompressed data sets to compare the results. Also note that all statistical parameters, except the dynamic range, were computed for both the magnitude and phase components of the complex data. The magnitude and phase components were used for the evaluation, since these components are important to form the outputs of SAR systems. The measured complex values are combined through SAR signal processing to form the Level 1 SAR product, while the phase is also important to produce higher level products, as discussed in Sections 2.3 and 2.4. For example, single-look complex (SLC) images use only the magnitude component, while for interferometric SAR (InSAR) the phase component is important. (See Section 2.4)

- Dynamic Range (DR)

The dynamic range, *DR*, is the ratio between the largest and smallest values that the data can represent and is defined as

$$DR = 20\log_{10}\left(\frac{V_{max}}{V_{min}}\right), \tag{5.2}$$

where V_{max} is the maximum value of the data, and V_{min} is the minimum value of the data. The dynamic range is computed using the magnitude component, and not the phase component. A reduction in the dynamic range leads to an improved compression ratio as fewer bits are required to represent the data.

- Mean (First order statistic)

The mean, μ, is defined as [61]

$$\mu = \frac{\sum_{i=1}^{N} X_i}{N}, \tag{5.3}$$

where X_i is the signal sample and N is the number of samples.

- Standard Deviation (Second order statistic)

The standard deviation, σ, is a measure of the variation of the data from the mean and is defined as [61]

$$\sigma = \sqrt{\frac{\sum_{i=1}^{N}(X_i-\mu)^2}{N}}. \tag{5.4}$$

- Skewness (Third order statistic)

The skewness, s, is a measure of how symmetrical the data are around the mean and is defined as [61]

$$s = \frac{\frac{1}{N}\sum_{i=1}^{N}(X_i-\mu)^3}{\left(\frac{1}{N}\sum_{i=1}^{N}(X_i-\mu)^2\right)^{3/2}}. \tag{5.5}$$

Certain compression algorithms, like the BAQ, exploit the fact that the I and Q components of raw SAR data follow a Gaussian distribution [60], [65]. In turn, this means that the amplitude component follows a Rayleigh distribution, while the phase component is uniformly distributed between $-\pi$ and π [64]. The skewness of a Rayleigh distribution and a uniform distribution are 0.63 and 0, respectively. Therefore, these values for the skewness can be used as a measure of how well the data components follow the applicable distributions. Skewness can thus be used to determine how much the compression algorithm caused the data to deviate from the distributions of the uncompressed data components.

- Kurtosis (Fourth order statistic)

The kurtosis, k, is a measure of how outlier-prone a distribution is or how heavy the tails of the distribution are and is defined as [61]

$$k = \frac{\frac{1}{N}\sum_{i=1}^{N}(X_i-\mu)^4}{\left(\frac{1}{N}\sum_{i=1}^{N}(X_i-\mu)^2\right)^2}. \tag{5.6}$$

Again, the kurtosis is an indication of how well the data follows a specific distribution by investigating the heaviness of the tails. The kurtosis of a Rayleigh distribution and a uniform distribution are 3.245 and 1.8, respectively. The kurtosis can therefore be used to determine whether the compression algorithm caused the data to deviate more from the applicable distribution compared to the uncompressed data.

- Entropy

The entropy, *H*, is a measure of the compressibility of the data or the randomness of the data and is defined as [61], [114]

$$H = -\sum_{i=1}^{N} \mathrm{p}(X_i)\cdot \log_2(\mathrm{p}(X_i)), \tag{5.7}$$

where $\mathrm{p}(X_i)$ is the probability of occurrence of X_i, a discrete random variable. A high entropy value means the data are difficult to compress, while a lower value indicates that the data can easily be compressed to a smaller size. The entropy after compressing and decompressing the data should be similar to the entropy of the uncompressed data.

5.2.3 Data histograms

The data histograms include the distributions of the in-phase (I), quadrature (Q), magnitude and phase components. The bin limits, binning method, and the normalisation scheme were specified for the standard *histogram* MATLAB function to ensure that the bins are equally spaced and all the values are well represented.

- The bin limits are specified as 3σ on the positive and negative side of the zero mean, as this represents 99.7 % of the data.

- The number of bins is computed using Scott's rule. Scott's rule is optimal if the data can be approximated as being normally distributed; therefore, it is a well suited algorithm for the raw SAR data.
- The histograms in this study were normalised to the probability of occurrence of each value.

By comparing the histograms before and after compression, the changes in the probability distribution caused by the compression algorithm can be visualised [62], [108].

5.2.4 Error measures

In this subsection, the amplitude and phase distortions of the complex SAR data after decompression are investigated. In essence, the errors and distortions caused by the quantiser are being investigated here. Take note of the definition of the variables being used in this subsection: g(x,y) is the pixels of the uncompressed data, f(x,y) is the pixels of the decompressed data, and M and N are the number of rows and columns of the data, respectively.

- Mean Square Error (MSE)

The MSE is a measure of the performance of the quantiser and gives the total absolute encoding error between the uncompressed and decompressed data set [26], [83], [108] and can be computed as

$$MSE = \frac{1}{M.N}\sum_{x=1}^{M}\sum_{y=1}^{N}(\mathrm{g}(x,y)\text{-}\mathrm{f}(x,y))^2 . \tag{5.8}$$

The MSE is computed using the magnitude components of the respective complex SAR data sets. The problem with using only the MSE to represent the distortion is that it depends strongly on the intensity scaling. Consequently, the MSE of different data sets can only be

compared after the MSE values have been normalised. Therefore, the signal-to-quantisation-noise ratio should also be evaluated.

- Mean Phase Error (MPE)

In SAR processing, the phase information is used to focus the SAR image, and therefore, knowing the phase error after decompression gives an indication of the focusing error that will be present in the final image [108]. The MPE [25], [26], [89] is computed for the phase component of the data using the following equation

$$MPE = \frac{1}{M.N}\sum_{x=1}^{M}\sum_{y=1}^{N}\left|\theta\left(g(x,y)\right)\text{-}\theta\left(f(x,y)\right)\right|, \tag{5.9}$$

where θ is the phase component of the complex SAR data of both sets being evaluated.

- Signal-to-Quantisation-Noise Ratio (SQNR)

The SQNR is an important parameter for image quality analysis since it is a measure of the signal-to-noise ratio after the compression and decompression of the data [26], [83], [89], [108]. SQNR is used to measure the average amplitude distortion of the complex SAR data after compression and decompression have been implemented [25] and can be computed as

$$SQNR = 10\log_{10}\left[\frac{\sum_{x=1}^{M}\sum_{y=1}^{N}\left(g(x,y)\right)^2}{\sum_{x=1}^{M}\sum_{y=1}^{N}(g(x,y)\text{-}f(x,y))^2}\right]. \tag{5.10}$$

The SQNR avoids the problem mentioned for the MSE by normalising the MSE. Therefore, both metrics are of use when investigating the quantisation effects caused by SAR compression algorithms.

5.3 IMAGE-DOMAIN METRICS

For conventional compression algorithms, the distortion is measured between the original and reconstructed data. However, for the compression of raw SAR data, the distortion is also measured in the image domain, after SAR processing [22]. Thus, the distortion is measured between the SLC image of the uncompressed data and the SLC image of the decompressed data [22]. However, only measuring distortion for the evaluation of compression algorithms for raw SAR data are not sufficient; since SAR has numerous outputs and applications that have different quality requirements. In most of the literature where compression algorithms for raw SAR data are evaluated, the only metrics used in the image domain are the signal-to-distortion noise ratio (SDNR) and/or the impulse response function (IRF) [25], [29], [82], [87], [114]. Although these are important metrics as they are strongly affected by compression algorithms, other metrics that evaluate factors other than visual quality should also be used to obtain a more complete quantification of the performance for a specific SAR application. The metrics to evaluate the effects of a compression algorithm in the image domain, are described below. These metrics also provide better validation than the data-domain metrics since they evaluate the quality of the SAR Level 1 output. As can be seen from Figure 4.1, this set of metrics is evaluated after processing the uncompressed data and the decompressed data to form the SLC SAR images that will be compared. The following metrics are proposed for image domain evaluation.

5.3.1 Statistical parameters

Higher order statistics can be used to characterise the distributions that the components of a data set follow. The statistical parameters of each data set are computed in the image domain to highlight the changes that occurred in the statistical characteristics of the SLC image [29], [62], [108]. Note that each metric is applied to the SAR image generated from the uncompressed data and the SAR image generated from the data after decompressing the compressed data to compare the results. For the equations of the metrics see Equations (5.2) to (5.6) in Section 5.2. Also note that all statistical parameters, except the dynamic range, are computed using the magnitude and phase components of the complex image data. Note

that the SLC image of the uncompressed data will act as the reference image for all comparisons.

- Dynamic Range

The dynamic range is computed using the magnitude component of the complex image data. There is a close correlation between the dynamic range and the contrast of the image; therefore, the change in this parameter can be compared to the change in the contrast ratio of the SAR images with and without compression. It should be noted that when the quality of an image is being evaluated, the dynamic range is generally seen as one of the image quality metrics. However, in this study it is evaluated as one of the statistical parameters to correspond with the statistical parameters of the data domain.

- Mean (First order statistic)

The compression algorithm should not drastically change the mean since the values are assumed to be quantized with only minor losses. The change in the mean should therefore be significantly smaller than the mean value of the uncompressed data. A change in the mean would introduce a bias in the final image, which would make the images more difficult to compare visually. However, if no clipping occurs (dynamic range is retained), the bias can be estimated and removed from the image. A large change in the mean would also indicate that the image exposure has been distorted by the compression algorithm, resulting in a loss of detail in the bright and/or dark regions of the image.

- Standard Deviation (Second order statistic)

Again, the compression algorithm is assumed to only quantize the data with minor losses. Therefore, the standard deviation of the image with the compression applied should be comparable with that of the image with no compression applied. A large change in the standard deviation would mean that the compression algorithm has increased the speckle content of the reference SAR image. Certain pixels are represented with a brighter or darker colour compared to the colour of the pixels in the reference image when the standard deviation changes. In this case the contrast of the SAR image will be affected.

- Skewness and Kurtosis (Third- and fourth-order statistics)

These parameters can be used to determine how well the algorithm retains the statistical distribution of the uncompressed SAR data and thus, how much the statistical analysis of the SAR images generated from the decompressed data can be trusted.

- Differential Entropy

Since the data in the image domain, after SAR processing, resemble a continuous random variable, differential entropy (or continuous entropy) needs to be calculated instead of entropy [114]. The entropy of a continuous random variable is infinite, since an infinite number of binary digits is required to fully represent the data. It is important to note that this parameter does not have the same physical meaning as entropy, calculated in the data domain. The differential entropy is calculated by replacing the summation in Equation (5.7) with an integral [114]. The differential entropy of the SAR image formed from the decompressed data should be similar to that of the SAR image formed from the uncompressed data, and can thus be used to verify this condition.

5.3.2 Image quality measures

Note that all the metrics in this subsection are computed for the SAR image formed from the uncompressed data, and for the SAR image formed from the decompressed data so that the results can be compared.

- Impulse Response Function (IRF)

A point target can be considered an impulse input to a SAR system. The point spread function (PSF) is equivalent to the IRF, since a SAR system can be modelled as a two-dimensional linear system [116], [117]. Generally, the PSF of an image is used to evaluate the performance or response of an imaging system like a SAR system [118], but in this case, the PSF or impulse response is used to determine the quality of a compression algorithm, as no other system changes are made. A good compression algorithm should not distort the IRF as this results in a loss of fidelity in the SAR images.

Illumination of a specifically designed scene is required to obtain the point target characteristics of a SAR system [119], [120]. The following elements are required within the scene:

1. point-like reflectors, and
2. reflectors positioned at the boundary between high and low backscatter areas.

Since only the data sets from the SAR system are available, the scene could not be set up with large point-like reflectors to measure the IRF. Although mission data generally have a scarcity of individual high signal-to-noise point targets in homogeneous areas of low reflectivity [120], [121], suitable geographical regions had to be identified from a real data set. See Section 7.4 for more information about the data set used in this study to evaluate the IRF.

The two metrics that are evaluated from the IRF are listed below [30], [83], [88]:

1. 3 dB impulse response width (IRW) in range and azimuth directions, which are related to the spatial resolutions. Spatial resolution, *SR*, is the ability of a system to distinguish between two adjacent point scatterers and can be computed as

$$SR = \frac{N_{-3dB}}{\rho_{pixel}}, \tag{5.11}$$

   where N_{-3dB} is the number of pixels between the -3 dB points, and ρ_{pixel} is the pixel size in the relevant direction [121].

2. Peak-to-side lobe ratio (PSLR) in the range and azimuth directions. PSLR provides an indication of whether the side lobe of a scatterer can mask an adjacent scatterer. It can be calculated as

$$PSLR = 20\log_{10}\left(\frac{IRF_{side}}{IRF_{main}}\right), \tag{5.12}$$

where IRF_{side} is the peak value of the first side lobe and IRF_{main} is the peak value of the main lobe of the IRF [121].

- Image Contrast (IC)

The image contrast is a metric to describe the quality of a SAR image [122], with a high image contrast ratio implying a crisp image and a low image contrast ratio suggesting a washed-out image [117]. IC is the ratio of the average intensity of a distributed clutter background to the average intensity of a no-return background [117] and can be computed as [65],

$$IC = \frac{\sigma_{image}}{\mu_{image}}. \tag{5.13}$$

The dynamic range and the IC are related. However, both metrics are useful since the dynamic range only considers the single highest and single lowest values of the image data, while the IC uses the mean and standard deviation, which are more representative of the variation of the dynamic range over the entire image.

- Global Contrast Factor (GCF)

GCF is a new approach in the field of image processing with applications in areas like rendering, tone mapping, volume visualization, and lighting design [122]. This metric has been added to the conventional metrics found in SAR literature, since it addresses the limitation of only using the darkest and brightest regions of an image to compute the IC. The GCF is indicative of the overall contrast of an image and is computed from the local contrasts of an image at various resolutions [122]. Local contrast ratio is the contrast ratio of any small part of an image, and the GCF is defined as the weighted sum of the local contrasts of a range of smaller image sizes.

Human visual experiments can be used to construct a GCF computation procedure which is indicative of human image perception. SAR images are not always interpreted by human

operators, so the weighting factors for human perception are not always relevant. Therefore, the method in [122] was adjusted to determine the GCF of the grayscale SAR images without applying the human perception adjustments. The steps below were followed.

1. Compute the linear luminance.

The linear luminance value for each pixel is computed by applying gamma correction to the image and scaling the result to be within the [0; 1] range. The linear luminance for the image is defined as

$$l = \left(\frac{k}{2^n\text{-}1}\right)\gamma, \tag{5.14}$$

where $\gamma = 2.2$ is the correction factor, $k \in \{0, 1, \ldots, 2^n\text{-}1\}$ is the original pixel value, and n is the number of bits of the SAR image data [122].

2. Compute the local contrast.

The local contrast for pixel i, l_{ci}, is computed as the average magnitude of the difference between the pixel and its four neighbouring pixels,

$$lc_i = \frac{|l_i\text{-}l_{i\text{-}1}|+|l_i\text{-}l_{i+1}|+|l_i\text{-}l_{i\text{-}w}|+|l_i\text{-}l_{i+w}|}{4}, \tag{5.15}$$

where the image has dimensions of $w \times h$. Note that for the corner pixels or pixels on the edges of the image, only the available neighbouring pixels are used in the computation.

3. Compute the average local contrast, LC_r, for the current resolution, r,

$$LC_r = \frac{1}{w\times h}\sum_{i=1}^{w\times h} lc_i\,. \tag{5.16}$$

Repeat step 1 to 3 for a number of resolutions of, for example $[1, 2, 4, 8, \ldots, 2^N]$ times the original resolution. A coarser image is obtained in each execution by taking the average of

4 pixels as the new pixel to halve the dimensions of the original image in both directions. This process continues until the coarsest resolution is reached. The number of chosen resolutions is defined as *N*.

4. Compute the global contrast factor as the average of the local contrasts for all resolutions. It is assumed that the system interpreting the SAR images is equally sensitive to changes at various frequencies and therefore a weighting function is not required to compute the global contrast, in contrast to the requirements in [122].

$$GCF = \frac{1}{N}\sum_{i=1}^{N} LC_r \,. \tag{5.17}$$

An image with a high GCF is variation-rich, while an image with a low GCF appears uniform with less information [122].

5.3.3 Image fidelity measures

Image fidelity measures evaluate the level of exactness with which the original SAR image is reproduced. Therefore, these measures are an important measure of the quality of a compression algorithm. The different metrics are discussed below. Take note of the definition of the variables used in this subsection: g(*x*,*y*) is the magnitude component of the uncompressed SLC image data, f(*x*,*y*) is the magnitude component of the decompressed SLC image data, and *M* and *N* are the number of rows and columns of the image, respectively.

- Mean Square Error (MSE) and Mean Phase Error (MPE)

The MSE and MPE in this domain [22], [26] are both pixel by pixel measures of the change between the pixel values in the SAR image formed from the uncompressed data, and the SAR image formed from the decompressed data. The MSE is computed for the magnitude component of the SAR images, while the MPE is computed for the phase component of the SAR images to measure the amplitude and phase distortions, respectively [25]. An important fact is that the MSE does not indicate whether the error is due to a large number of small

errors, or whether it is due to a few large errors [108], [117]. It also depends strongly on the image intensity scaling. Therefore, the signal-to-distortion-noise ratio is also evaluated as part of this study. According to [117], the MSE is the most widely used image fidelity measure in SAR compression studies since it is mathematically and computationally simple to evaluate. To compute the MSE see Equation (5.8) [65], [117]. The MPE can be computed using Equation (5.9), where θ is the phase components of the two SLC images being compared.

- Signal-to-Distortion Noise Ratio (SDNR)

SDNR [25], [29], [30], [62], [65] is a more global measure of the change and thus addresses the limitation mentioned for the MSE by normalising the MSE. It is also mathematically and computationally simple and therefore widely used in the literature [117]. To compute the SDNR see Equation (5.10) [65], [117].

- Error Images

The error image [65], [108] can be computed as

$$e(x,y) = |g(x,y)-f(x,y)|. \tag{5.18}$$

The error image can be computed for the magnitude and phase of the complex images in order to investigate both components. This metric can be used to visualise some of the corruptions that have occurred in the SAR images formed. It is important to note that many of the corruptions cannot be easily visualised by the human perceptual system and therefore, this metric is not able to fully represent the degradation that may have occurred.

5.4 SAR TECHNOLOGIES AND THEIR METRICS OF IMPORTANCE

In Section 2.4, well-known SAR technologies and their applications were discussed. Single frequency, single polarisation SAR systems produce a SLC image, with or without further corrections. UWB SAR has applications in medical imaging and the detection of concealed

Table 5.1 Summary of important metrics for well-known SAR technologies and applications. Adapted from [83], © 1995 IEEE.

SAR Technology	Primary Application	Main requirement(s)	Important Metric(s)
Single frequency, single polarisation SAR	Image classification	- High image contrast	- Statistical parameters - IC and GCF
	Detection of man-made targets	- High sensitivity to point targets - Magnitude component	- Impulse response function: o 3 dB IRW o PSLR - IC and GCF - MSE
	Global monitoring (Change detection)	- Noise should not mask changes	- SDNR
UWB SAR	Imaging through unconventional mediums	- High radiometric resolution	- SDNR
InSAR	Surface topography	- Very high phase accuracy	- Phase error: o MPE o Error Image of phase
	Measurement of displacements		
PolSAR	Change detection and feature tracking	- High phase accuracy	- Phase error: o MPE o Error Image of phase
Image Fusion	Fusion of Visible-Infrared (VIR) sensor data and SAR images	- Geometric and radiometric accuracy	- SDNR
	Fusion of multi-frequency or multi-temporal SAR images		

objects due to its high resolution and low operating frequencies. Since the phase of a single SAR image is not exploitable, InSAR and PolSAR use the phase difference between multiple images for various advanced SAR applications. Image fusion is a means of gaining complementary information by either combining data from different imaging systems, or by combining data from SAR systems with different operating characteristics. In this way, the advantages of each imaging system are exploited to produce unique information and improve interpretation. Since these technologies use different components of the SAR data, different

metrics will be of importance for each technology when compression has to be implemented on board the platform. The important metrics for each technology are discussed below and also summarised in Table 5.1. It is important to note that all data-domain metrics are of importance for every SAR technology, thus emphasis will be placed on the image-domain metrics that need to be preserved in each case.

5.4.1 Single frequency, single polarisation basic SAR systems

For image classification automatic target recognition (ATR) is increasingly being used as it is a time-consuming process for a human operator to search through all the data [42]. The important metrics for these algorithms are the mean, variance and entropy of the SAR images, since these metrics are used to divide the image into homogeneity categories [41]. Furthermore, high image contrast is required for initial detection of areas of change within an image, so the IC and GCF are also important metrics for this application.

The detection of man-made targets is mainly utilised in military systems and requires good resolution and geometric accuracy [42]. When detecting and classifying man-made targets in military applications, it is important that the estimated location of the target corresponds to the real location with only a minimal margin of error. To ensure that the location is accurate, the IRF must be preserved. As part of the detection of targets, the magnitude or modulus of the SAR image is calculated [2] and the phase information is of less importance for the output. This means that the magnitude component should be preserved as well as possible when investigating the compression of the raw SAR data for man-made target detection. This condition can be monitored by comparing all the error measures of the magnitude component which include the MSE and SDNR.

Global monitoring is used for earth observation and the study of climate change where the global carbon cycle, the global energy/water cycle and other human activities are monitored [44]. The SAR system needs to be sensitive to small changes when monitoring a global cycle and thus, the radiometric resolution of the SAR system is an important factor. The

radiometric resolution of an imaging system is its ability to detect miniscule differences in the reflected energy. In order to preserve the radiometric resolution of a system, frequent calibrations are required [44]. A high SNR indicates that the signal level is greater than the noise level and therefore the noise does not mask any of the small changes that may appear in a scene. The metrics of importance for this application are the MSE and SDNR.

5.4.2 Ultra-wideband (UWB) SAR systems

UWB imaging utilises time or frequency domain techniques [45]. The frequency domain technique is widely applied for UWB imaging applications. This technique operates by performing a frequency sweep and only measuring one very narrow frequency which will achieve the highest possible dynamic range. The image quality depends strongly on the measurement accuracy and the dynamic range of the system [45]. For landmine detection, regions of interest are identified by measuring the amplitude difference between targets and the background noise [46]. To avoid a high number of false alarms, the noise in the system should be minimised. Therefore, dynamic range and SDNR are the metrics of importance and should be preserved when implementing a compression algorithm on board the platform.

5.4.3 Interferometric SAR (InSAR)

As previously mentioned, InSAR uses the phase difference between two SAR images acquired at two distinct times or from slightly different positions to measure changes to a specific surface [7], [42], [51]. With InSAR data it is possible to detect and measure miniscule path length differences, very small velocities and height differences with very high accuracy. This is due to the high accuracy of the range information derived from the phase of each pixel [5], [7], [42]. It is therefore evident that preserving the phase content is important for this application. The metrics of importance include the MPE and the error image of the phase component as it can provide a visual representation of the error between two SAR images.

5.4.4 Polarimetric SAR (PolSAR)

PolSAR is an advanced imaging system where the radar transmits and receives multiple polarisations. PolSAR is highly suited for change detection and feature tracking applications [7], [123]. For these applications, the phase information of the SAR image is required [2], so it is important that the phase information be preserved when compressing the raw data. The metrics of importance include the phase MSE and the error image of the phase component as a visual representation of the error between two SAR images.

5.4.5 Image fusion

Image fusion has numerous applications which include topographic mapping, land-use mapping, disaster monitoring, ice and snow monitoring and other geological applications [53]. Image fusion improves the reliability of the results, extends the classification capabilities and provides robust operational performance [53].Three image fusion methods exist and they are performed at three different processing levels. Thus, fusion can take place at pixel level, feature level, or decision level [53], [57]. A prerequisite for image fusion is pre-processing the data [53], [57]. Pre-processing includes calibration, geocoding, registration, resampling to conform different images to be compatible, to only mention a few [53], [57]. All the sensor-specific corrections need to be performed before image fusion, since the contributions from the different sensors are indistinguishable after image fusion. For VIR data, it is important that radiometric distortions present in the imagery are corrected to ensure that the data sets are compatible. Speckle reduction is a critical pre-processing step when SAR imagery is used.

Pixel-level methods are widely used since they are highly advantageous and easy to implement [57]. To avoid artefacts, consequently causing misinterpretation, in the results of pixel-based image fusion, geometric accuracy is critical [53]. Generally, the geometry and radiometry of the individual sensor outputs are optimised as much as possible, before fusion is applied [53]. An input image of low SNR is also known to cause a blurring effect in the

fused output [53]. Therefore, it is evident that the radiometry and SNR of the input images are of importance. Thus, in this study the SDNR would be the important metric to preserve.

5.5 CHAPTER SUMMARY

Despite the importance of being able to quantify the performance of SAR data-compression algorithms, there does not appear to be a widely-accepted set of metrics in the literature [28]. The problem is compounded by the fact that different publications on SAR-data compression often propose new metrics to emphasise the unique benefits of the proposed algorithms (e.g. [29] and [30]). Therefore, the metrics available in the literature have been reviewed to establish a standardised set of metrics that evaluate the algorithms in both the data and image domains.

The evaluation metrics that will serve as a standardised set of metrics for the performance evaluation of raw SAR-data compression algorithms were established in this chapter. The majority of the metrics were taken from known SAR-data compression literature, except where it was mentioned that the metric was added from another field to address a limitation. The metrics were proposed as two sets to be evaluated in the first two important domains for SAR data production. Firstly, the data-domain metrics, established in Section 5.2, can be evaluated to determine the effects of the compression algorithm in the data domain. After SAR processing, another set of metrics, established in Section 5.3, can be evaluated to determine the degradation in the image domain. Here, the emphasis is on the quality of the SAR image that was produced from the data that had undergone compression on board the SAR platform. Finally, in Section 5.4 the SAR technologies discussed in Chapter 2, were revisited and the metrics of importance for each application were discussed.

CHAPTER 6 IMPLEMENTATION OF SAR COMPRESSION ALGORITHMS

6.1 CHAPTER OVERVIEW

In Chapter 3 it was found that a careful assessment of the statistical properties of the data to be compressed, must be performed before an efficient compression algorithm can be chosen. In this way the chosen algorithm can exploit the data characteristics and thus achieve better performance. Therefore, the statistical characteristics of the data sets used in this study, are analysed in Section 6.2. Thereafter, the three SAR compression algorithms that were chosen to conduct the research explained in Chapter 4, are discussed. The compression algorithms include the block adaptive quantiser (BAQ), the fast Fourier transform BAQ (FFT-BAQ), and the flexible dynamic BAQ (FDBAQ), and are discussed in Subsections 6.3.1 to 6.3.3, respectively. The discussions of the algorithms are divided into the compression and decompression steps, while the computational complexity is also investigated.

6.2 STATISTICAL ANALYSIS OF SAR DATA SETS

The acquired data were stored as a raw binary format. This file type contains the data exactly as it was captured by the ADCs, without loss of quality and without compression. The raw file content was then converted to complex, double-precision, floating-point format to be processed in MATLAB. Thereafter, the data were downsampled in the slow time dimension, since a very high PRF was achieved during the flight tests. The downsampling increased the signal-to-noise ratio (SNR) by lowering the noise floor and also made the size of the data more manageable in a MATLAB environment. Although the SAR system is described as

having 14-bit quantisation in Subsection 4.3.1, the received echoes from the scene only fill about 9 of the lower bits. The remaining bits are the recorded leakage signal of the SAR system.

The signal also had to be adjusted to ensure that discrete data are used for the research, since discrete ADC data are usually the input to raw SAR data compression algorithms. Thus, after the pre-processing required to remove the system artefacts present in this prototype SAR system, the data of each scene were discretised to 12 bit in-phase (I) and quadrature (Q) samples, respectively.

As mentioned in Chapter 4, raw SAR data are the received echoes, without any SAR processing performed. The received echoes are sampled into I and Q components, and then digitised to the required bit rate by a uniform quantiser. Although the data used in this research are not directly from the uniform quantiser of the ADC, since pre-processing is performed, the data are still categorised as Level 0 data since no focusing of the data have occurred [31], [112].

Although it was concluded in SAR-data literature that the I and Q components can be assumed to follow a Gaussian distribution with zero mean [22], [25], [60], [62], [63], another consideration is the scene type and the level of urbanisation. This is important since a high level of urbanisation leads to higher levels of return and ultimately leads to a distribution with heavy tails [70]. In some cases, the data then follow other types of distributions and the Gaussian distribution assumptions, mentioned in Section 2.5, may cause severe image degradation after SAR processing.

Terrain clutter is normally categorised as homogeneous speckle in SAR imagery, while cultural or man-made clutter can be a mixture of homogeneous and inhomogeneous speckle [70]. Natural terrain produces low average returns, while cultural clutter is responsible for strong, point-scatterer-like returns. In [70] data sets are categorised according to the cultural clutter coverage in the scene.

- Low urban data: scenes that typically consist of natural clutter with limited cultural clutter, covering only one-third or less of the scene.
- Mid urban data: scenes that typically consist of some natural clutter as well as moderately urbanised areas, like a residential area, covering one-third to two-thirds of the scene.
- High urban data: scenes that typically consist of dense residential areas or city capitals, with the cultural clutter covering two-thirds or more of the scene.

Therefore, since different scene types were used in this study, the data sets were statistically analysed to determine their characteristics and whether a Gaussian probability distribution function (PDF) can be assumed. The data sets were also categorised as high, mid or low urban data, following the approach in [70]. As mentioned in Section 4.3, three data sets of different scenes were used in this study. The data sets are introduced in Table 6.1 and discussed in more detail in Subsections 6.2.1 to 6.2.3, respectively.

Table 6.1 Information about data sets used.

Data Set Number	Scene Type	Features
1	Farm	Vegetation, river, gravel roads
2	Mine	Different surface levels, piles, gravel roads
3	Peri-urban	Golf course, housing, dam

For the current application, the compression problem can be simplified if the raw data can be assumed to follow a standard normal (Gaussian) distribution. Therefore, the distributions of the raw data of all three data sets were investigated. Various goodness-of-fit tests were executed in MATLAB. The tests that were implemented in MATLAB include the Chi-square goodness-of-fit test, the Jarque-Bera test, the one-sample Kolmogorov-Smirnov test, and the Lilliefors test. These tests were found to be too strict for the raw SAR data, since all of these tests rejected the null hypothesis that the data follow a standard normal distribution.

Therefore, the function *allfitdist*, written by Mike Sheppard[1], was used to fit all valid parametric probability distributions to the data. In this way, the distributions that best fit the data could be identified. The function evaluates the Bayesian information criterion (BIC) and sorts the valid distributions according to this criterion. BIC [124] is a widely known statistical model selection criterion due to its computational simplicity and effective performance in many modelling selection or evaluation problems. BIC was derived to serve as an asymptotic approximation to a transformation of the Bayesian posterior probability of a candidate model. For large samples, the BIC favours the model that the data is most probable to follow. The computation of BIC is based on the empirical log-likelihood and therefore, does not require the specification of prior probability distributions. Thus, BIC is ideal for Bayesian applications where prior distributions are difficult to find. In a model selection application, the most plausible model is identified by the minimum value of BIC. Model selection based on BIC is advantageous since the BIC is known for its consistency. The results for the three data sets are illustrated in the form of PDFs as can be seen in Figure 6.1.

The results of the *allfitdist* function show that the normal distribution is not the best fit to the data. However, when comparing the values for the different parametric probability distributions fitted to the data, summarised in Table 6.2, it can be seen that the BIC value for the normal distribution is close to that of the distribution that fits the data best. The best fit seems to either be the t location-scale distribution or the logistic distribution. The t location-scale distribution has heavier tails, which means it is more prone to outliers than the normal distribution. The logistic distribution has longer tails and a higher kurtosis than the normal distribution.

Despite the result that the normal distribution is not the best fit for the raw data, the assumption that the I and Q components of raw SAR data follow a Gaussian distribution is

[1] Copyright ©2012, Mike Sheppard

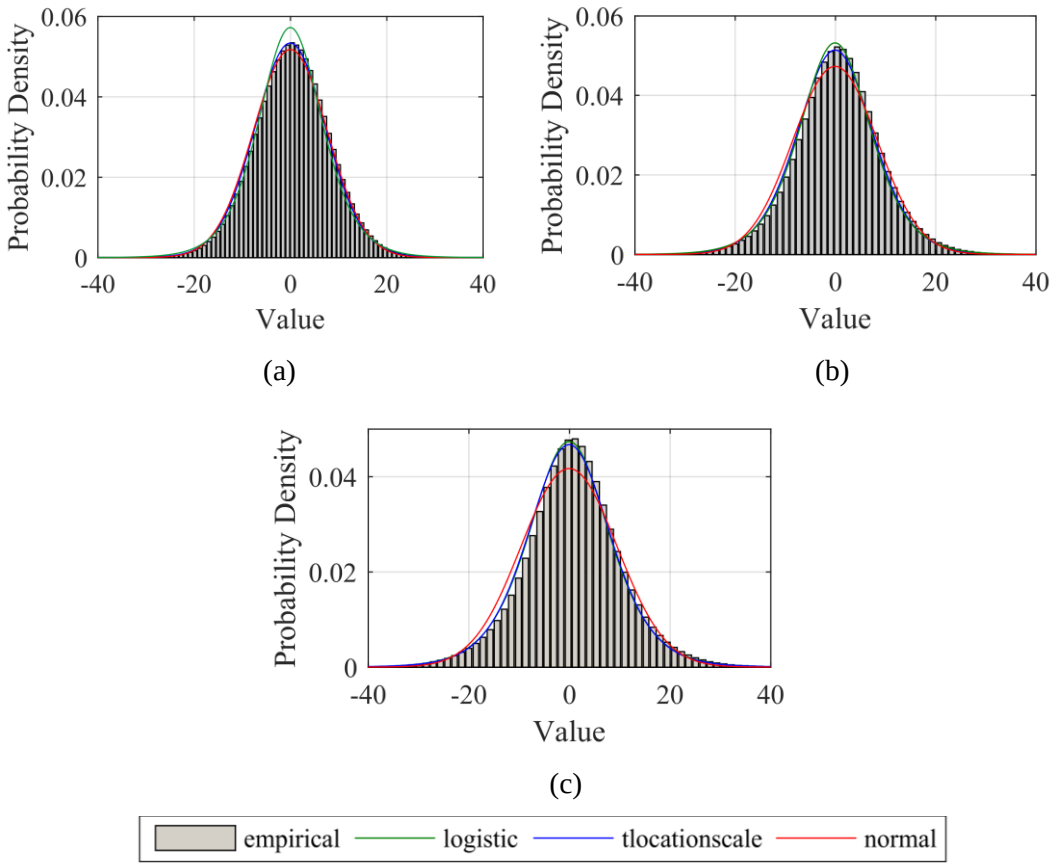

Figure 6.1 PDFs of the three data sets with the three best distributions fitted to the data. (a) Data set 1. (b) Data set 2. (c) Data set 3.

made in SAR compression literature [22], [25], [60], [62], [63]. However, this assumption is valid since the number of elementary phasor contributions can be considered to be extremely large, therefore the I and Q components of the received signal are sums of a very large number of independent random variables [60], [125]. It then follows from the central limit theorem that these components are Gaussian with unknown variances [125]. To verify this assumption, the PDFs and cumulative distribution functions (CDFs) of the data sets were plotted. Statistical parameters, like the skewness and kurtosis were also used to assess the deviation of the distribution of the SAR data from a standard normal distribution. The validity of the assumption that the I and Q components of each data set are Gaussian distributed, is investigated in the subsections to follow.

Table 6.2 Summary of the BIC values of the distributions fitted to each data set.

Data set 1		**Data set 2**		**Data set 3**	
Top five distributions	**BIC ($\times 10^8$)**	**Top five distributions**	**BIC ($\times 10^8$)**	**Top five distributions**	**BIC ($\times 10^8$)**
t Location-scale	1.3842	t Location-scale	1.4177	Logistic	1.4658
Normal	1.3846	Logistic	1.4178	t Location-scale	1.4660
Logistic	1.3861	Normal	1.4207	Normal	1.4710
Generalised extreme value	1.3950	Generalised extreme value	1.4349	Generalised extreme value	1.4886
Extreme value	1.4210	Extreme value	1.4649	Extreme value	1.5183

6.2.1 Data set 1: Rural scene

The first data set is a farm with a river flowing through the area. Therefore, the data set was classified as low urban data since it consists of mostly natural clutter. The other statistical characteristics of the set are summarised in Table 6.3.

Table 6.3 Characteristics of data set 1.

Parameter	**Value**	
Quantisation	12 bits	
Level of urbanisation	Low urban	
Mean	I: -0.0368	Q: -0.6599
Variance	I: 951.4096	Q: 942.1072
Skewness	I: -0.0043	Q: -0.0091
Kurtosis	I: 3.27	Q: 3.26
Entropy	I: 10.31 bits	Q: 10.31 bits

In raw SAR data compression literature, it is stated that raw SAR data are difficult to compress and pose unique compression challenges due to the high entropy and dynamic range of the raw data [31], [83].

The statistical parameters in Table 6.3 confirm these characteristics for the raw SAR data of data set 1. It can be seen that the entropy is between 10 and 11 bits for the 12 bit quantisation, implying that the compressibility of the data is low.

The CDFs in Figure 6.2, as well as the PDFs in Figure 6.3, show that the I and Q components of data set 1 closely follow a Gaussian distribution. It can also be seen that the magnitude component follows a Rayleigh distribution, while the phase is uniformly distributed between $-\pi$ and π. The statistical parameters, like the skewness and kurtosis can also be investigated to determine how well the data follow a Gaussian distribution. For example, the skewness and kurtosis of a Gaussian distribution are 0 and 3, respectively. Therefore, the summarised characteristics in Table 6.3 also confirm that the I and Q components of data set 1 closely follow a Gaussian distribution, since the skewness and kurtosis are close to 0 and 3, respectively.

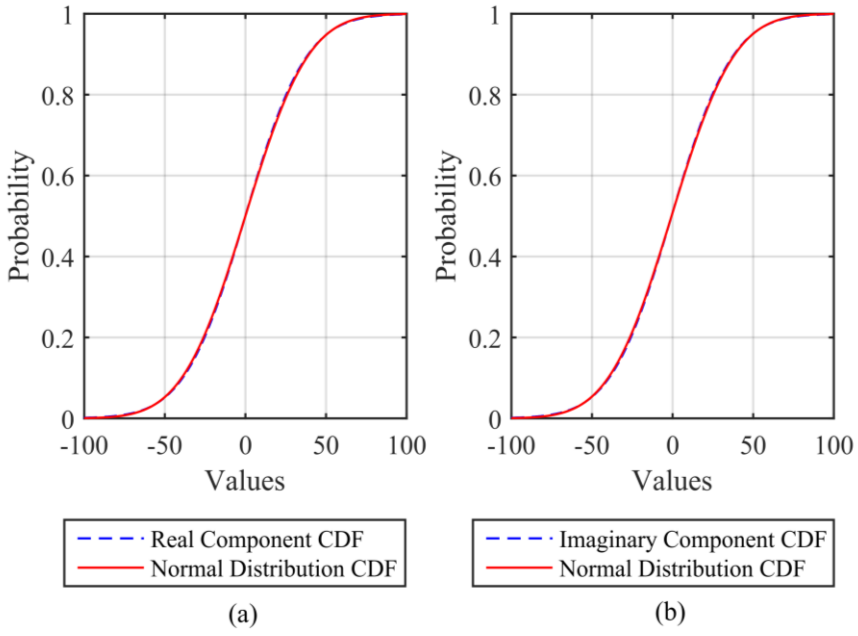

Figure 6.2 Empirical CDFs of data set 1. (a) I component. (b) Q component.

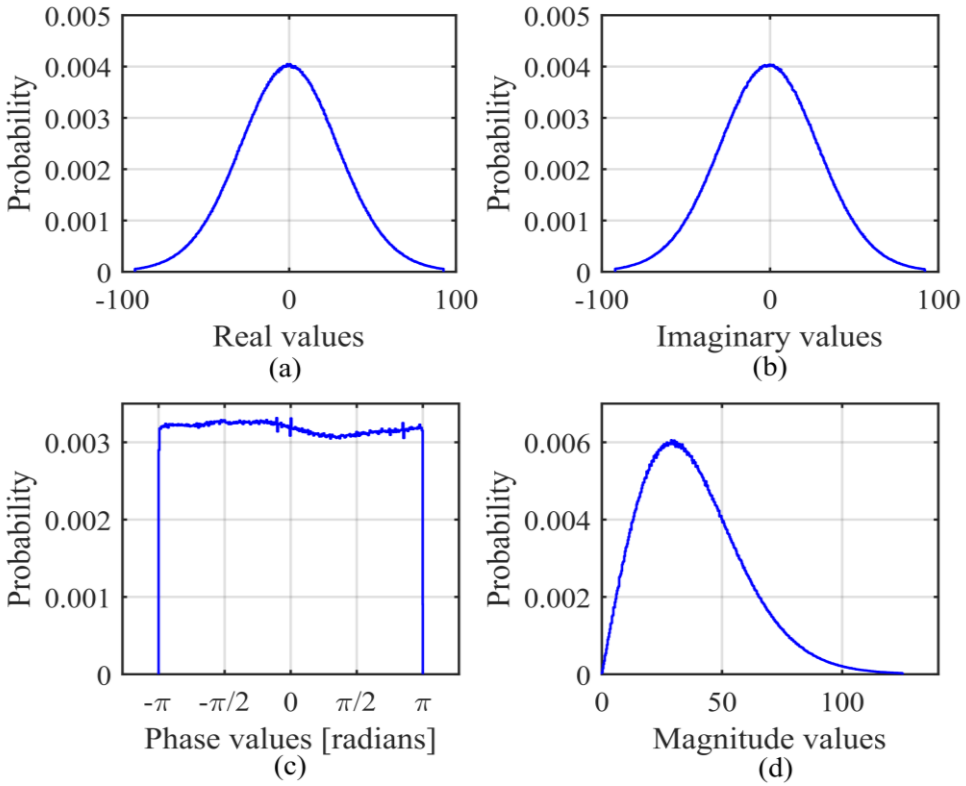

Figure 6.3 PDFs of the components of data set 1. (a) Real component. (b) Imaginary component. (c) Phase. (d) Magnitude.

6.2.2 Data set 2: Mine scene

Data set 2 is an image of a mine. Therefore, the data set was classified as low urban data since it consists of natural clutter with less than one-third of the scene consisting of cultural clutter. The other statistical characteristics of the set are summarised in Table 6.4.

The statistical parameters in Table 6.4 confirm that the entropy and dynamic range of the raw SAR data of data set 2, are indeed high. It can be seen that the entropy is between 10 and 11 bits for the 12 bit quantisation, implying that the compressibility of the data is low.

The CDFs in Figure 6.4, as well as the PDFs in Figure 6.5, show that the I and Q components of data set 2 closely follow a Gaussian distribution. It can also be seen that the magnitude component follows a Rayleigh distribution, while the phase is uniformly distributed between

–π and π. The statistical parameters, like the skewness and kurtosis were investigated to determine how well the data follow a Gaussian distribution. The summarised characteristics in Table 6.4 also confirm that the I and Q components of data set 2 closely follow a Gaussian distribution, since the skewness and kurtosis are close to 0 and 3, respectively.

Table 6.4 Characteristics of data set 2.

Parameter	**Value**	
Quantisation	12 bits	
Level of urbanisation	Low urban	
Mean	I: -0.2059	Q: -0.0915
Variance	I: 1139.1	Q: 1167.7
Skewness	I: 0.0087	Q: -0.0285
Kurtosis	I: 3.73	Q: 3.82
Entropy	I: 10.11 bits	Q: 10.13 bits

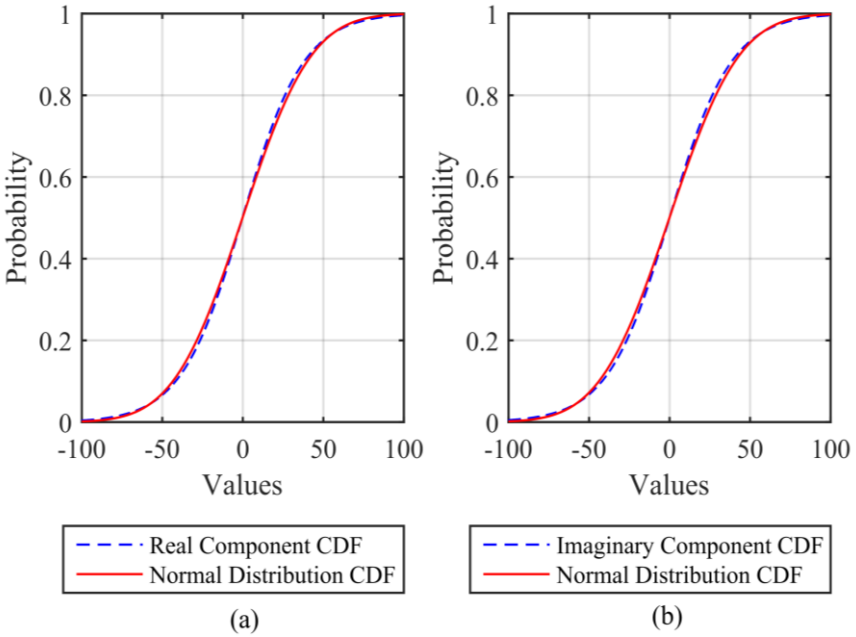

Figure 6.4 Empirical CDFs of data set 2. (a) I component. (b) Q component.

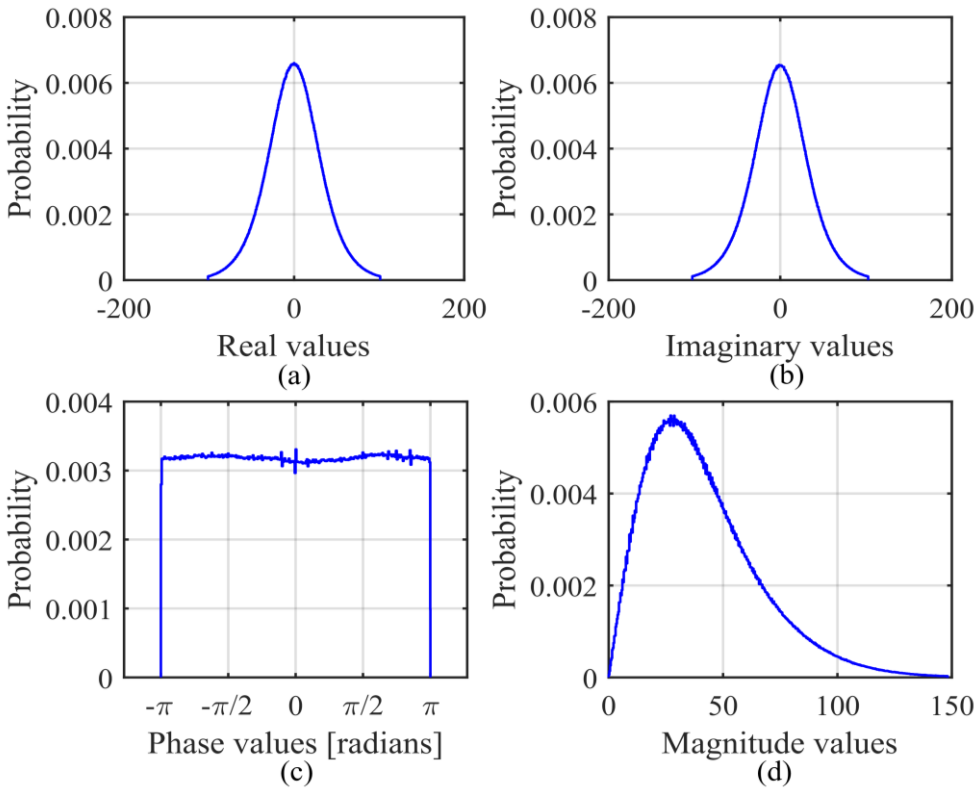

Figure 6.5 PDFs of the components of data set 2. (a) Real component. (b) Imaginary component. (c) Phase. (d) Magnitude.

6.2.3 Data set 3: Peri-urban scene

The last data set covers a residential area on a golf course in Hartbeespoort, called Pecanwood Estate, and also a part of the Hartbeespoort Dam. Therefore, the data set was classified as mid urban data since it consists of some natural clutter with cultural clutter covering one to two thirds of the scene. The other statistical characteristics of the set are summarised in Table 6.5.

The statistical parameters in Table 6.5 confirm that the entropy and dynamic range of the raw SAR data of data set 3, are indeed high. It can be seen that the entropy is between 10 and 11 bits for the 12 bit quantisation, implying that the compressibility of the data is low. It was also noted that data set 3 has the highest variance, which corresponds to the power of the data, and therefore, indicates that this scene produces higher returns than the other two

scenes. This observation corresponds to the fact that cultural clutter produces a higher level of backscatter, since data set 3 is a residential area and was categorised as mid urban data, while data sets 1 and 2 are low urban data.

The CDFs in Figure 6.6, as well as the PDFs in Figure 6.7, show that the I and Q components of data set 3 closely follow a Gaussian distribution. It can also be seen that the magnitude component follows a Rayleigh distribution, while the phase is uniformly distributed between $-\pi$ and π. The statistical parameters, like the skewness and kurtosis were investigated to determine how well the data follow a Gaussian distribution. The summarised characteristics in Table 6.5 also confirm that the I and Q components of data set 3 closely follow a Gaussian distribution, since the skewness and kurtosis are relatively close to 0 and 3, respectively.

Table 6.5 Characteristics of data set 3.

Parameter	**Value**	
Quantisation	12 bits	
Level of urbanisation	Mid urban	
Mean	I: -0.2729	Q: 1.1528
Variance	I: 1465.3	Q: 1498.1
Skewness	I: -0.0045	Q: 0.1339
Kurtosis	I: 3.99	Q: 4.06
Entropy	I: 10.29 bits	Q: 10.3 bits

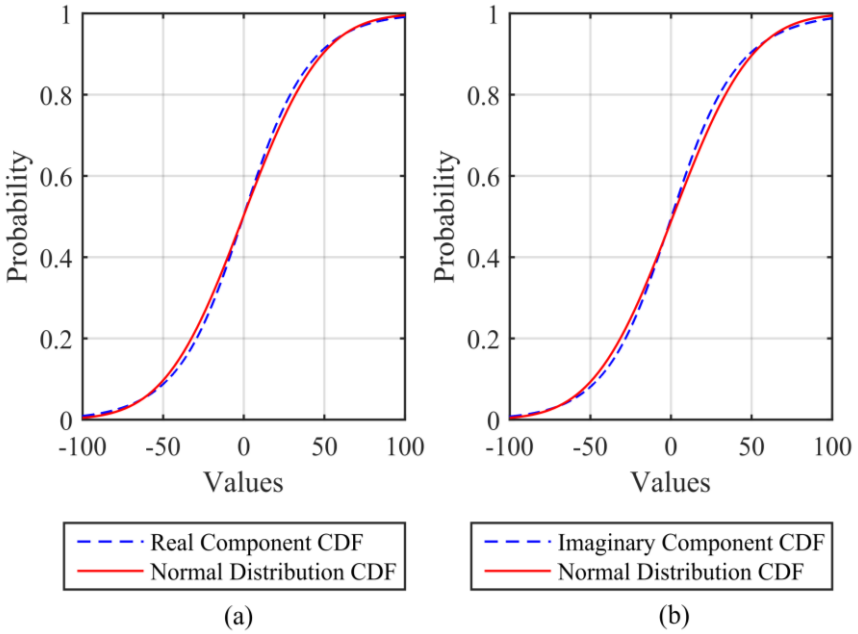

Figure 6.6 Empirical CDFs of data set 3. (a) I component. (b) Q component.

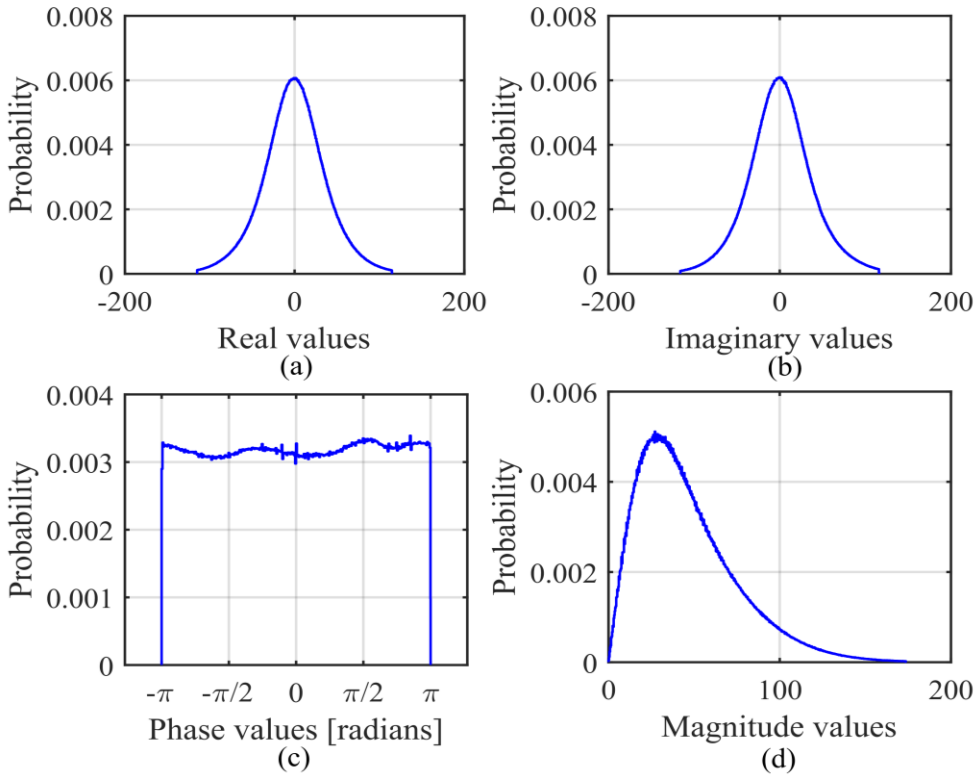

Figure 6.7 PDFs of the components of data set 3. (a) Real component. (b) Imaginary component. (c) Phase. (d) Magnitude.

6.3 IMPLEMENTATION OF COMPRESSION ALGORITHMS

In Chapter 3 it was seen that raw SAR data are difficult to compress due to their high entropy and lack of statistical dependency. Therefore, it has been noted that compressing the focused SAR image, instead of the raw SAR data, would be much easier as the data then contain dependency and redundancy that can be exploited by compression algorithms [28], [96]. However, the SAR focusing process is too complex for real-time, on board implementation, and therefore, raw SAR data compression is a critical requirement for modern SAR systems.

It was also concluded that lossless compression algorithms, which utilises predictive coding, are ill-suited for the compression raw SAR data since these methods take advantage of sample to sample correlation. Since conventional lossy compression techniques utilise transform coding, which also exploit the correlation between samples, these techniques are also rendered ill-suited for the compression of raw SAR data [65], [84]. The characteristics of raw SAR data and the above mentioned factors imply that quantisation is a suited method for the compression for raw SAR data [84].

The results in the previous section show that it can be assumed that the I and Q components of all three data sets used for this research, follow a Gaussian distribution with zero mean. Therefore, a compression algorithm that exploits these characteristics of the raw data would be highly suited to compress the raw SAR data on board a SAR platform. As seen in Subsection 3.3.3, lattice vector quantisation is usually applied when the data have a known PDF with a mean of zero [85]. However, although vector quantisation (VQ) performs well, the computational complexity renders it ill-suited for on board implementation [96]. A very well-known algorithm that was designed for the compression of raw SAR data, with Gaussian distributed I and Q components, is the BAQ [31], [34], [60]. It has been observed that combining algorithms can lead to improved results at some cost. The BAVQ algorithm, for example, produces an image of better quality compared to an image produced after the BAQ, but the increased amount of computations required for this algorithm cannot be justified [99]. A lot of literature focuses on the fusion of the time and frequency domain,

since it had been observed that the best results have been achieved when the BAQ is applied in the frequency domain [83], [99].

Where the application is the onboard compression of raw SAR data, BAQ is preferred, primarily because it is a good trade-off between performance and simplicity [62], [83]. A thorough literature study showed that the main candidates for SAR raw data compression are the standard BAQ, some of the BAQ variations (which have been implemented on recent SAR satellites), like the FDBAQ, and the FFT-BAQ [5], [83], [99].

The FFT-BAQ algorithm achieved promising results. It is known to outperform the BAQ, but again leads to increased computational complexity [83]. The BAQ can be applied in the frequency domain since one of the properties of the Gaussian random process is that the response of a linear system to a Gaussian random process is also a Gaussian random process [114]. Until recently, FFT-BAQ was not considered a viable solution due to the high computational requirements, but technological advances in hardware design could see the implementation of FFT-BAQ on board a future SAR platform.

The FDBAQ is the latest extension of the standard BAQ method by adaptively selecting the encoding bitrate according to the local SNR [21], [92], [93]. The FDBAQ algorithm has been implemented on board the Sentinel-1 satellite, launched in 2014. FDBAQ achieves an average bit rate comparable to that of a BAQ with an output bit rate of 3 bits, but with the added benefit of improved SNR in the high-reflectivity areas in the scene, while also not degrading the quality of the low-reflectivity areas. The added flexibility of the bit rate per block is important for modern SAR systems, since different operating modes and applications have different image quality and data volume requirements [5], [63].

6.3.1 BAQ algorithm

As seen in Chapter 3, BAQ is categorised as scalar quantisation, and is therefore a lossy compression algorithm [71], [73]. It is also categorised as an adaptive quantiser, meaning it estimates the statistics of the data and then adjusts the quantiser to match the observed

statistics [60]. In order to design an optimal quantiser, the statistics of the data must be known. The input to the BAQ is the uniformly quantised samples from the analogue to digital converters (ADCs) in the SAR system. Although it is known that raw SAR data are not highly compressible, a reduction in the number of bits is possible for the BAQ method, since the entropy for a block of data is much less than that of the entire data set [31], [83]. BAQ has been designed to compress raw SAR data, since a Gaussian statistic signal, with slowly varying power, forms the basis of the BAQ design [31], [34], [60]. The BAQ then adaptively varies the step sizes of a non-uniform quantiser, based on the estimated variance of the block, to minimise the distortion error of that block. This non-uniform quantiser, called the Lloyd-Max quantiser, achieves a wider overall dynamic range at the output, for the same number of quantization levels than simple uniform quantization of the data [62]. The quantiser rate is measured in bits/sample, and is fixed for the BAQ algorithm.

The choice of the block size is a trade-off between the upper and lower limits. Therefore, the selection of the block size is critical for good performance. The guidelines for selecting a block size are given below [31], [34].

1. The lower bound of the block size is that the block should contain enough samples to ensure Gaussian statistics for the block. Thus, 50 to 100 samples are the required minimum number of samples.
2. The upper bound of the block size is determined by the range extent and must ensure that the signal power is constant within a block. A maximum variation of 1 to 2 dB in signal power is acceptable.
3. The blocks should also be small in range relative to the number of samples in one pulse. Thus, the block size should be smaller than a ¼ to a ½ of the uncompressed pulse width in fast time.
4. The blocks should also be small in azimuth relative to the synthetic aperture length. Thus, the block size should be smaller than a ¼ to a ½ of the synthetic array time in slow time.

In some literature, for example the BAQ implementation on board the ENVISAT system, one-dimensional blocks were used to save memory [99]. However, two-dimensional blocks have been recommended [99]. Experiments by Kuduvalli, Dutkiewicz, and Cumming, showed that the BAQ algorithm is not sensitive to the changes in the block size in the range of 64 to 512 samples [62]. For the data sets used in this research, a block size of 200×200 samples was selected.

The figures below show that the guidelines for the block size were followed. These figures were plotted for the real (I) component of data set 1 for illustration purposes, although the outcome is the same for all the data sets, and both components. Figure 6.8 shows that the lower limit is adhered to, since the blocks of size 200×200 have Gaussian statistics. This is confirmed by the skewness and kurtosis, 0 and 3 respectively for a Gaussian distribution, that are maintained well after dividing the data into blocks of size 200×200, while the mean and standard deviation deviate slightly more from the value of the entire data set. Table 6.6 shows that the upper limit has not been surpassed, since the power does not vary more than 2 dB within the 200×200 blocks. The values in Table 6.6 were calculated using Equation (6.1), with the assumption that each block contains a homogenous scene. It is assumed that these power variation values for a specific block size are true for all the blocks of the data set.

$$Power\ variation = 10\log_{10}\left(\frac{(R_{start}+\Delta R)^4}{R_{start}{}^4}\right). \tag{6.1}$$

Table 6.6 Power variation for each block size.

Block Size	20×20	50×50	100×100	200×200	250×250	500×500
Power Variation (dB)	0.1729	0.4290	0.8476	1.6557	2.0461	3.8764

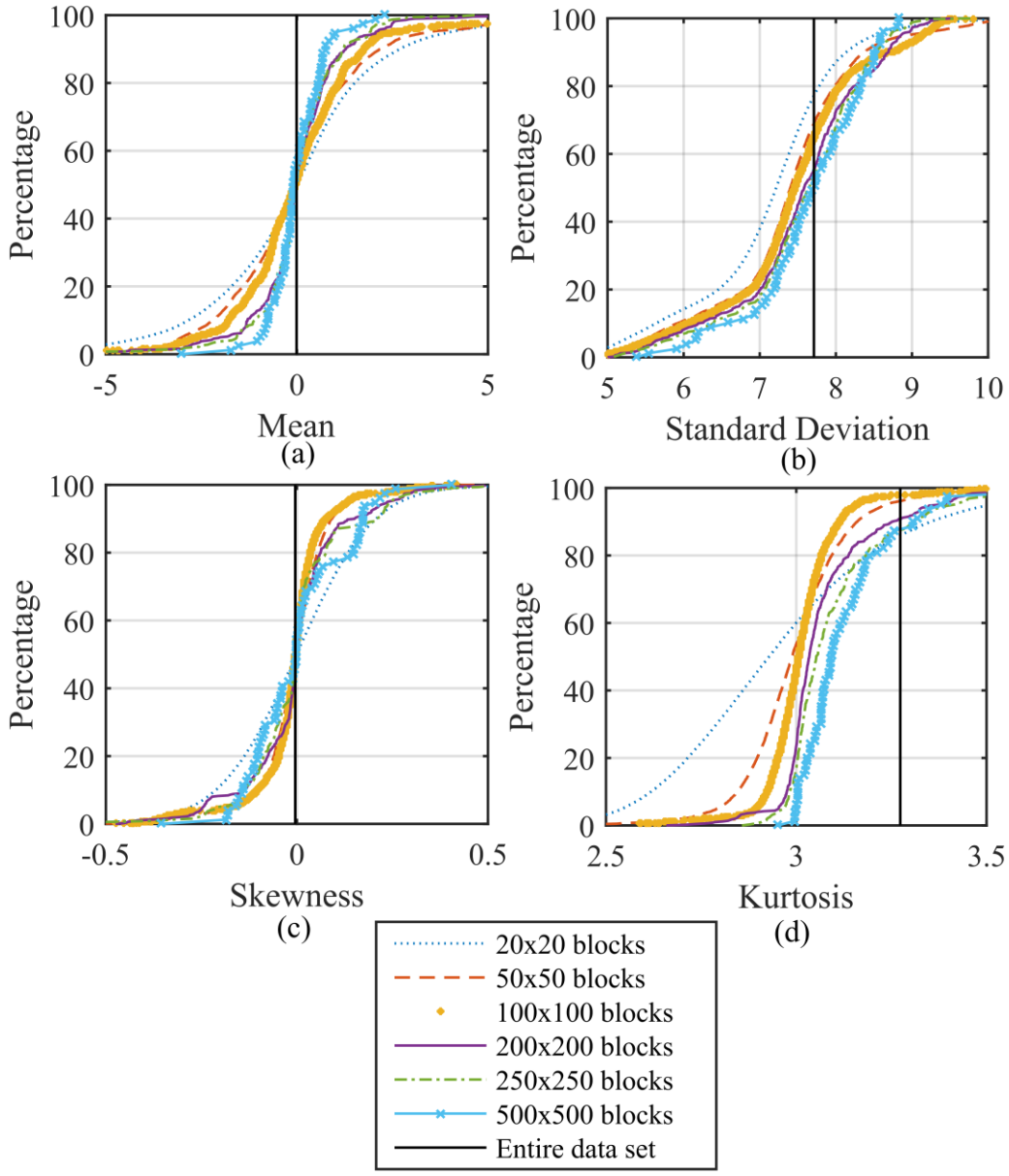

Figure 6.8 Statistical parameters measured for different block sizes. (a) Mean. (b) Standard deviation. (c) Skewness. (d) Kurtosis.

Compression bit rates of 2 bits/sample and 3 bits/sample were selected for this research, since most of the literature use these bit rates for comparison. 2 bits/sample is also the best achievable compression bit rate for the standard BAQ method. This means the quantiser outputs the chosen number of bits per I and Q sample. The BAQ algorithm will serve as the

baseline for comparison of the performance of the variants of the BAQ algorithm used in this study, namely the FFT-BAQ and the FDBAQ. Table 6.7 is an extract of the threshold and reconstruction values provided by Max [86], and shows the required values for this study. Note that the reconstruction values differ slightly from the output values given in [86], since these values are for an ideal uniform quantiser. According to the additive quantisation noise model (AQNM), a quantiser can be approximated by a linear gain with additive white noise [126]. Therefore, due to saturation effects, the uniform quantiser has an effective gain equal to 1 minus the coding error (found in [86]), resulting in the reconstruction values below.

Table 6.7 Parameters for an optimum 2-bit and 3-bit quantiser with $\sigma \neq 1$ [86].

Levels = 4		**Bits = 2**
Threshold Value	**Encoded Value**	**Reconstruction Value**
0	00	0.5131σ
± 0.9816σ	01	1.7110σ
	10	-0.5131σ
	11	-1.7110σ
Levels = 8		**Bits = 3**
Threshold Value	**Encoded Value**	**Reconstruction Value**
0	000	0.2539σ
± 0.5006σ	001	0.7830σ
± 1.050σ	010	1.3921σ
± 1.748σ	011	2.2290σ
	100	-0.2539σ
	101	-0.7830σ
	110	-1.3921σ
	111	-2.2290σ

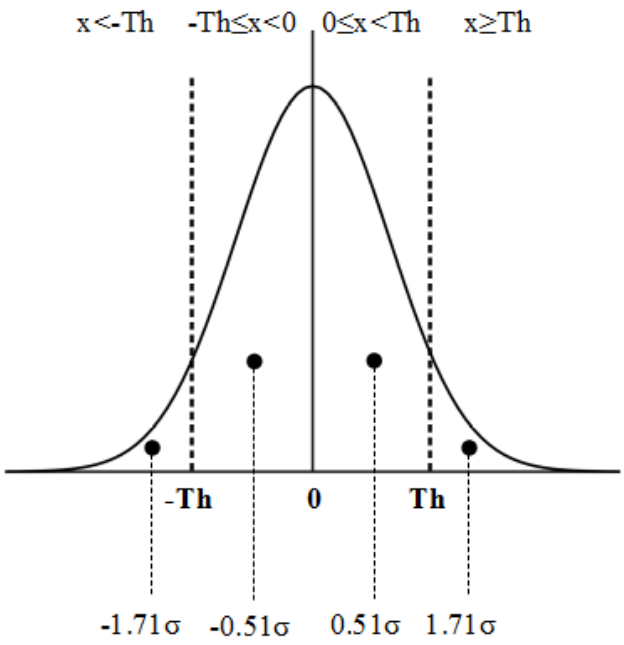

Figure 6.9 Illustration of BAQ thresholds and reconstruction values for the 2-bit quantisation case. Adapted from [65], with permission.

Figure 6.9 illustrates the operation of the BAQ algorithm and shows how the threshold values and reconstruction values for $N = 4$ levels are determined [65], [86]. The BAQ algorithm will now be further discussed by explaining the compression and decompression steps separately.

6.3.1.1 Compression

The compression steps of the BAQ algorithm [31], as implemented in this study, are summarised below. The process is also illustrated in Figure 6.10.

1. Split the raw, complex data into I and Q components.
2. Divide the I and Q components into 200 × 200 blocks.
3. Compute the standard deviation (σ) of the block (perform for each block).
4. Encode each sample in the block (perform for each block).

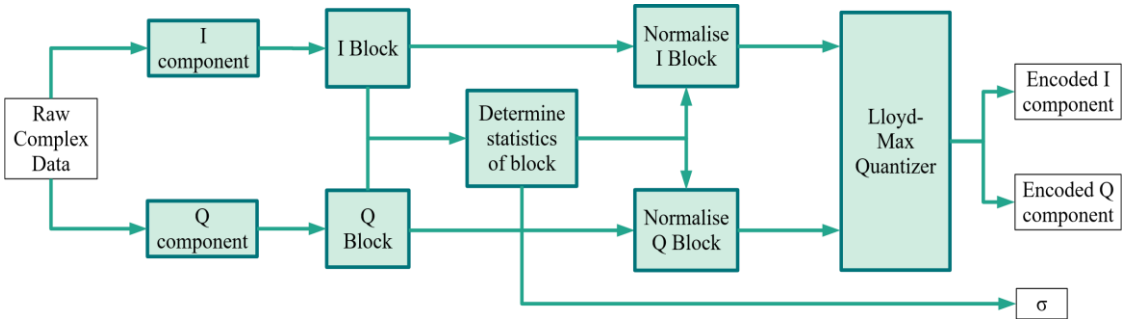

Figure 6.10 Flow diagram of the compression steps of the standard BAQ. Adapted from [83], © 1995 IEEE.

It should be noted that the standard Cartesian format of the BAQ algorithm is used in this study, since the I and Q channels are encoded independently. In some implementations of the BAQ, the statistics of the previous block are used for the encoding of the block, instead of the statistics of the current block [62], [90]. However, in this study the statistics of the current block are used.

For each sample within a block, a sign bit and a magnitude bit(s) are assigned, according to Table 6.7 and Figure 6.9 [60]. The sign bit indicates whether the sample value is positive or negative, while the magnitude bit(s) indicates whether the sample value is above or below the threshold. It is important to note that the BAQ algorithm has an overhead that is transmitted with the encoded data, required for the decompression process [31], [34], [60]. The overhead of the BAQ algorithm consists only of the σ of each block. The added bits per sample (*bps*), due to the overhead, were computed using Equation (6.2), where σ is of type double and thus 64 bits in size (for a conservative case).

$$added\ bps = \frac{\sigma_{bit\ size}}{block\ size} \tag{6.2}$$
$$= \frac{64}{200\times200}$$
$$= 1.6\times10^{-3}$$

This result shows that the added *bps* is insignificant for the specific data set size and block size used in this study.

6.3.1.2 Decompression

To reconstruct the encoded data [60], [65], the reconstruction values in Table 6.7 are used as well as the transmitted standard deviation of each block, included in the overhead data. The reconstruction values represent the centroids of each region (see Figure 6.9) [86]. Output values are assigned according to the threshold interval they are contained in. By using these optimal thresholds and reconstruction values, the mean square error in the reconstructed signal is minimised, leading to optimal quantization of the recovered SAR data.

6.3.1.3 Computational complexity

Although certain conclusions can be made about what algorithm would be best for a certain application based on the metrics, another factor is the computational complexity. An algorithm may perform very well in terms of reduction rate and also cause the least degradation of the final SAR product, but being an order of magnitude more complex than another method may be the one reason the algorithm is not feasible to implement in a SAR. Therefore, the computational complexity of each algorithm was investigated and compared. Big O notation was used to describe the complexity of the compression steps of each algorithm in a simplified manner. Only the complexity of the compression operations was considered since the encoding will take place on board the SAR platform where SWAP limitations apply, while the decoding operations will be performed at the ground station.

Table 6.8 Complexity of each step in the compression process of the BAQ algorithm.

Compression Steps	**Complexity**
1. Split data into I & Q components	O(1)
2. Break data into [200×200] blocks	O(1)
3. Calculate the σ of each bock	O($4N$ + 3)
4. Encode the data	O(N)

The complexity of the compression part of the BAQ method was computed as below,

$$O(\text{BAQ}) = O(1+1+4N+3+N) \quad (6.3)$$

$$= O(5N+5) \quad (6.4)$$

$$\approx O(5N) \quad (6.5)$$
$$\approx O(N) \quad (6.6)$$

where N is the number of elements in the data set.

Therefore, the computational complexity of the BAQ method is a linear function of the number of elements in the data set, which relates to the volume of data.

6.3.2 FFT-BAQ algorithm

The FFT-BAQ algorithm consists of transforming the data from the time domain to the frequency domain, and then applying the standard BAQ to reduce the data rate [83]. By transforming the data, the correlation present in the transform domain can now be exploited [127]. Raw SAR data are frequency modulated in the range direction due to the modulation present in the transmitted pulse, while in the azimuth direction, the data are frequency modulated due to the natural movement of the platform, known as the Doppler effect [83]. Since raw SAR data are frequency modulated in both directions, the transformed coefficients show energy compaction. Therefore, performing the data reduction in the frequency domain allows the encoding to be adapted to the energy levels in the transform domain, since the average envelope of the transformed data is known after the transformation. This means that regions with higher energy levels are quantised with more bits, while for example, the region that falls outside the processed bandwidth is omitted. This means that the FFT-BAQ automatically performs digital filtering of oversampled data [99], [127]. Note that it was assumed that the processed bandwidth corresponds with 85 % of the full signal bandwidth [83]. Therefore, a code scheme is established after investigating the envelope in the transform domain.

Although the standard BAQ is applied in the time domain, it can also be applied in the transform domain given that the transformed data are also Gaussian distributed [83]. As discussed in Section 2.5 and Section 6.2, raw SAR data can be assumed to follow a Gaussian distribution. One of the known properties of a Gaussian random process is that the response

of a linear system to a Gaussian random process, is also a Gaussian random process [114]. Therefore, after applying the 2D-FFT, the BAQ can be applied to the transformed data, since the Fourier transform is a linear operation. The FFT-BAQ algorithm will now be further discussed by explaining the compression and decompression steps separately.

6.3.2.1 Compression

The compression steps of the FFT-BAQ algorithm [83], [99], as implemented in this study, are summarised below. The process is also illustrated in Figure 6.11.

1. Split the raw, complex data into I and Q components.

BAQ Stage 1

2. Divide the I and Q components into 200 × 200 blocks.
3. Compute the standard deviation (σ_1) of the block. (perform for each block)
4. Normalise each sample in the block by the σ_1 of the block. (perform for each block)

Transform

5. Divide the normalised, complex data into 1024 × 1024 blocks.
6. Perform a 2D-FFT on every block of complex data.

BAQ Stage 2

7. Split the complex, transformed data into I and Q components.
8. Divide the I and Q components into 200 × 200 blocks.
9. Compute the standard deviation (σ_2) of the block. (perform for each block)
10. Encode each sample in the block according to the established code scheme. (perform for each block)

It is important to note that the FFT-BAQ implementation for this research consists of two BAQ stages [83]. The first BAQ stage serves as a normaliser, without reducing the bit rate of the data, and is executed in the time domain. The data are normalised to decrease the dynamic range of the power of the signal. Also note that maximum precision should be used to prevent digitisation loss during the computation of the FFT. The same block size as that of the standard BAQ algorithm, 200 × 200, was also used for the two BAQ stages in this algorithm.

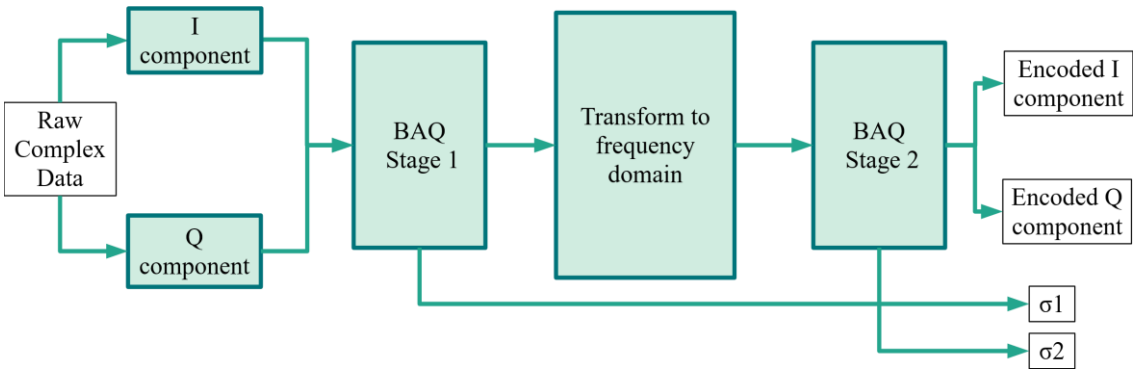

Figure 6.11 Flow diagram of the compression steps of the FFT-BAQ. Adapted from [83], © 1995 IEEE.

For the transformation stage, as seen in Figure 6.11, large blocks need to be used. A block size of 1024 × 1024 is the norm for practical cases [83], and was therefore also used in this implementation of the FFT-BAQ algorithm. In this stage of the algorithm, the data are transformed from the time domain to the transform domain. This can be achieved using the FFT, discrete cosine transform (DCT), or the Walsh-Hadamard transform (WHT) [83]. In this implementation a 2D-FFT was used to transform the data to the frequency domain.

The final stage in the compression process is the stage 2 BAQ. At this stage, quantisation of the transformed data is performed adaptively, according to the code scheme. This means that a variable rate BAQ is used. In contrast with the standard BAQ, the stage 2 BAQ is applied in the transform domain.

The code scheme used in this implementation of the FFT-BAQ algorithm is shown in Figure 6.13 and was adapted from the code scheme in [83]. The code scheme is applied to the I and Q components in the transform domain. The assumption that the processed bandwidth in both the azimuth and range directions is 85 % is assumed to be valid in this study, since it is true for most practical SAR systems [83]. A processed bandwidth of 85 % means that the

data rate is reduced by 15 % without any degradation of the image quality. The spectrums of the data sets used in this study were investigated to determine the energy variation present in the transform domain.

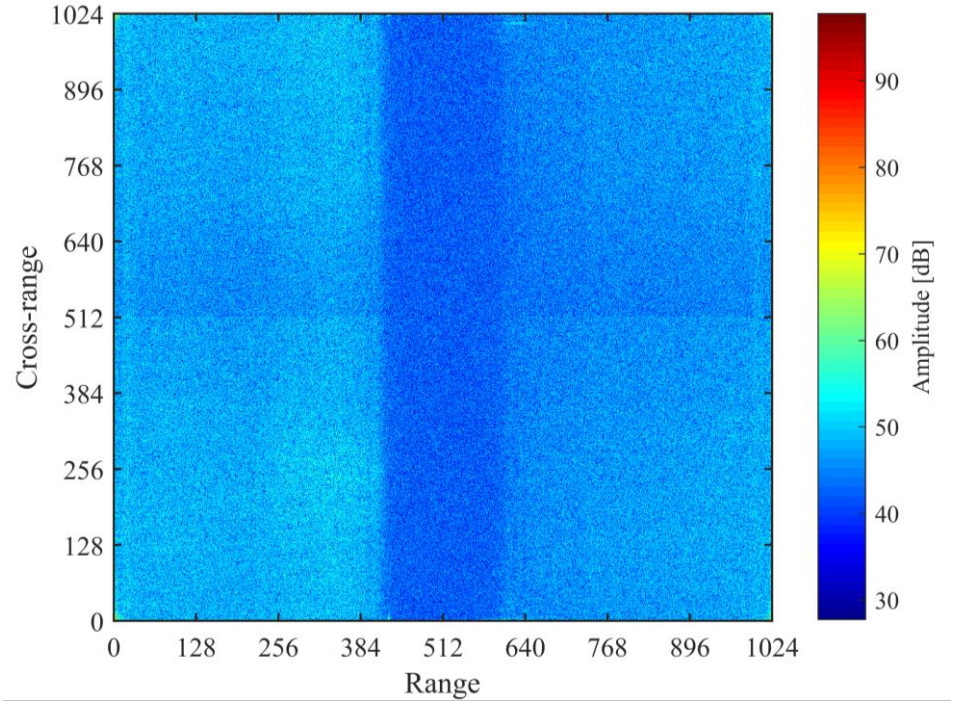

Figure 6.12 Average spectrum (over all blocks) of the farm scene.

The spectrums of the data sets are shown in Figure 6.12, Figure 6.13, and Figure 6.14, respectively, as an example of the energy levels in the frequency domain after the 2D FFT was performed. In the range direction, the energy levels vary, and therefore, different regions are encoded with different number of bits [83].

- The values in the frequency regions with little energy are set to zero and corresponds to the allowable 15 % in both range and azimuth directions.
- The values in the frequency regions that contain the highest energy levels, are quantised with (b+1) bits.
- The values in the frequency regions that contain lower energy levels, are quantised with b bits.

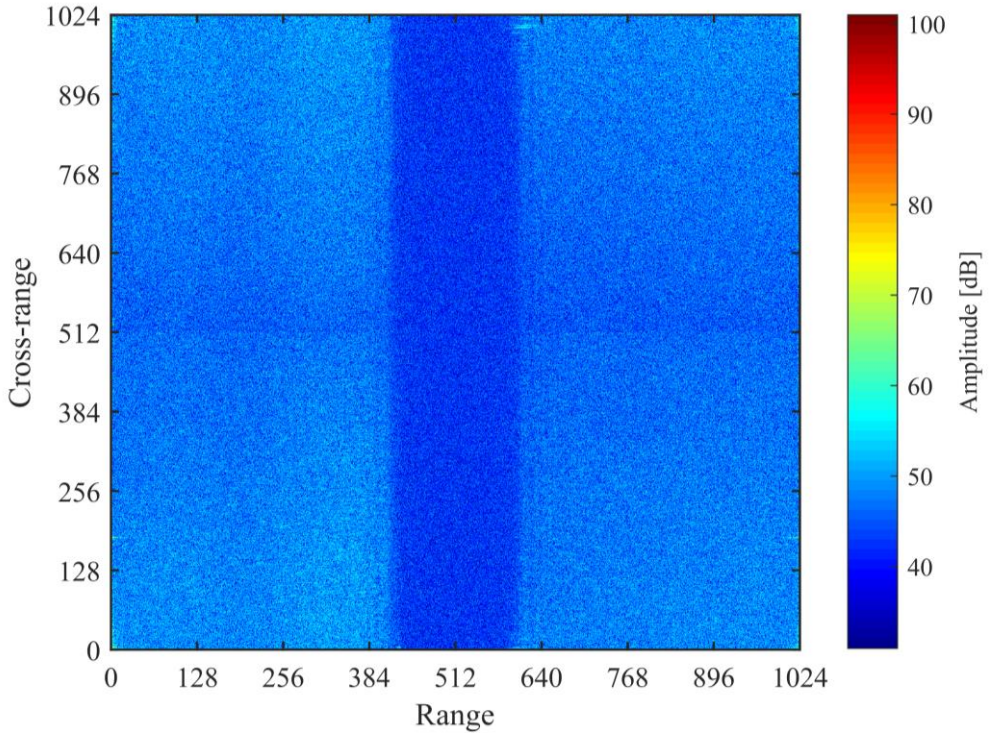

Figure 6.13 Average spectrum (over all blocks) of the mine scene.

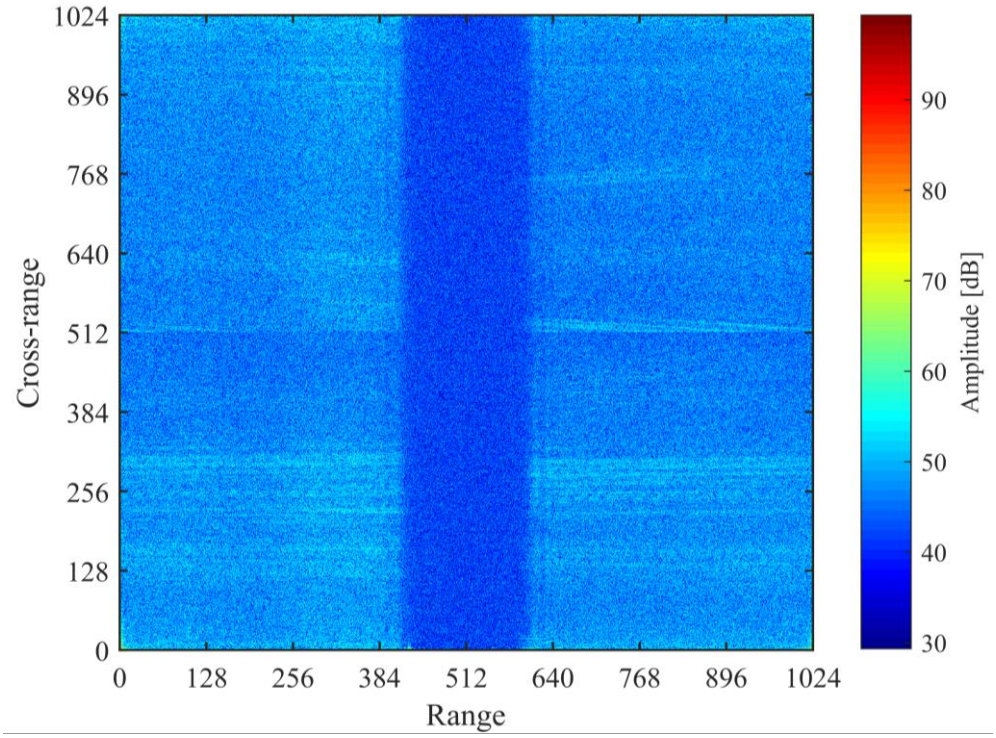

Figure 6.14 Average spectrum (over all blocks) of the peri-urban scene.

The transition value [83] between the regions encoded with *(b+1)* bits and *b* bits, $transition_R$, is calculated as

$$transition_R = \frac{b_{mean} - b \times percent_{AZ} \times percent_R}{percent_R}, \tag{6.7}$$

where b_{mean} is the average encoding bit rate and $percent_{AZ} = percent_R = 0.85$, as previously explained. Also note the following conditions that must be met [83]:

$$b+1 > b_{mean},$$

$$0 \leq transition_R \leq percent_R.$$

Thus, for the 2-bit compression case, b_{mean} was set equal to 2 and different values of *b* were used in Equation (6.7) to find a transition value and *b* value that meet both of the conditions. It was found that $b = 2$ bits and $transition_R = 65$ % met both conditions.

It is important to note that the FFT-BAQ algorithm has an overhead that is transmitted with the encoded data, required for the decompression process [83]. The overhead of the FFT-BAQ algorithm consists of σ_1 and σ_2 of each block. The added bits per sample (*bps*), due to the overhead, were computed using Equation (6.8) where σ_1 and σ_2 are of type double and thus 64 bits in size.

$$\begin{aligned} added\ bps &= \frac{\sigma_{1\_bit\ size} + \sigma_{2\_bit\ size}}{block\ size} \\ &= \frac{64+64}{200 \times 200} \\ &= 3.2 \times 10^{-3} \end{aligned} \tag{6.8}$$

This result shows that the added bps is insignificant for the specific size of the data set and block size used in this study, but compared to the BAQ result, the bps is greater.

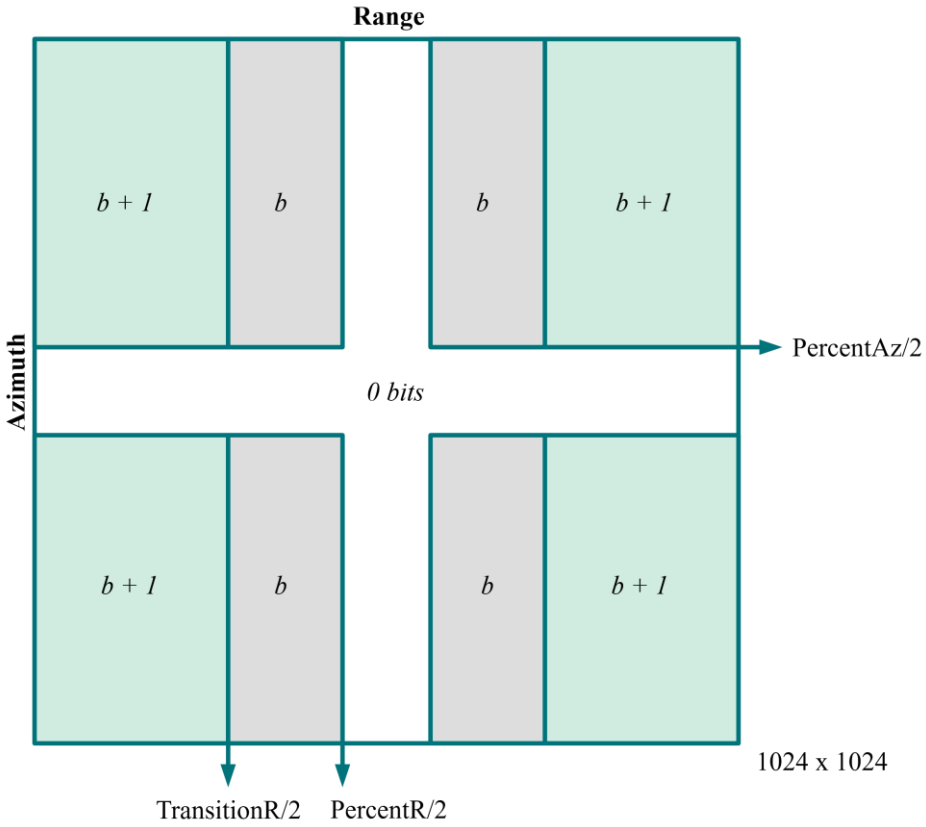

Figure 6.15 Code scheme used for the FFT-BAQ algorithm. Adapted from [83], © 1995 IEEE.

6.3.2.2 Decompression

The encoded data set is reconstructed by executing the inverse of the encoding steps. Firstly, BAQ decompression is executed using the standard deviation of the stage 2 BAQ in the compression process, σ_2. The second step is to perform a two-dimensional inverse FFT with the same block size, 1024×1024, used during the compression. Lastly, BAQ denormalisation is executed using the standard deviation computed in the first BAQ stage of the compression process, σ_1. Since the compression ratio of the first BAQ stage was 1, this decompression step only entails multiplying or descaling by σ_1.

6.3.2.3 Computational complexity

Table 6.9 Complexity of each step in the compression process of the FFT-BAQ algorithm.

Compression Steps	Complexity
1. Split data into I & Q components	O(1)
2. Break data into [200×200] blocks	O(1)
3. Calculate the σ_1 of each bock	O($4N$ + 3)
4. Normalise the data by σ_1	O(N)
5. Break data into [1024×1024] blocks	O(1)
6. Perform 2D FFT on each block	O(K (LM log(LM))
7. Break data into [200×200] blocks	O(1)
8. Calculate the σ_2 of each bock	O($4N$ + 3)
9. Encode the data	O(N)

The complexity of the compression part of the FFT-BAQ method was computed as below,

$$\begin{aligned} \mathrm{O}(\text{FFT-BAQ}) &= \mathrm{O}(10N+10+K(LM\log LM)) && (6.9)\\ &\approx \mathrm{O}(N+K(LM\log LM)) && (6.10)\\ &\approx \mathrm{O}\left(N+\frac{N}{LM}(LM\log LM)\right) && (6.11)\\ &\approx \mathrm{O}(N+N\log LM) && (6.12)\\ &\approx \mathrm{O}(N+N\log\tfrac{N}{K}) && (6.13)\\ &\approx \mathrm{O}(N+N\log N) && (6.14) \end{aligned}$$

where N is the number of elements in the data set, M is the number of rows in each FFT block, L is the number of columns in each FFT block and K is the number of blocks to perform the 2D FFT on, thus $K=\frac{N}{LM}$.

Therefore, it can be seen that the computational complexity of the FFT-BAQ method is a logarithmic function of the number of elements in the data set, which relates to the volume of data.

6.3.3 FDBAQ algorithm

FDBAQ is the latest variation of the standard BAQ algorithm, currently implemented on the Sentinel-1 platform [21], [93]. The FDBAQ adaptively changes the encoding bit rate according to the local SNR, and therefore exploits the dynamic range of the received signal.

This algorithm addresses the limitation of the poor response that weaker targets have in the presence of stronger targets, that other compression algorithms face. This limitation is addressed by encoding the bright scatterers with an increased number of bits. FDBAQ also allows encoding with non-integer rates, which in turn allows the information throughput to be optimised for different types of scenes and downlink scenarios by considering the trade-off between thermal and quantization noise. This compression algorithm allows for a multi-mode measurement system, each mode with different output data rates and quality requirements [5].

The FDBAQ algorithm will now be further discussed by explaining the compression and decompression steps separately.

6.3.3.1 Compression

The compression steps of the FDBAQ algorithm [21], as implemented in this study, are summarised below. The process is also illustrated in Figure 6.16.

1. Split the raw, complex data into I and Q components.
2. Divide the I and Q components into 200 × 200 blocks.
3. Compute the standard deviation (σ) of the block, as well as the noise power $\hat{\sigma}_T^{\,2}$, and the signal power $\hat{\sigma}_{cr}^{\,2}$ (perform for each block).
4. Select the encoding bit rate, R (or number of output levels, L) based on the SNR threshold value (perform for each block).
5. Encode each sample in the block using the selected bit rate (perform for each block).

The initial steps of the FDBAQ algorithm are similar to that of the standard BAQ, where the I and Q components are divided into blocks of size 200 × 200. Thereafter, the statistics of each block, required for this algorithm, are estimated. These statistics include the standard deviation, signal power, $\hat{\sigma}_{cr}^{\,2}$, and noise power, $\hat{\sigma}_T^{\,2}$, of the block. Note that the noise power is a characteristic of the system's receiver and is generally known. In this study, however, the noise power had to be estimated due to a lack of information about the prototype SAR

system. The noise power was assumed to only be due to thermal noise and was thus computed from/using the minimum variance of the block. The signal power was computed as the difference between the variance of the block and the minimum variance of the block. The SNR was estimated using the equation [21],

$$SNR = \frac{1}{\frac{\hat{\sigma}_T^{\,2}}{\hat{\sigma}_{cr}^{\,2}}\left(1+\frac{1}{SQNR}\right)+\frac{1}{SQNR}}, \tag{6.15}$$

where the signal-to-quantisation noise ratio (SQNR) is provided by the quantiser. To get the SQNR, the error value corresponding with the number of output levels, L, is extracted from Table I in [86]. In this study L was restricted to $(n_{levels}\text{-}1) \leq L \leq (n_{levels}\text{+}1)$, where n_{levels} is the number of output levels for the average encoding bit rate (R_{mean}), for example $n_{levels} = 4$ for $R_{mean} = 2$ bits. The outcome of Equation (6.15) is that when the signal power, $\hat{\sigma}_{cr}^{\,2}$, is small compared to the thermal noise, $\hat{\sigma}_T^{\,2}$, good quantisation is not required and therefore less bits can be used, while when the signal power reaches higher levels, more bits can be used to quantise the data with a smaller error and better retain the values [21].

The FDBAQ selects the number of output levels, L, for the block based on an estimation of the local signal-to-thermal-noise ratio of the block of data being compressed [5]. The block *SNR* was estimated using the lowest output level, as well as for one level higher, and then the two estimates were subtracted. The result was then compared to an SNR threshold. If the estimated SNR improvement that would be achieved by adding another output level exceeded the SNR threshold, the higher L value was used as the number of output levels of the BAQ applied to that block. If the threshold was not exceeded, the lower L value was used as the number of output levels. The SNR threshold was chosen to ensure that the required average encoding bit rate was achieved.

It is important to note that the FDBAQ algorithm has an overhead that is transmitted with the encoded data required for the decompression process. The overhead of the FDBAQ algorithm consists of the σ and L of each block. The added bits per sample (*bps*), due to the overhead of this method, were computed using Equation (6.16). σ is of type double and thus 64 bits in size, for the conservative case, while L only requires 2 bits of storage since L can only be one of three values in this study.

$$\begin{aligned} added\ bps &= \frac{\sigma_{bit\ size}+L_{bit\ size}}{block\ size} \\ &= \frac{64+2}{200\times200} \\ &= 1.65\times10^{-3} \end{aligned} \tag{6.16}$$

This result shows that the added *bps* is insignificant for the data set size and block size used in this study, but compared to the bps for the BAQ method, the bps is slightly greater.

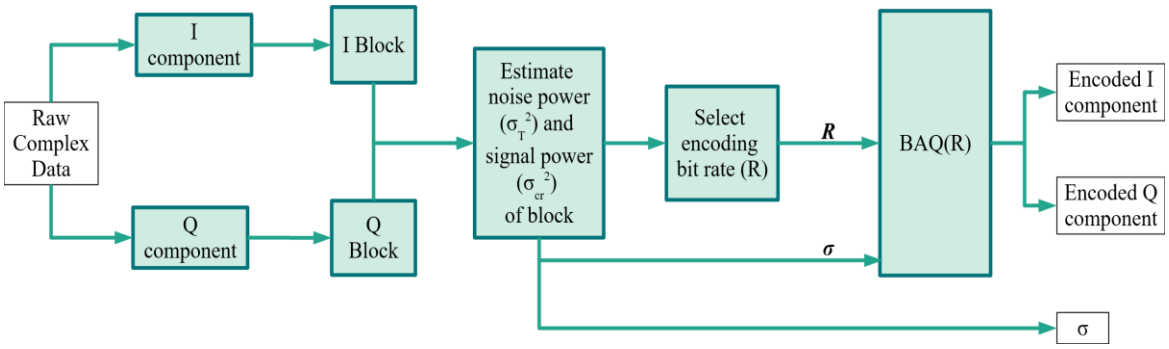

Figure 6.16 Flow diagram of the compression steps of the FDBAQ. Adapted from [21], © 2010 IEEE.

6.3.3.2 Decompression

To reconstruct the encoded data, the decompression steps of the BAQ algorithm are applied. The only difference is that the corresponding number of output levels, L, for the block, first needs to be extracted from the overhead data, since a varying encoding bit rate is a

characteristic of the FDBAQ operation. Thereafter, the relevant reconstruction values [86], adjusted by the effective gain, are used to decompress the data.

6.3.3.3 Computational complexity

Table 6.10 Complexity of each step in the compression process of the FDBAQ algorithm.

Compression Steps	**Complexity**
1. Split data into I & Q components	O(1)
2. Break data into [200×200] blocks	O(1)
3. Calculate the signal power and noise power of each bock	O($4N$ + 3)
4. Select bit rate for encoding	O(P)
5. Encode the data	O(N)

The complexity of the compression part of the FDBAQ method was computed as below,

$$\begin{aligned} \mathrm{O(FDBAQ)} &= \mathrm{O}(1+1+4N+3+P+N) && (6.17)\\ &= \mathrm{O}(5N+P+5) && (6.18)\\ &\approx \mathrm{O}(5N) && (6.19)\\ &\approx \mathrm{O}(N), && (6.20) \end{aligned}$$

where N is the number of elements in the data set and P is the number of blocks that the data set is split into.

Therefore, the computational complexity of the FDBAQ method is also a linear function of the number of elements in the data set, which relates to the volume of data.

6.4 CHAPTER SUMMARY

Firstly, the statistical characteristics of the three data sets used in this study were investigated. This was done to ensure that the assumptions made in literature are also valid in this study. It was found that the normal distribution is not the best fit for the data, but the data do closely follow the normal distribution. Therefore, the raw I and Q components can be assumed to be zero-mean Gaussian distributions. In turn this means the BAQ is a suitable

choice for a compression algorithm since this algorithm exploits the Gaussian statistics of the data.

The three SAR compression algorithms, identified as suitable solutions for implementation on board resource constrained SAR platforms, the BAQ, the FFT-BAQ, and the FDBAQ, were discussed in terms of the compression and decompression steps. The computational complexity of each algorithm was also investigated. It is clear that the 2D FFT required for the FFT-BAQ algorithm greatly increases the computational complexity, confirming why this algorithm has not been implemented on board any practical SAR system to date.

CHAPTER 7 SAR OUTPUT AND EVALUATION OF METRICS

7.1 CHAPTER OVERVIEW

In a modern SAR system, the decompression and SAR processing are performed at a ground station after the compressed data have been transmitted from the platform or read from platform data storage.

In this chapter, the metrics that were presented in Chapter 5 are evaluated to compare the performance of the three chosen SAR compression algorithms. The three algorithms that were implemented to illustrate how the metrics can be applied, are the block adaptive quantiser (BAQ), fast Fourier transform BAQ (FFT-BAQ) and the flexible dynamic BAQ (FDBAQ), and were discussed in detail in Section 6.3. In the literature, these algorithms were found to be best suited for the compression of raw SAR data in a processing and cost constrained environment due to their simplicity, reliability and current uses in SAR sensor systems [5], [60], [83], [99]. Implementing these algorithms represents compression of raw SAR data in the time and frequency domains, respectively. The performance of these algorithms was evaluated by implementing the process described in Figure 4.1.

Note that the compression ratio and processing parameters were kept constant when comparing the different algorithms for the same data set. This was done to ensure that the compression algorithm was the only changing variable while all other parameters were constant. For example, the same SAR signal processor was used for all data sets, and the metrics were computed using the same equations and at the same stage of the process, with

the compression algorithms being the only varying factor. This experimental setup ensured that the results of each compression algorithm could be compared. Also note that the main evaluation was performed for 2-bit compression of the scenes. 3-Bit compression was however, also implemented for one data set (peri-urban scene), in order to also consider the effect of a higher bit rate.

As discussed in Chapter 6, three data sets were used in this study.

1. Data set 1: Rural Scene (farm).
2. Data set 2: Mine Scene.
3. Data set 3: Peri-urban Scene (Pecanwood Estate).

7.2 SAR IMAGES

In this section the scenes are introduced by Google Maps representations of the areas covered during the flight tests. The SAR images of the scenes, before and after compression, are given to compare the results of the study visually.

7.2.1 Original, uncompressed Images

7.2.1.1 Data set 1: Rural scene

Figure 7.1 Rural scene on Google Earth © 2017.

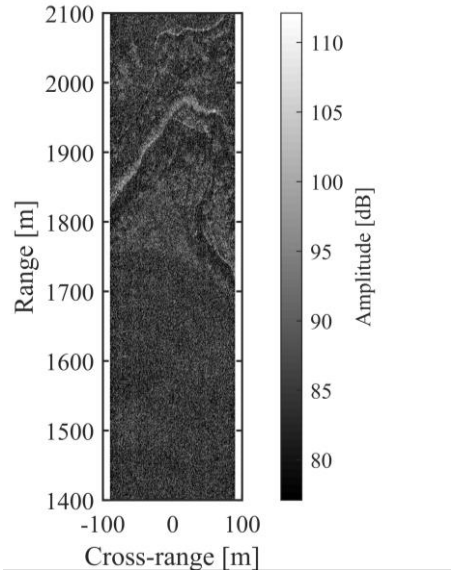

Figure 7.2 SAR image of uncompressed data (rural scene).

7.2.1.2 Data set 2: Mine scene

Figure 7.3 Mine scene on Google Earth © 2017.

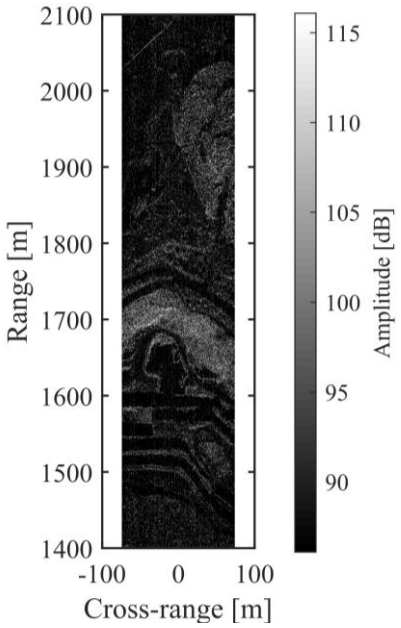

Figure 7.4 SAR image of uncompressed data (mine scene).

7.2.1.3 Data set 3: Peri-urban scene

Figure 7.5 Peri-urban scene on Google Earth © 2017.

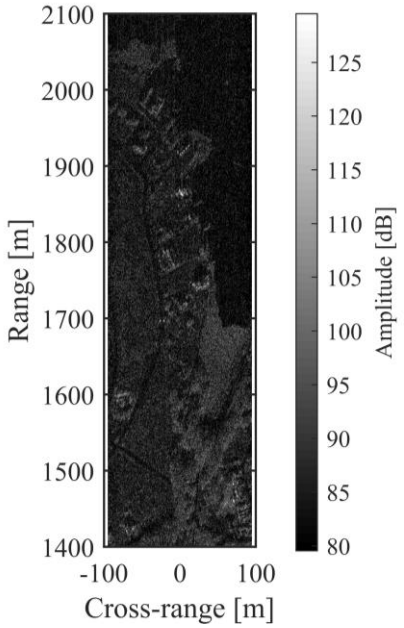

Figure 7.6 SAR image of uncompressed data (peri-urban scene).

7.2.2 2-Bit compression

7.2.2.1 Data set 1: Rural scene

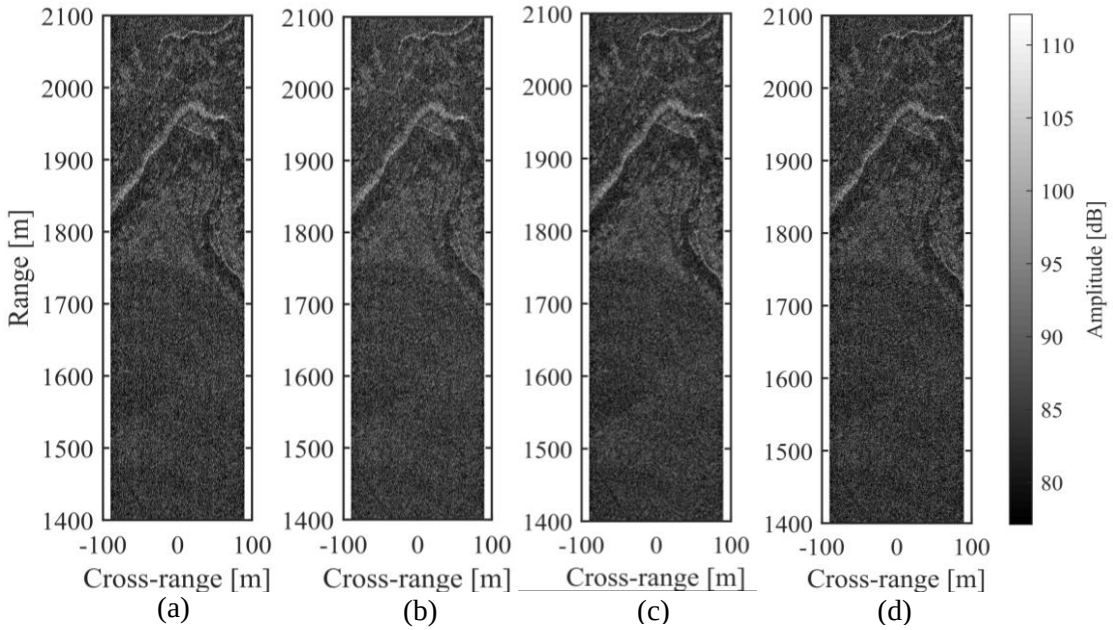

Figure 7.7 SAR Images of the rural scene. (a) Uncompressed data. (b) BAQ applied. (c) FFT-BAQ applied. (d) FDBAQ applied.

7.2.2.2 Data set 2: Mine scene

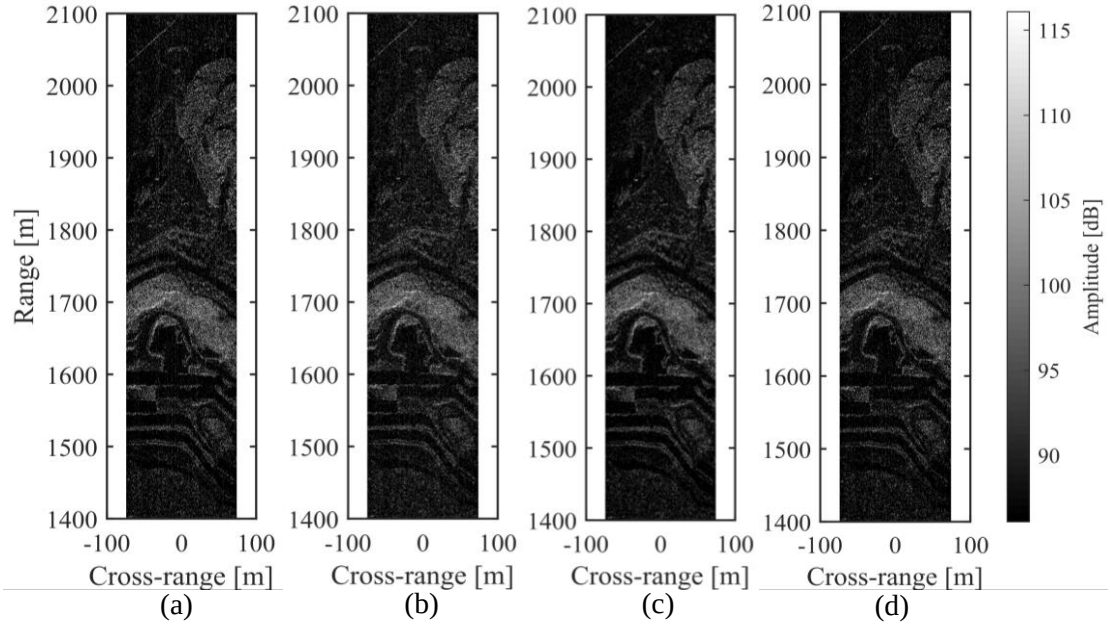

Figure 7.8 SAR Images of the mining scene. (a) Uncompressed data. (b) BAQ applied. (c) FFT-BAQ applied. (d) FDBAQ applied.

7.2.2.3 Data set 3: Peri-urban scene

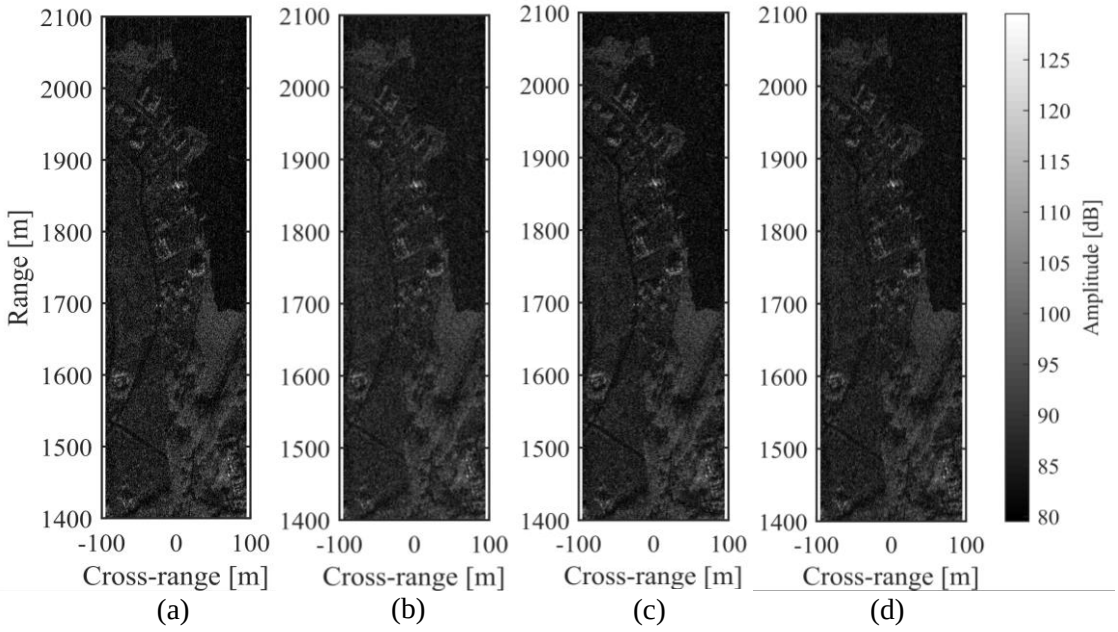

Figure 7.9 SAR Images of the peri-urban scene. (a) Uncompressed data. (b) BAQ applied. (c) FFT-BAQ applied. (d) FDBAQ applied.

7.2.3 3-Bit compression

7.2.3.1 Data set 3: Peri-urban scene

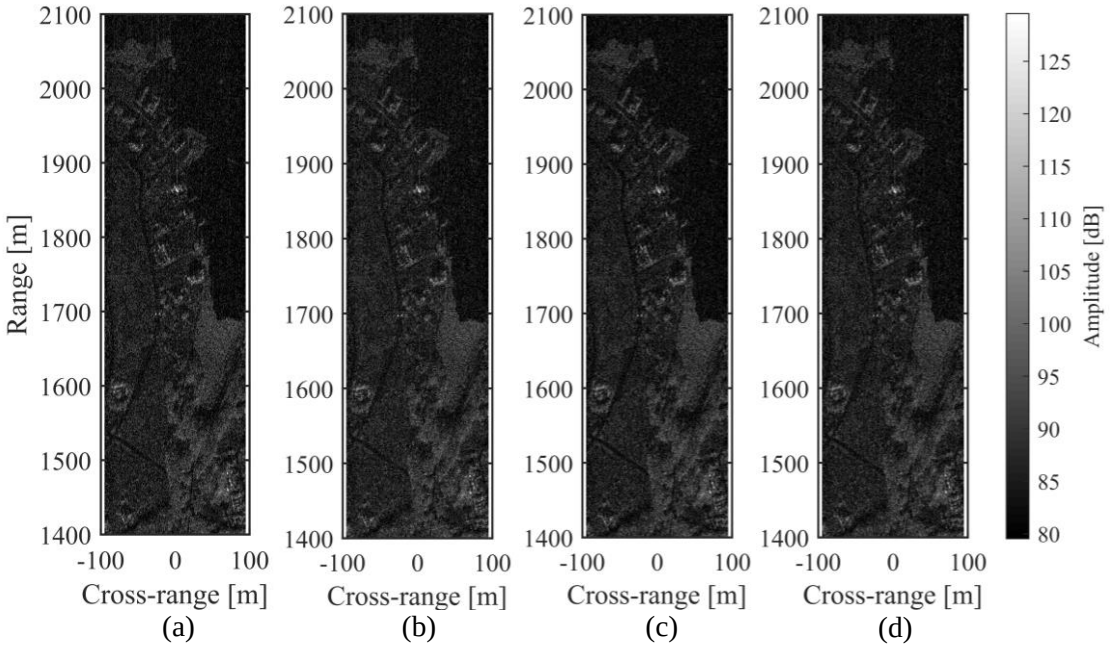

Figure 7.10 SAR Images of the peri-urban scene. (a) Uncompressed data. (b) BAQ applied. (c) FFT-BAQ applied. (d) FDBAQ applied.

7.3 EVALUATION OF DATA-DOMAIN METRICS

The metrics proposed in Section 5.2 were evaluated and the results are summarised below. All three of the compression algorithms were evaluated for all three data sets with similar tendencies being observed. Note that the data-domain metrics are evaluated after decompressing the compressed data, and before any SAR processing occurs. As mentioned in Section 6.2, the original data were discretised to 12 bit in-phase (I) and quadrature (Q) samples, respectively, before performing the compression. Therefore, the magnitude and phase components of the decompressed data were also discretised to 12 bits before computing the metrics. The rounding was performed to ensure that, before and after implementing the compression process, the same number of bits is compared to evaluate the

associated information loss or introduced distortions. It is also important to note that in practical SAR systems the computations would be executed on hardware that inherently performs fixed-point calculations. The data used in the rest of the SAR system were stored as the default MATLAB variable type, and not rounded, causing the data to have more fractional bits than the original data.

Firstly, all the results in the data domain are summarised by means of tables and figures. Thereafter, the results are discussed in detail.

7.3.1 Data set 1: Rural scene

7.3.1.1 2-Bit results

Table 7.1 Statistical parameters of the rural scene in the data domain.

Metric	**Uncompressed Value**	**Value after BAQ method**	**Value after FFT-BAQ method**	**Value after FDBAQ method**
Compression Ratio	-	6	6	6
Dynamic Range	64.82 dB	15.71 dB	67.73 dB	12.43 dB
Mean (mag)	38.19	41.59	31.02	36.04
Mean (phase)	-21.68×10^{-3}	-21.68×10^{-3}	-5.05×10^{-3}	53×10^{-3}
Standard deviation (mag)	20.87	19.24	16.8	17.34
Standard deviation (phase)	1.81	1.79	1.81	1.76
Skewness (mag)	0.82	0.23	0.72	0.02
Skewness (phase)	25.64×10^{-3}	23.38×10^{-3}	5.37×10^{-3}	32.61×10^{-3}
Kurtosis (mag)	3.88	1.66	3.45	2.10
Kurtosis (phase)	1.8	1.73	1.8	1.83
Entropy (mag)	10.33 bits	9.07 bits	10.02 bits	8.73 bits
Entropy (phase)	12.64 bits	3.42 bits	12.65 bits	3.74 bits

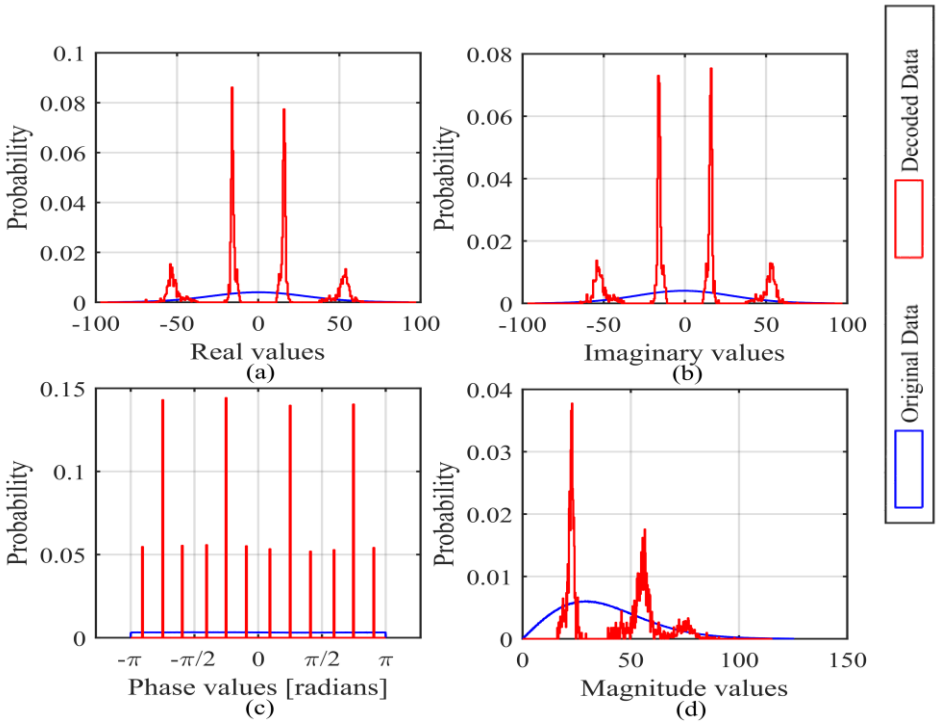

Figure 7.11 Distribution of data set 1 before and after implementing the BAQ algorithm. (a) I component. (b) Q component. (c) Phase component. (d) Amplitude component.

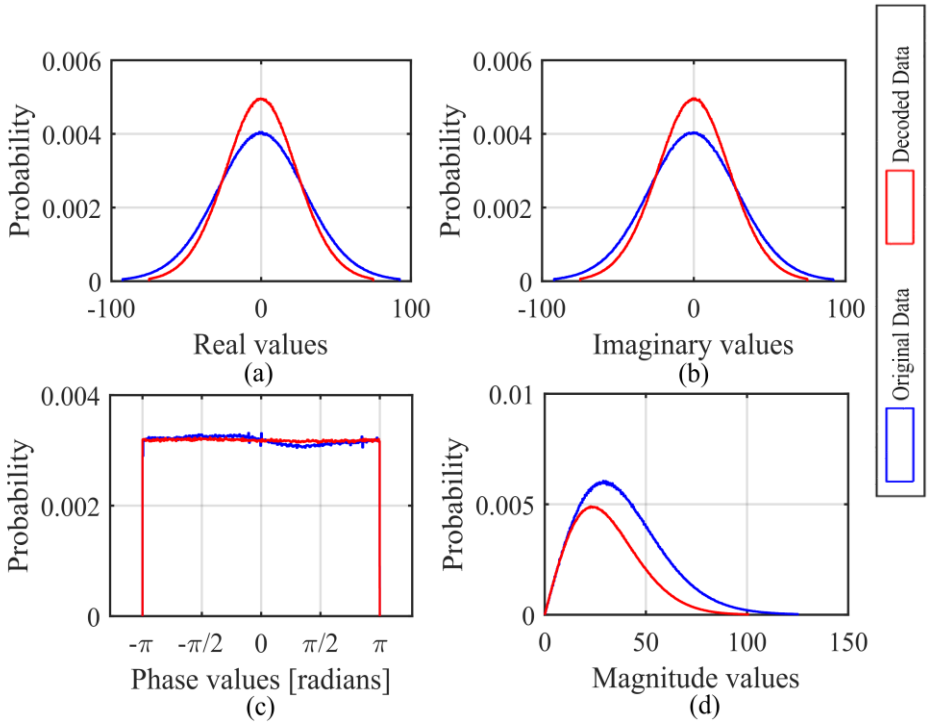

Figure 7.12 Distribution of data set 1 before and after implementing the FFT-BAQ algorithm.

(a) I component. (b) Q component. (c) Phase component. (d) Amplitude component.

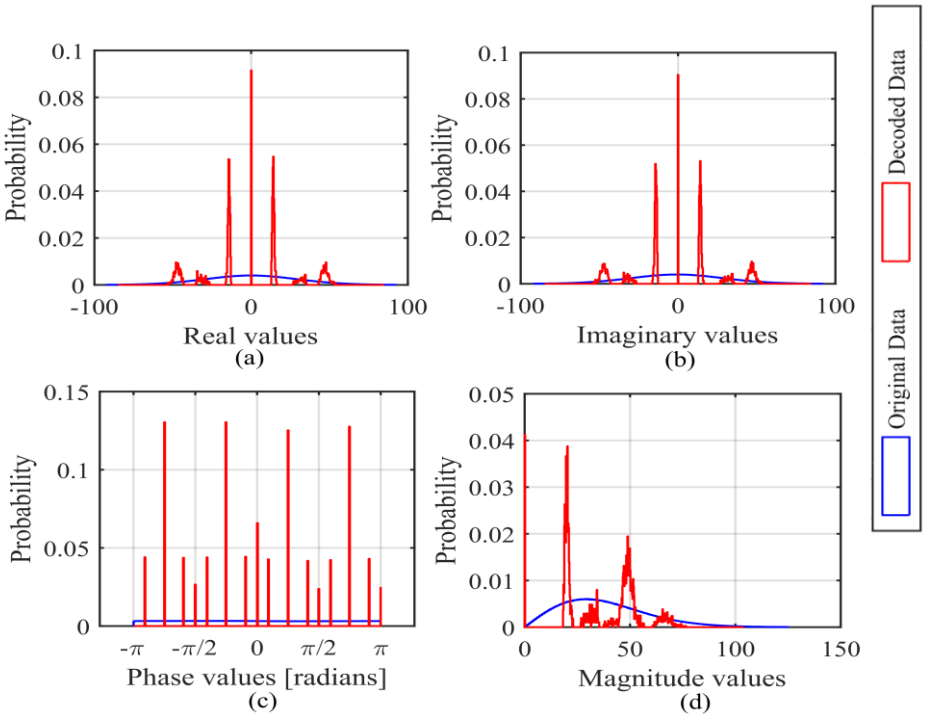

Figure 7.13 Distribution of data set 1 before and after implementing the FDBAQ algorithm. (a) I component. (b) Q component. (c) Phase component. (d) Amplitude component.

Table 7.2 Error measures for the rural scene in the data domain.

Metric	**Value after BAQ method**	**Value after FFT-BAQ method**	**Value after FDBAQ method**
MSE	163.21	329.94	168.32
SQNR	10.65 dB	7.59 dB	10.51 dB
MPE (rad)	0.2507	0.3633	0.2954
MPE (degrees)	14.36	20.82	16.93

7.3.2 Data set 2: Mine scene

7.3.2.1 2-Bit results

Table 7.3 Statistical parameters of the mine scene in the data domain.

Metric	**Uncompressed Value**	**Value after BAQ method**	**Value after FFT-BAQ method**	**Value after FDBAQ method**
Compression Ratio	-	6	6	6
Dynamic Range	67.13 dB	17 dB	70.78 dB	15.55 dB
Mean (mag)	41.18	44.88	35.14	38.41
Mean (phase)	2.2×10^{-3}	2.2×10^{-3}	877×10^{-6}	227×10^{-3}
Standard deviation (mag)	24.71	23.38	21.77	22.4
Standard deviation (phase)	1.82	1.79	1.81	1.71
Skewness (mag)	1.06	0.6	1.11	0.34
Skewness (phase)	1.2×10^{-3}	-565×10^{-6}	-619×10^{-6}	49.6×10^{-3}
Kurtosis (mag)	4.48	2.34	4.47	2.99
Kurtosis (phase)	1.79	1.72	1.8	2
Entropy (mag)	9.51 bits	9.61 bits	10.31 bits	8.93 bits
Entropy (phase)	12.64 bits	3.41 bits	12.65 bits	3.81 bits

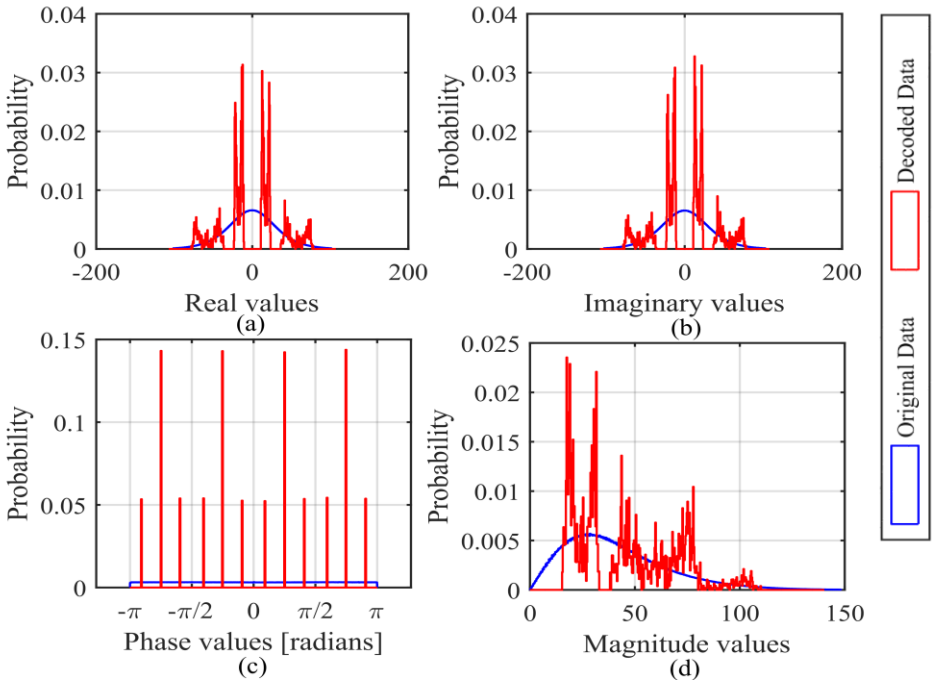

Figure 7.14 Distribution of data set 2 before and after implementing the BAQ algorithm. (a) I component. (b) Q component. (c) Phase component. (d) Amplitude component.

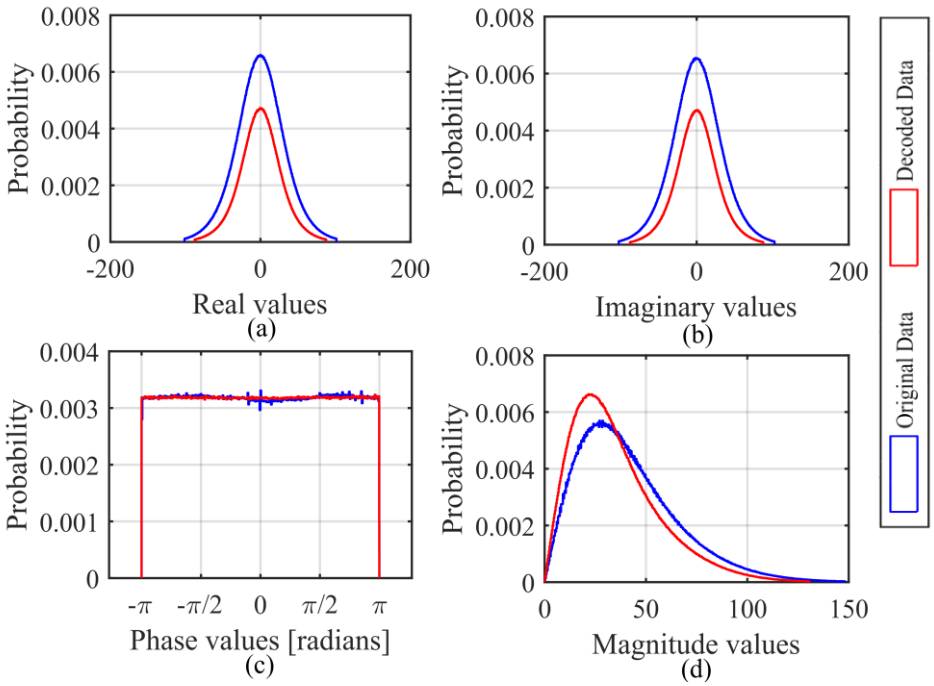

Figure 7.15 Distribution of data set 2 before and after implementing the FFT-BAQ algorithm. (a) I component. (b) Q component. (c) Phase component. (d) Amplitude component.

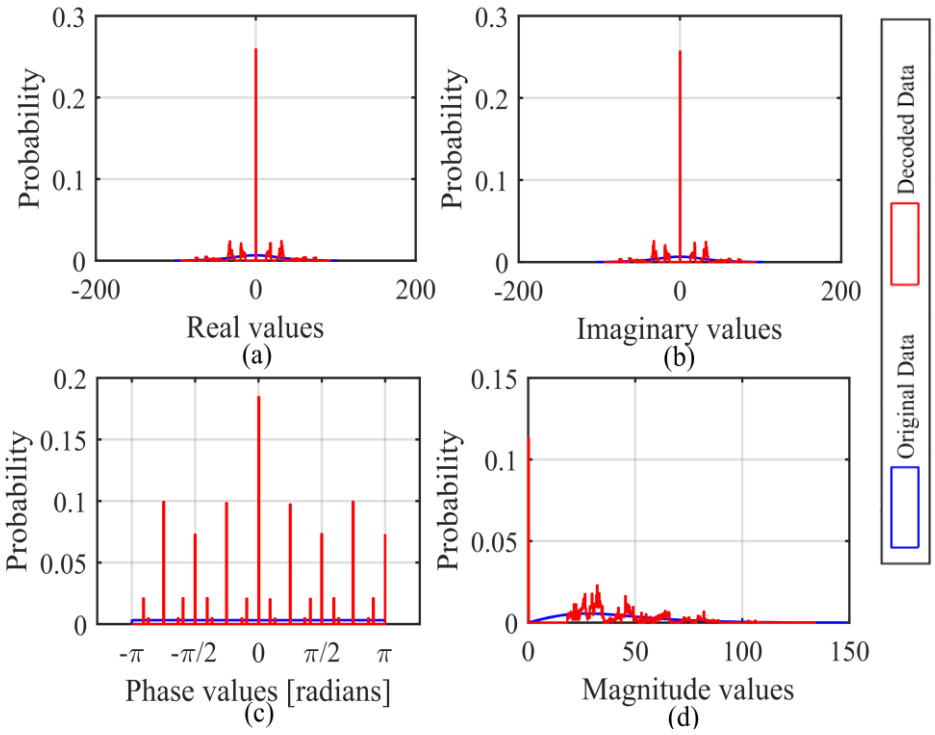

Figure 7.16 Distribution of data set 2 before and after implementing the FDBAQ algorithm. (a) I component. (b) Q component. (c) Phase component. (d) Amplitude component.

Table 7.4 Error measures for the mine scene in the data domain.

Metric	**Value after BAQ method**	**Value after FFT-BAQ method**	**Value after FDBAQ method**
MSE	201.82	328.22	203.5
SQNR	10.58 dB	8.47 dB	10.54 dB
MPE (rad)	0.2523	0.3442	0.3653
MPE (degrees)	14.46	19.72	20.93

7.3.3 Data set 3: Peri-urban scene

7.3.3.1 2-Bit results

Table 7.5 Statistical parameters of the peri-urban scene in the data domain.

Metric	**Uncompressed Value**	**Value after BAQ method**	**Value after FFT-BAQ method**	**Value after FDBAQ method**
Compression Ratio	-	6	6	6
Dynamic Range	67.83 dB	19.59 dB	67.2 dB	18.04 dB
Mean (mag)	46.11	50.06	37.49	42.81
Mean (phase)	25.2×10^{-3}	24.8×10^{-3}	3.9×10^{-3}	269.8×10^{-3}
Standard deviation (mag)	28.96	27.63	24.66	26.37
Standard deviation (phase)	1.82	1.79	1.82	1.72
Skewness (mag)	1.12	0.74	1.26	0.62
Skewness (phase)	-19.6×10^{-3}	-20.8×10^{-3}	-3.9×10^{-3}	27.4×10^{-3}
Kurtosis (mag)	4.58	2.7	4.99	3.36
Kurtosis (phase)	1.79	1.72	1.8	1.98
Entropy (mag)	9.71 bits	9.51 bits	9.44 bits	8.96 bits
Entropy (phase)	12.64 bits	3.42 bits	12.65 bits	3.88 bits

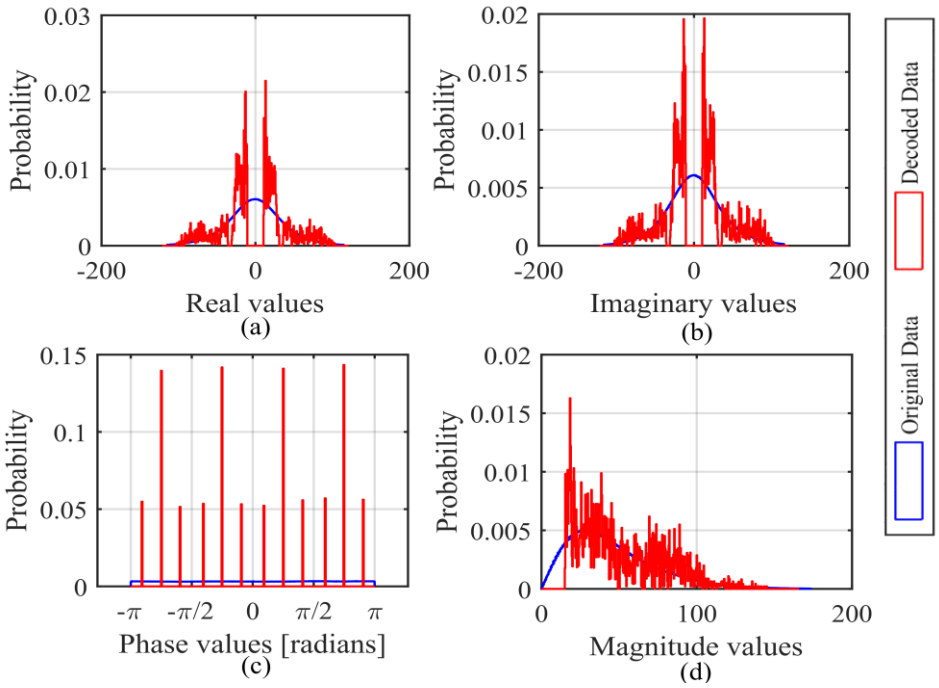

Figure 7.17 Distribution of data set 3 before and after implementing the BAQ algorithm.

(a) I component. (b) Q component. (c) Phase component. (d) Amplitude component.

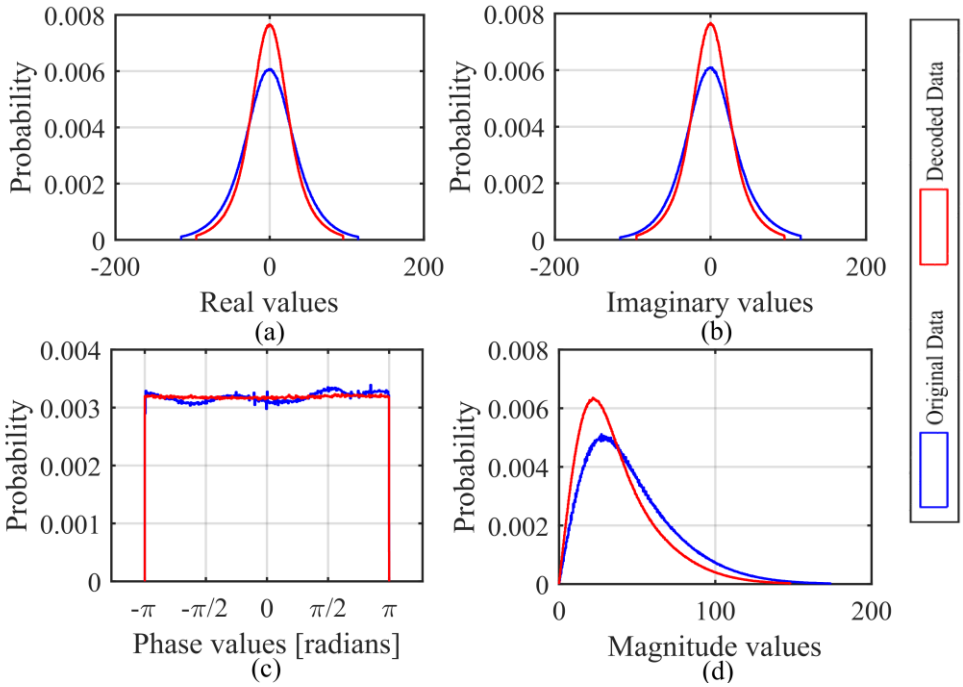

Figure 7.18 Distribution of data set 3 before and after implementing the FFT-BAQ algorithm.

(a) I component. (b) Q component. (c) Phase component. (d) Amplitude component.

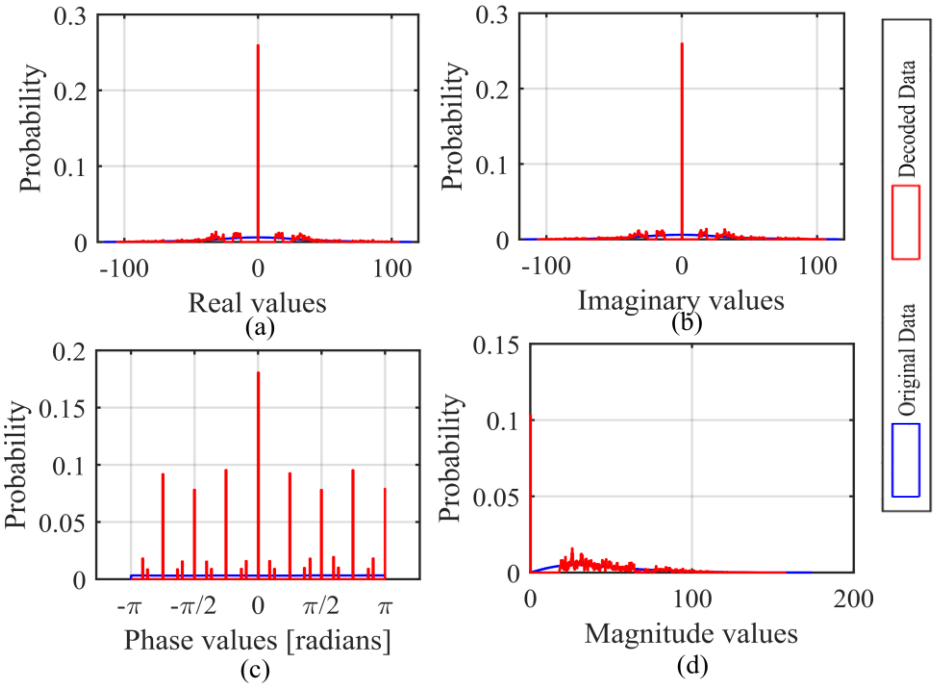

Figure 7.19 Distribution of data set 3 before and after implementing the FDBAQ algorithm. (a) I component. (b) Q component. (c) Phase component. (d) Amplitude component.

Table 7.6 Error measures for the peri-urban scene in the data domain.

Metric	**Value after BAQ method**	**Value after FFT-BAQ method**	**Value after FDBAQ method**
MSE	254.24	476.45	233.79
SQNR	10.67 dB	7.94 dB	11.03 dB
MPE (rad)	0.2502	0.3598	0.3402
MPE (degrees)	14.34	20.62	19.49

7.3.3.2 3-Bit results

Table 7.7 Statistical parameters of the peri-urban scene in the data domain.

Metric	**Uncompressed Value**	**Value after BAQ method**	**Value after FFT-BAQ method**	**Value after FDBAQ method**
Compression Ratio	-	4	4	4
Dynamic Range	67.83 dB	28.02 dB	66.66 dB	24.79 dB
Mean (mag)	46.11	47.04	37.47	45.05
Mean (phase)	25.2×10^{-3}	25×10^{-3}	5.1×10^{-3}	238.7×10^{-3}
Standard deviation (mag)	28.96	28.44	24.82	27.62
Standard deviation (phase)	1.82	1.81	1.82	1.79
Skewness (mag)	1.12	0.95	1.27	0.92
Skewness (phase)	-19.6×10^{-3}	-20.8×10^{-3}	-4.9×10^{-3}	-10.5×10^{-3}
Kurtosis (mag)	4.58	3.68	5.03	3.85
Kurtosis (phase)	1.79	1.76	1.79	1.85
Entropy (mag)	9.71 bits	10.25 bits	9.44 bits	10.07 bits
Entropy (phase)	12.64 bits	5.17 bits	12.65 bits	5.58 bits

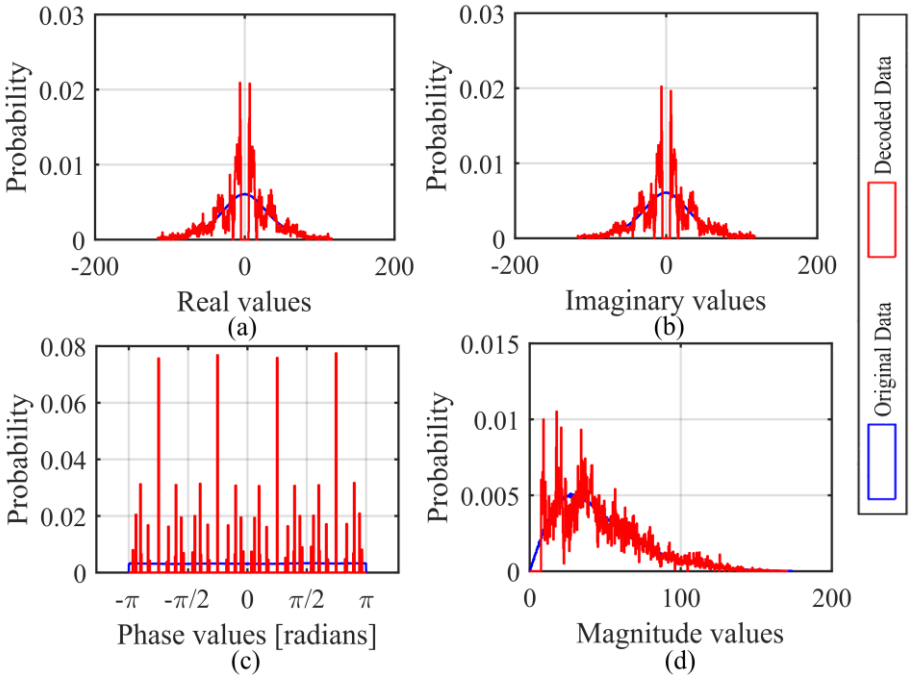

Figure 7.20 Distribution of data set 3 before and after implementing the BAQ algorithm. (a) I component. (b) Q component. (c) Phase component. (d) Amplitude component.

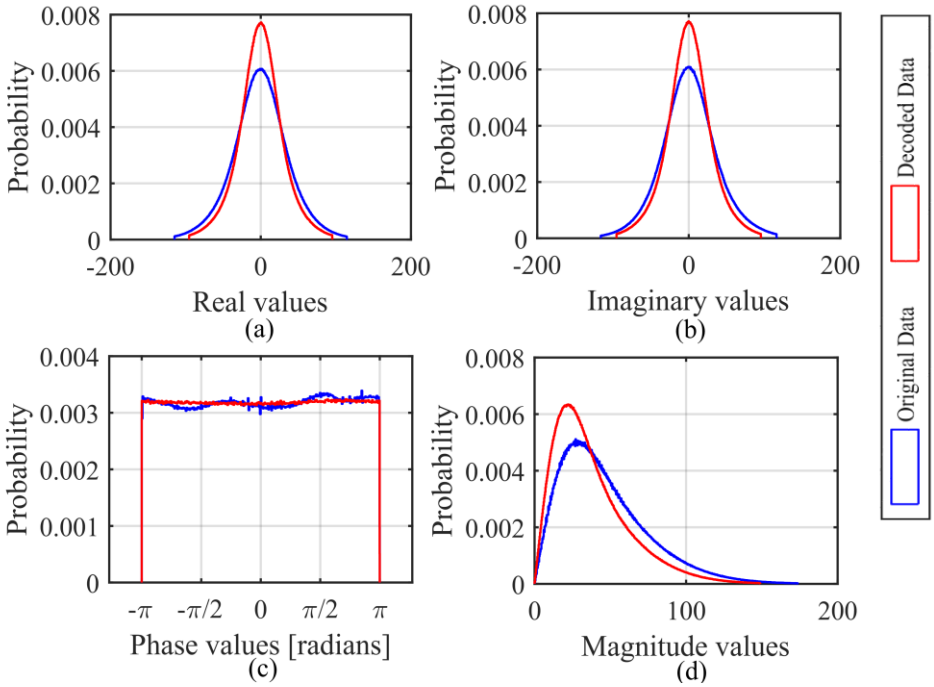

Figure 7.21 Distribution of data set 3 before and after implementing the FFT-BAQ algorithm. (a) I component. (b) Q component. (c) Phase component. (d) Amplitude component.

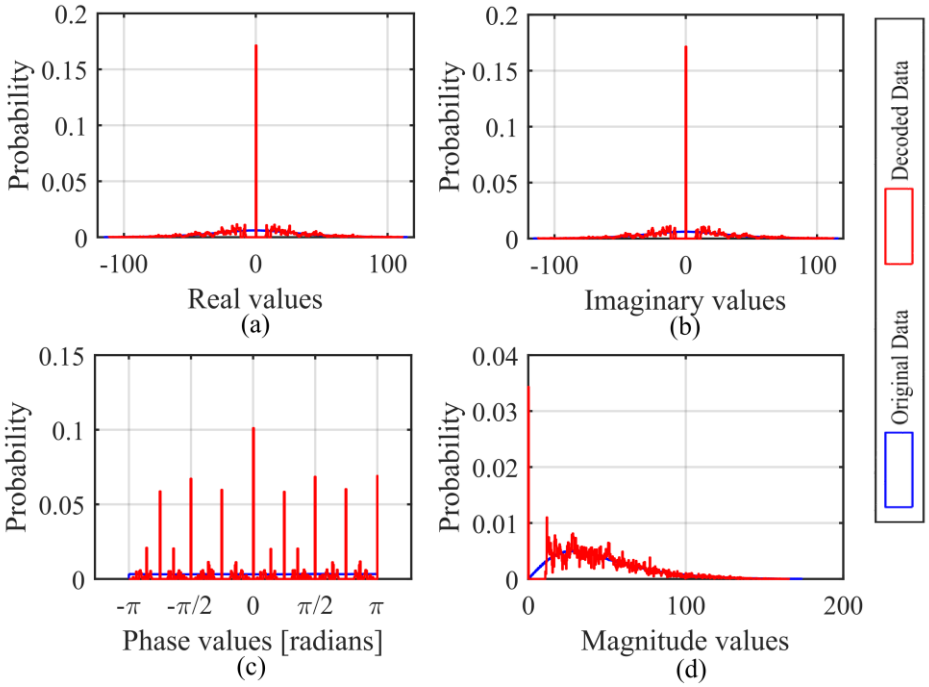

Figure 7.22 Distribution of data set 3 before and after implementing the FDBAQ algorithm. (a) I component. (b) Q component. (c) Phase component. (d) Amplitude component.

Table 7.8 Error measures for the peri-urban scene in the data domain.

Metric	Value after BAQ method	Value after FFT-BAQ method	Value after FDBAQ method
MSE	73.02	415.64	73.4
SQNR	16.09 dB	8.53 dB	16.06 dB
MPE (rad)	0.1453	0.3363	0.1677
MPE (degrees)	8.33	19.27	9.61

7.3.4 Discussion of the data-domain metrics results

7.3.4.1 Statistical parameters

In Table 7.1, Table 7.3, and Table 7.5, the results of the statistical parameters for each scene are summarised, respectively. There is a difference of about 50 dB between the dynamic

range of the results obtained using a time-domain method (FDBAQ or BAQ methods), and the FFT-BAQ method. The dynamic range after applying the FFT-BAQ method compares very well with the dynamic range of the uncompressed data set, while after applying the other two methods, the dynamic range is less than that of the uncompressed data. The reason for the high dynamic range result of the FFT-BAQ method is because the compression takes place in the frequency domain while the metrics are computed in the time domain, where various levels are represented after implementing the FFT-BAQ decompression steps. The wide range of values represented in the time domain is confirmed by a high dynamic range. For the two time-domain methods only certain output levels are possible, consequently reducing the dynamic range.

When considering the other statistical parameters, all the methods perform well as the values differ only slightly from the original, uncompressed values. The skewness and kurtosis are two metrics that are of importance since they are representative of the deviation of the distributions of the magnitude and phase components from the original distributions. The results show that the FFT-BAQ method causes minimal deviation from the original distributions and thus does not cause the statistical characteristics of the data to change significantly. For a Rayleigh distribution the skewness should be close to 0.63, while the kurtosis should have a value of 3.245. The results show that even after applying the compression algorithms, each component can still be assumed to have similar characteristics to the original distribution of the uncompressed data sets.

Entropy is another important measure in the data domain since it is an indication of the information content of the data set. The results show that the entropy of the magnitude component remains well preserved for all methods, with the FFT-BAQ result being the closest to the entropy of the uncompressed data. This shows that the encoding and decoding steps did not cause severe loss of magnitude information, meaning most of the information could be recovered. However, the entropy of the phase component is not well preserved for the two time-domain methods. The FFT-BAQ method preserves both the magnitude and phase information very well. Overall, the time-domain methods show an average of about

7 bits of information loss for the two components, compared to the information loss of less than a bit for the FFT-BAQ method.

7.3.4.2 Data histograms

In Figure 7.11 to Figure 7.13, the variation of the statistical parameters of data set 1 due to the compression methods is represented visually by the histograms of each component before compression and after the decompression. Similarly, Figure 7.14 to Figure 7.16, are the histograms of data set 2, and Figure 7.17 to Figure 7.19 are the histograms of data set 3. The effect of compression in the time domain, as is a characteristic of the BAQ and FDBAQ methods, can be seen since only certain values are represented after decompression. For the FFT-BAQ method, it can be seen that the decompressed data closely follow the original distribution since compression was performed in the frequency domain and, thus, the quantisation effect is spread across the time domain values. Consequently, applying the FFT-BAQ method results in all possible values still being represented in the time domain. The operation of the FDBAQ method can be visualised as it can be seen that the values represented after decoding are highly variable, since the BAQ used in this algorithm was applied for more than one output bit rate. Figure 7.20 to Figure 7.22 are the histograms of data set 3 after 3-bit compression, and the higher output bit rate can be confirmed by the increased number of values represented after decoding of the BAQ method. The results show that the data histograms are an important visual aid in determining the effects of a compression algorithm on the raw SAR data in the data domain.

7.3.4.3 Error measures

The error measures for each data set are summarised in Table 7.2, Table 7.4, and Table 7.6, respectively. The FFT-BAQ method achieves the worst results for the error measures, although it achieved the best statistical parameter results. This can be attributed to the variable compression ratio of the code scheme used in the FFT-BAQ method. The code scheme encodes a portion of the data that has the lowest amount of energy in the frequency domain with 0 bits, whereas the high energy frequency components are encoded with more bits. Encoding data with 0 bits represents a loss of information and has an effect on the mean

squared error (MSE), mean phase error (MPE), and the signal-to-quantisation-noise ratio (SQNR), which are all measures of the distortion caused by the quantiser computed as the absolute encoding error between every sample of the uncompressed and decompressed data sets. Due to the nature of operation of the FFT, an error is introduced to each element in the set, which is then used in the computation of these metrics. It is thus evident that these metrics are used to determine the effects of the quantisation for each method in the data domain, which will differ from the effects they have in the image domain as will be seen in the next subsection.

The MSE was further investigated to determine the size of the error relative to the 12 bits of data. The results of the Pecanwood scene are summarised in Table 7.9 and are representative of the other two data sets. It can be seen that the two time-domain methods achieve an error of less than 10 %, while the error introduced by the FFT-BAQ method is slightly higher than 10 %.

Table 7.9 MSE and the corresponding percentage error for the peri-urban scene.

	BAQ	**FFT-BAQ**	**FDBAQ**
MSE	254.24	476.45	233.79
% Error	6.21 %	11.63 %	5.71 %

From the phase error metrics, it seems that the BAQ method has the smallest effect on the phase in the data domain. However, when considering the entropy of the phase component of the decompressed data, it can be seen that the information content of the phase component is not well preserved compared to the entropy of the phase of the uncompressed data. This shows that although the computed errors are smaller for the time-domain methods, these methods have a detrimental effect on the phase information content of the data in the data domain.

The MPE was further investigated to determine whether the error is due to distortion or a bias. This was determined by computing the variance of the phase error (VPE). The results

of the Pecanwood scene are summarised in Table 7.10 and are representative of the other two data sets. It can be seen that the FFT-BAQ and FDBAQ methods introduce a distortion to the phase component, since the VPE is relatively high. The BAQ method on the other hand, does not distort the phase component of the data since the VPE is only 2.3 degrees.

Table 7.10 MPE and VPE results for the peri-urban scene.

	BAQ	**FFT-BAQ**	**FDBAQ**
MPE (rad)	0.2502	0.3598	0.3402
MPE (degrees)	14.34	20.62	19.49
VPE (rad)	0.0401	0.6614	0.2936
VPE (degrees)	2.3	37.9	16.82

To better visualise the distortion that the different compression methods introduce, the error between the phases of the uncompressed data and the decompressed data, is plotted for each method. The results can be seen in Figure 7.23 to Figure 7.25.

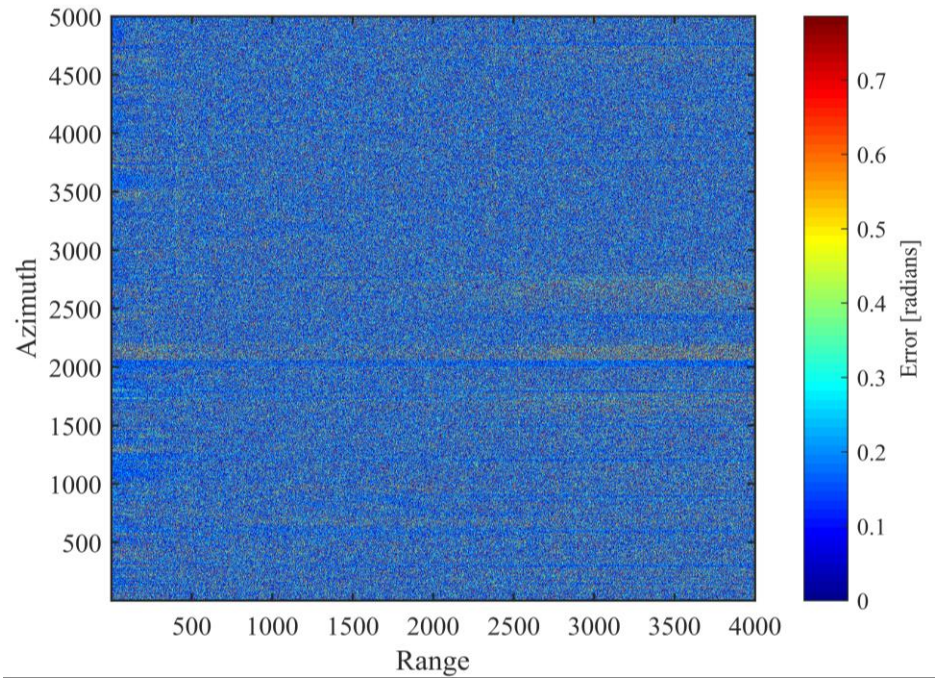

Figure 7.23 Visual representation of the phase error between the original data and the data after the BAQ decompression.

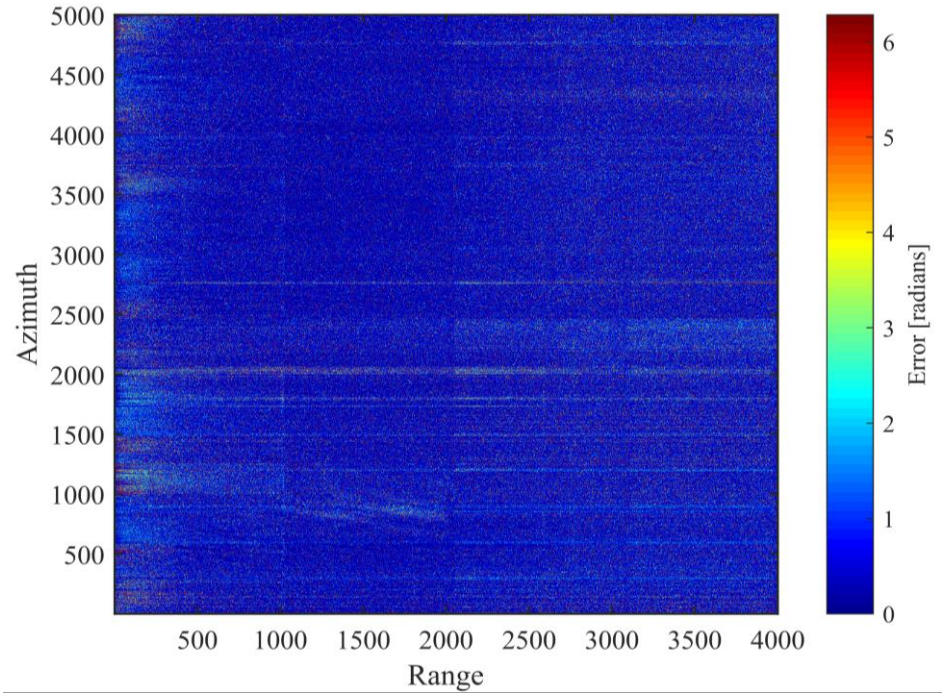

Figure 7.24 Visual representation of the phase error between the original data and the data after the FFT-BAQ decompression.

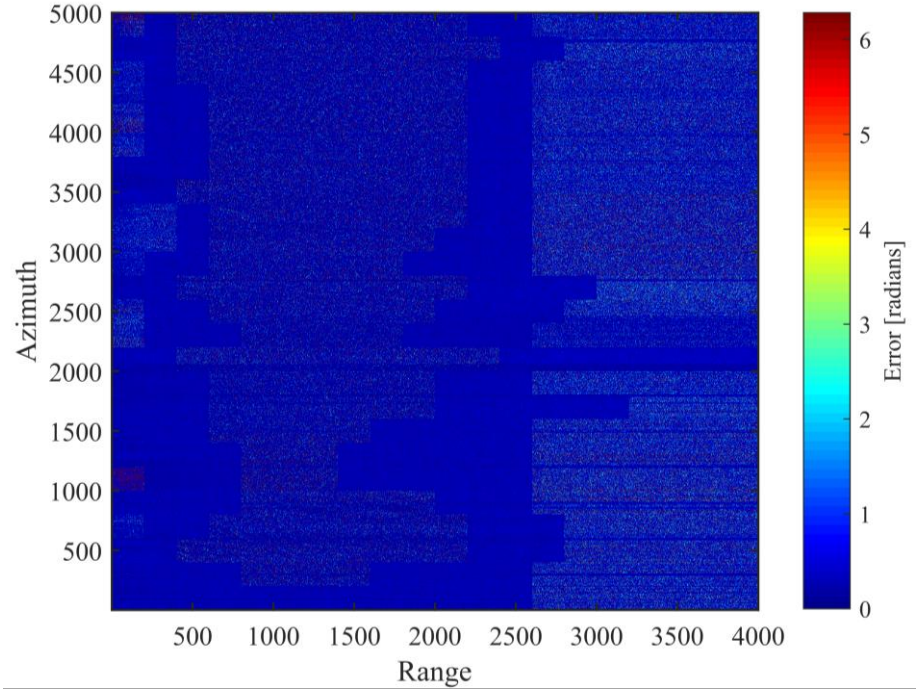

Figure 7.25 Visual representation of the phase error between the original data and the data after the FDBAQ decompression.

It can be seen that the BAQ method introduces small phase errors across the entire scene, while it seems like the FFT-BAQ method revealed a cyclic feature in the data and then distorts it further. The FDBAQ method shows areas in the scene with greater errors than other areas.

After investigating the results in the data domain, it was seen that some metrics favoured the time-domain methods, while some metrics favoured the frequency-domain method. Therefore, a decision on the performance of a raw SAR data compression algorithm cannot be made by only considering the metrics in the data domain alone. The metrics in the image domain also need to be considered when choosing a suitable algorithm for an application.

7.4 EVALUATION OF IMAGE-DOMAIN METRICS

The metrics discussed in Section 5.3 were evaluated and the results are summarised below. All three of the compression algorithms were evaluated for all three data sets with similar tendencies being observed. These metrics are evaluated in the image domain, which means they are evaluated after the SAR processing has been implemented, as can be seen in Figure 4.1. Firstly, all the results in the image domain are summarised by means of tables and figures, thereafter, the results are discussed.

7.4.1 Data set 1: Rural scene

7.4.1.1 2-Bit results

Table 7.11 Statistical parameters of the rural scene in the image domain.

Metric	Image of uncompressed data	Image after BAQ method	Image after FFT-BAQ method	Image after FDBAQ method
Dynamic Range	95.34 dB	94.37 dB	93.32 dB	94.56 dB
Mean (mag)	21 259.02	22 570.96	20 591.05	19 876.46
Mean (phase)	1.13×10^{-4}	-2.51×10^{-4}	-1.07×10^{-4}	-2.05×10^{-4}
Standard deviation (mag)	12 934.97	13 465.02	12 750.12	11 868.82
Standard deviation (phase)	1.81	1.81	1.81	1.81
Skewness (mag)	1.89	1.71	2.03	1.71
Skewness (phase)	-1.87×10^{-5}	2.49×10^{-5}	1.45×10^{-5}	8.14×10^{-6}
Kurtosis (mag)	14.9	12.84	16.46	12.88
Kurtosis (phase)	1.8	1.8	1.8	1.8
Differential Entropy	16.12	16.21	16.08	16.03

Table 7.12 Image quality measures for the rural scene.

Metric	Image of uncompressed data	Image after BAQ method	Image after FFT-BAQ method	Image after FDBAQ method
Image Contrast	0.6084	0.5966	0.6192	0.5971
Global Contrast Factor	0.1535	0.1547	0.1465	0.1546

Table 7.13 Image fidelity measures for the rural scene.

Metric	**Image after BAQ method**	**Image after FFT-BAQ method**	**Image after FDBAQ method**
SDNR	11.54 dB	13.03 dB	11.91 dB
MSE	4.34×10^7	3.08×10^7	3.99×10^7
MPE (rad)	0.5839	0.5889	0.5836
MPE (degrees)	33.46	33.74	33.44

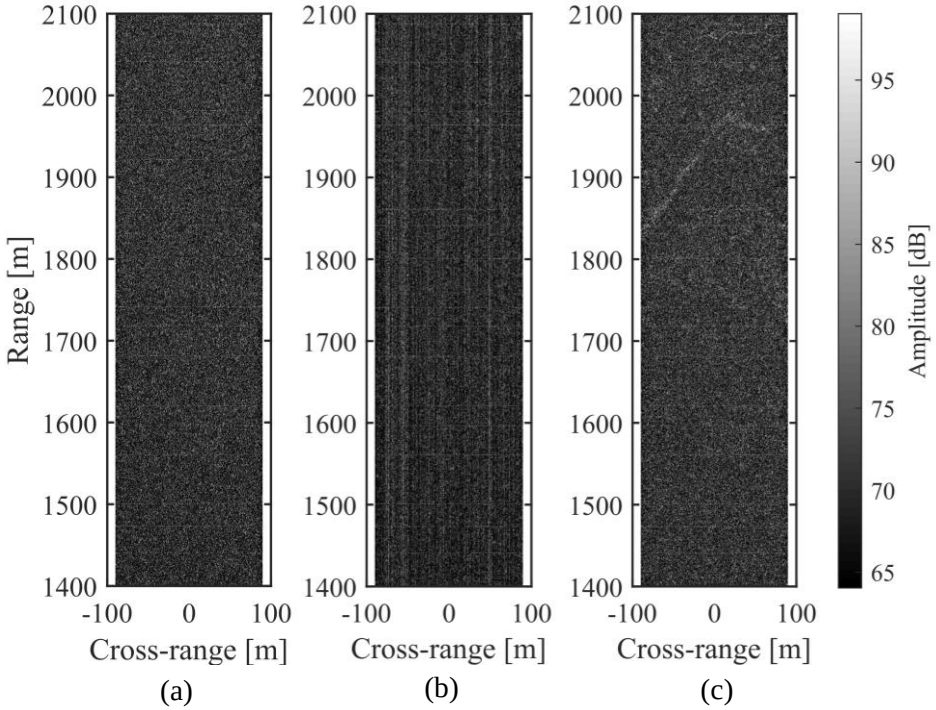

Figure 7.26 Error images of the rural scene. (a) BAQ applied. (b) FFT-BAQ applied. (c) FDBAQ applied.

7.4.2 Data set 2: Mine scene

7.4.2.1 2-Bit results

Table 7.14 Statistical parameters of the mine scene in the image domain.

Metric	Image of uncompressed data	Image after BAQ method	Image after FFT-BAQ method	Image after FDBAQ method
Dynamic Range	94.66 dB	92.09 dB	95.36 dB	99.03 dB
Mean (mag)	27 911.63	29 711.97	26 752.46	26 287.95
Mean (phase)	-1.95×10^{-4}	1.99×10^{-4}	-1.90×10^{-4}	-1.75×10^{-5}
Standard deviation (mag)	22 352.76	22 682.12	22 329.6	20 363.61
Standard deviation (phase)	1.81	1.81	1.81	1.81
Skewness (mag)	3.21	3.01	3.31	3.08
Skewness (phase)	4.35×10^{-5}	9.62×10^{-6}	-4.84×10^{-6}	8.53×10^{-5}
Kurtosis (mag)	24.77	22.73	25.56	23.5
Kurtosis (phase)	1.8	1.8	1.8	1.8
Differential Entropy	16.54	16.63	16.48	16.45

Table 7.15 Image quality measures for the mine scene.

Metric	Image of uncompressed data	Image after BAQ method	Image after FFT-BAQ method	Image after FDBAQ method
Image Contrast	0.8008	0.7634	0.8347	0.7746
Global Contrast Factor	0.1538	0.1547	0.1480	0.1523

Table 7.16 Image fidelity measures for the mine scene.

Metric	**Image after BAQ method**	**Image after FFT-BAQ method**	**Image after FDBAQ method**
SDNR	12.46 dB	13.25 dB	12.98 dB
MSE	7.25×10^{7}	6.04×10^{7}	6.44×10^{7}
MPE (rad)	0.5585	0.5582	0.5595
MPE (degrees)	32	31.98	32.06

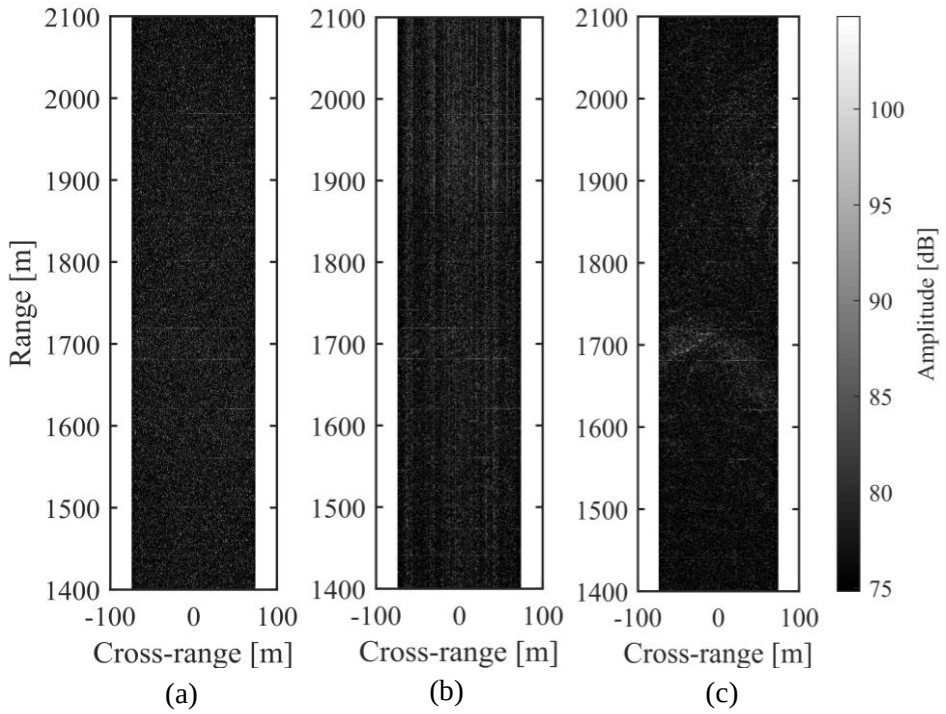

Figure 7.27 Error images of the mine scene. (a) BAQ applied. (b) FFT-BAQ applied. (c) FDBAQ applied.

7.4.3 Data set 3: Peri-urban scene

7.4.3.1 2-Bit results

Table 7.17 Statistical parameters of the peri-urban scene in the image domain.

Metric	Image of uncompressed data	Image after BAQ method	Image after FFT-BAQ method	Image after FDBAQ method
Dynamic Range	114.55 dB	114.77 dB	115.01 dB	112.09 dB
Mean (mag)	22 762.81	25 095.08	22 532.18	22 063.778
Mean (phase)	-3.08×10^{-4}	-3.3×10^{-4}	-1.62×10^{-5}	-4.04×10^{-5}
Standard deviation (mag)	22 280.39	22 785.34	22 070.9	20 478.46
Standard deviation (phase)	1.81	1.81	1.81	1.81
Skewness (mag)	19.27	19.04	18.04	18.9
Skewness (phase)	1.33×10^{-5}	5×10^{-6}	-9.76×10^{-5}	-2.58×10^{-6}
Kurtosis (mag)	1 346.54	1 320.88	1 167.46	1 295.15
Kurtosis (phase)	1.8	1.8	1.8	1.8
Differential Entropy	16.23	16.37	16.22	16.19

Table 7.18 Image quality measures for the peri-urban scene.

Metric	Image of uncompressed data	Image after BAQ method	Image after FFT-BAQ method	Image after FDBAQ method
IRW (range)	1.06 m	0.9994 m	1.12 m	0.9994 m
IRW (azimuth)	9.68 m	9.62 m	9.74 m	9.68 m
PSLR (range)	-18.94 dB	-16.9 dB	-16.55 dB	-16.39 dB
PSLR (azimuth)	-25.12 dB	-23.26 dB	-24.65 dB	-24.59 dB
Image Contrast	0.9788	0.9080	0.9795	0.9281
Global Contrast Factor	0.0947	0.0917	0.0931	0.0911

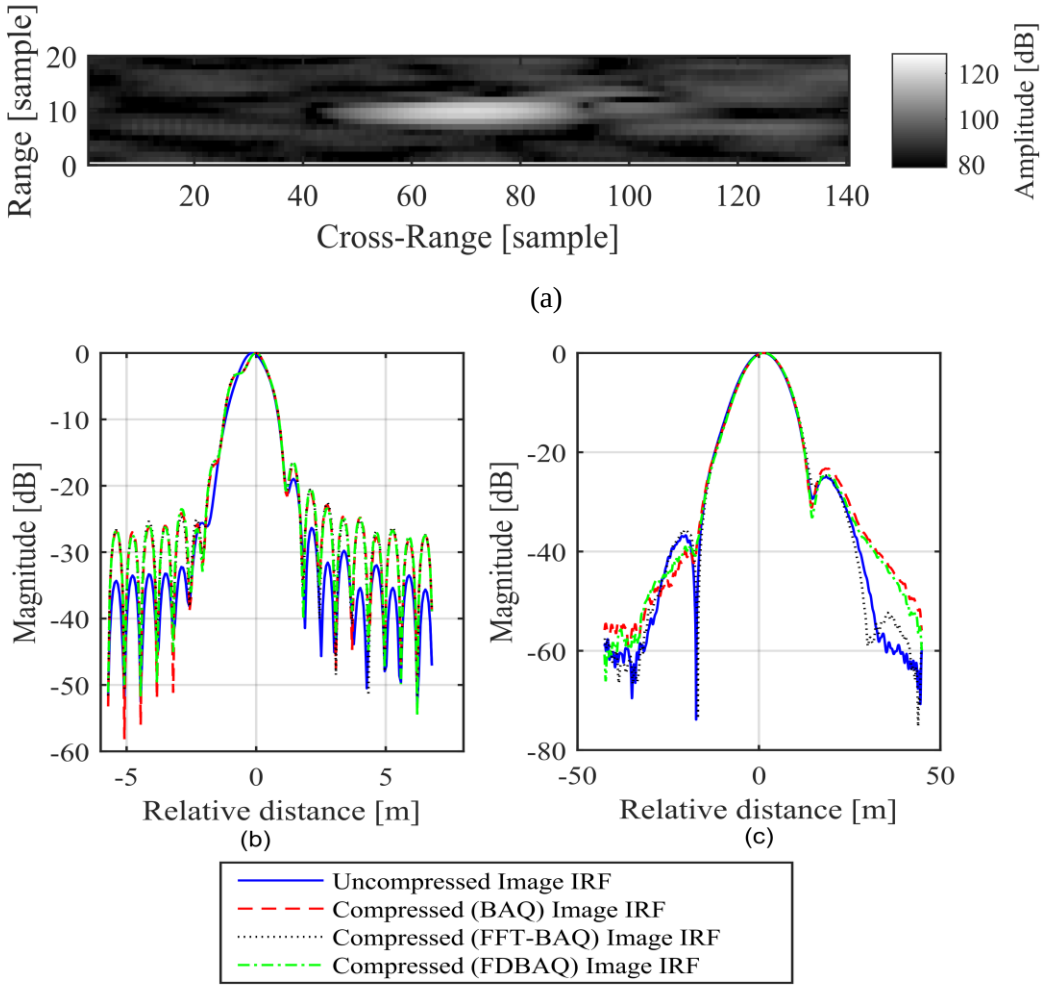

Figure 7.28 IRF of the peri-urban scene before and after 2-bit compression. (a) Extracted target. (b) Range direction. (c) Cross-range direction.

Table 7.19 Image fidelity measures for the peri-urban scene.

Metric	**Image after BAQ method**	**Image after FFT-BAQ method**	**Image after FDBAQ method**
SDNR	11.41 dB	14.27 dB	12.5 dB
MSE	7.34×10^{7}	3.79×10^{7}	5.71×10^{7}
MPE (rad)	0.5779	0.5924	0.5810
MPE (degrees)	33.11	33.94	33.29

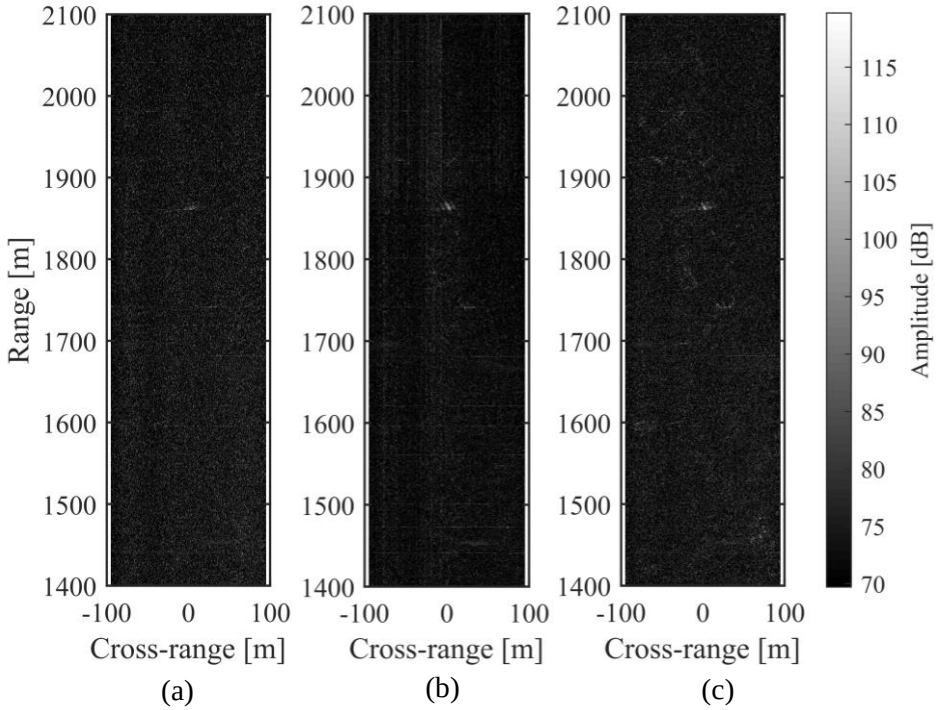

Figure 7.29 Error images of the peri-urban scene for 2-bit compression. (a) BAQ applied. (b) FFT-BAQ applied. (c) FDBAQ applied.

7.4.3.2 3-Bit results

Table 7.20 Statistical parameters of the peri-urban scene in the image domain.

Metric	Image of uncompressed data	Image after BAQ method	Image after FFT-BAQ method	Image after FDBAQ method
Dynamic Range	114.55 dB	114.08 dB	121.71 dB	122.90 dB
Mean (mag)	22 762.81	23 358.8	22 063.5	22 499.6
Mean (phase)	-3.08×10^{-4}	5.71×10^{-5}	-2.55×10^{-4}	-2.36×10^{-4}
Standard deviation (mag)	22 280.39	22 490.74	22 209.73	21 745.14
Standard deviation (phase)	1.81	1.81	1.81	1.81
Skewness (mag)	19.27	19.59	19.11	19.6
Skewness (phase)	1.33×10^{-5}	-7.27×10^{-5}	-2.1×10^{-5}	-1.06×10^{-5}
Kurtosis (mag)	1 346.54	1 360.82	1 287.63	1 359.97
Kurtosis (phase)	1.8	1.8	1.8	1.8
Differential Entropy	16.23	16.27	16.19	16.22

Table 7.21 Image quality measures for the peri-urban scene.

Metric	Image of uncompressed data	Image after BAQ method	Image after FFT-BAQ method	Image after FDBAQ method
IRW (range)	1.06 m	0.9994 m	1.06 m	1.06 m
IRW (azimuth)	9.68 m	9.68 m	9.68 m	9.68 m
PSLR (range)	-18.94 dB	-17.1 dB	-16.77 dB	-16.87 dB
PSLR (azimuth)	-25.12 dB	-24.28 dB	-24.26 dB	-24.36 dB
Image Contrast	0.9788	0.9628	1.0066	0.9665
Global Contrast Factor	0.0947	0.0925	0.0927	0.0924

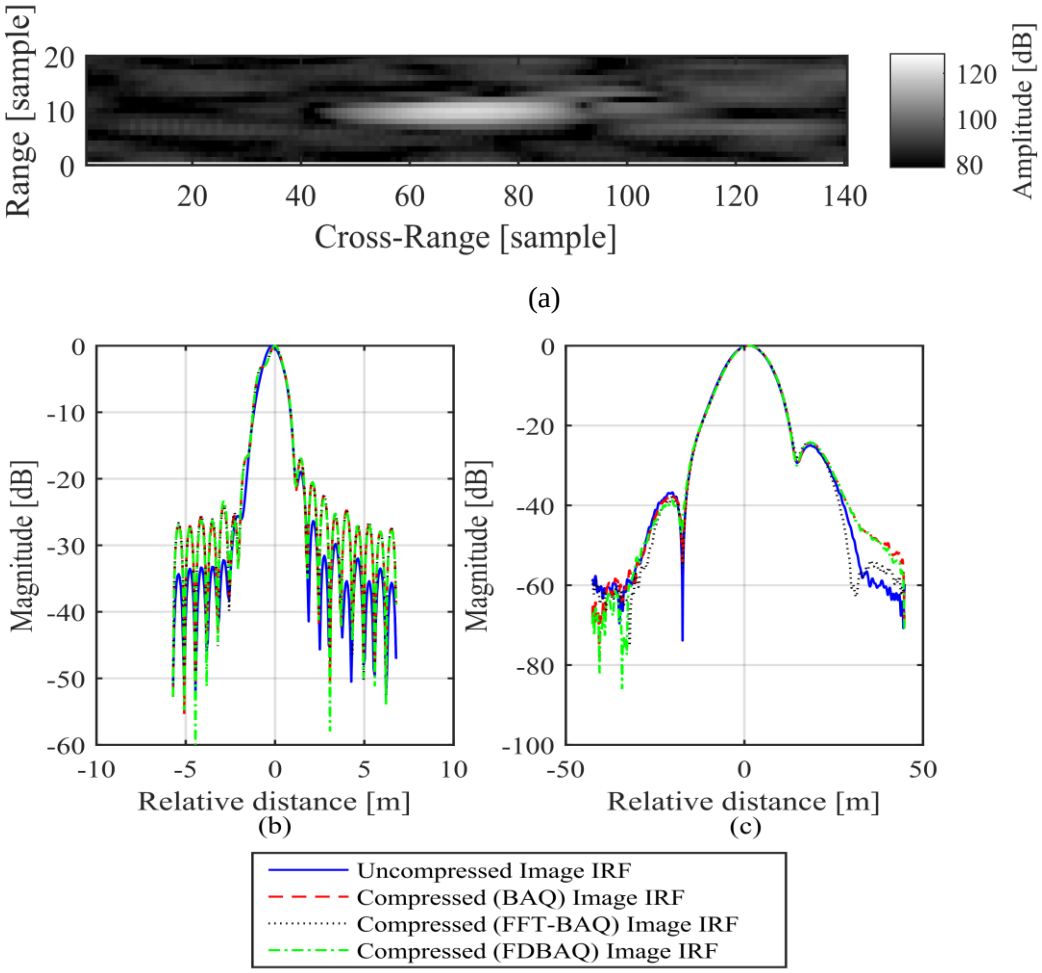

Figure 7.30 IRF of the peri-urban scene before and after 3-bit compression. (a) Extracted target. (b) Range direction. (c) Cross-range direction.

Table 7.22 Image fidelity measures for the peri-urban scene.

Metric	**Image after BAQ method**	**Image after FFT-BAQ method**	**Image after FDBAQ method**
SDNR	15.84 dB	16.92 dB	16.22 dB
MSE	2.64×10^{7}	2.06×10^{7}	2.42×10^{7}
MPE (rad)	0.6044	0.6097	0.6051
MPE (degrees)	34.63	34.93	34.67

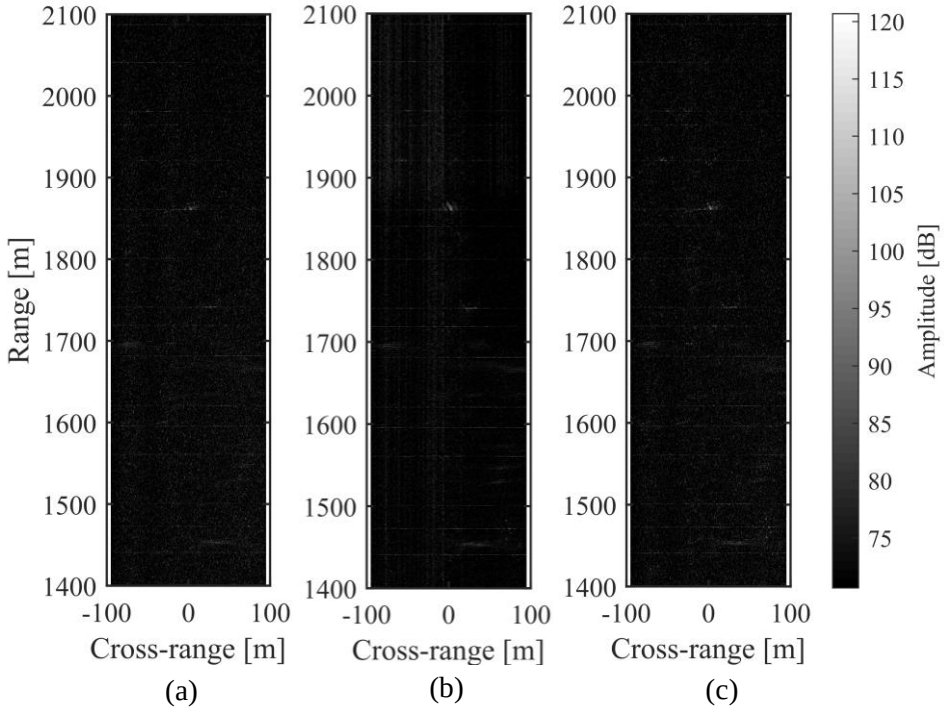

Figure 7.31 Error images of the peri-urban scene for 3-bit compression. (a) BAQ applied. (b) FFT-BAQ applied. (c) FDBAQ applied.

7.4.4 Discussion of the image-domain metrics results

7.4.4.1 Statistical parameters

In Table 7.11, Table 7.14, and Table 7.17, the results of the statistical parameters for each scene are summarised, respectively. The results suggest that all methods perform equally well in this domain, since the statistical characteristics of the original SAR image did not change significantly after applying any of the compression algorithms. Therefore, since the mean and standard deviation did not change significantly, it implies that no bias was introduced in the images after decompression, nor did the speckle content of these images change significantly. The results of the skewness and kurtosis parameters also show that the distributions of the magnitude and phase components of the reference SAR image did not deviate significantly when applying the compression algorithms. The differential entropy

after applying the compression methods did not change significantly compared to the differential entropy computed for the reference SAR image.

The one statistical parameter that needs more attention, is the dynamic range. In the data domain, there was about a 50 dB difference between the dynamic ranges of the time-domain methods and the frequency-domain method. However, in the image domain, the dynamic range of the FDBAQ method is slightly greater than that of the FFT-BAQ method in most cases. This shows that in the image domain, a greater range of values are represented in the SAR image after implementing the FDBAQ method than that of the SAR image after the FFT-BAQ method. This therefore implies that the coherent SAR processing exploits averaging to reduce the effects caused by the quantisation in the data domain, so that great differences in the data domain have little effect in the image domain.

7.4.4.2 Image quality measures

After SAR processing, the SAR image is produced and the visual quality of the image can be determined by the image quality measurements. These metrics include the impulse response function (IRF), the image contrast (IC), and the global contrast factor (GCF) and are summarised in Table 7.12, Table 7.15, and Table 7.18, for the respective scenes. When considering the IC ratio, which directly relates to the dynamic range, it can be seen that the SAR image after applying the FFT-BAQ method has the highest contrast ratio. This result can also be confirmed visually, since a higher contrast ratio means a crisper image. When comparing the images of the farm scene after the different compression methods in Figure 7.7, Figure 7.8 for the mine scene, and Figure 7.9 for the

scene, a slightly higher level of crispness of the SAR image after the FFT-BAQ method can be observed. The boundaries in the images between, for example, the water of the dam and the residential area in the peri-urban scene, can be distinguished more easily for the image with FFT-BAQ applied. Quantising the data in the frequency domain causes less image degradation than quantising the data in the time domain. It has a visible effect on the dynamic range and the image contrast of the SAR images, which are slightly higher when the FFT-BAQ method is applied.

Another important image quality metric is the IRF of the SAR system. It is the response of the SAR system to a point scatterer. For this investigation, the peri-urban scene data set was used since this scene contained more bright scatterers than the rural or mine scenes. Usually, the IRF of a SAR system is determined by placing targets with a known RCS, like a transponder or reflector, in the scene to measure the response. However, to compare the IRF after applying different compression algorithms, using the available data sets, a target of opportunity had to be used. Thus, the method explained in [128] was executed and the extracted target can be seen in Figure 7.28 (a). The IRF was determined for the case where no compression algorithm was applied to the data to serve as the reference, as well as for the case where compression was applied. The effect that each compression algorithm has on the impulse response can then be determined.

The IRF results for the 2-bit compression case are summarised in Table 7.18. The IRF in the range and cross-range directions is plotted in Figure 7.28 (b) and (c). The 3 dB widths after applying the respective compression methods correspond well to the reference values. Although the side lobes are higher in the range direction, observed for all three compression methods, the overall shape of the reference IRF is maintained. Therefore, none of the compression methods has a detrimental effect on the impulse response of the original SAR image without any compression applied. If the goal of the SAR mission was to identify man-made targets, the compression algorithm with the smallest effect on the IRF would be preferred. Since man-made targets have similar scattering characteristics to point scatterers, the impulse response of the system needs to be preserved.

7.4.4.3 Image fidelity measures

The image fidelity measures are an indication of the exactness with which the SAR image, with compression applied, was reproduced compared to the reference SAR image. In this domain, these metrics are a measure of the distortions that propagated into the image domain caused by quantising in the data domain. The results are summarised in Table 7.13, Table 7.16, and Table 7.19, for the respective scenes. It can be seen that the FFT-BAQ method has

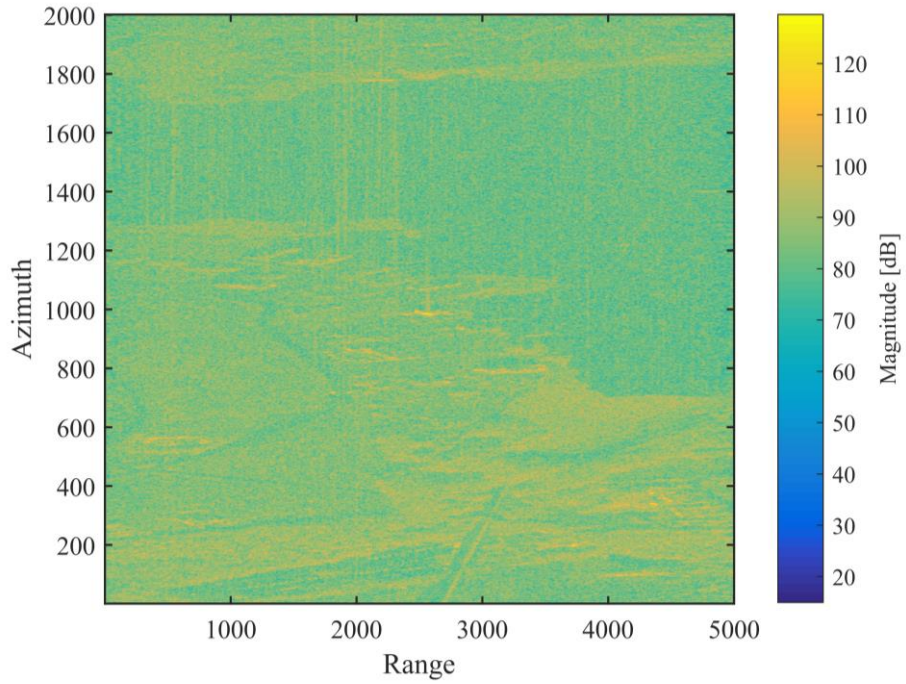

Figure 7.32 Magnitude component of the peri-urban scene SAR image.

the smallest errors in this domain, since it achieves the highest signal-to-distortion-noise ratio (SDNR), while the MSE and MPE are slightly smaller than for the two time-domain methods.

The MSE was further investigated to determine whether the errors caused by the compression algorithms are present throughout the scene or confined to only the bright scatterers. The squared error of the magnitude component is plotted for the Pecanwood scene and are representative of the other two data sets. The magnitude component of the original Pecanwood SAR image is plotted in Figure 7.32 to serve as the reference image. The magnitude error for the three different algorithms are plotted in Figure 7.33 to Figure 7.35. in the reference figure it can be seen that cyclic components are present in the final SAR image. It can be seen that the cyclic components are no longer present after implementing the time domain compression. However, these components are still present after implementing the frequency domain method, FFT-BAQ. FFT-BAQ causes large errors on the cyclic components as can be seen in Figure 7.34. The BAQ method causes errors across the scene, while the FDBAQ method causes greater errors for the large bright scatterers.

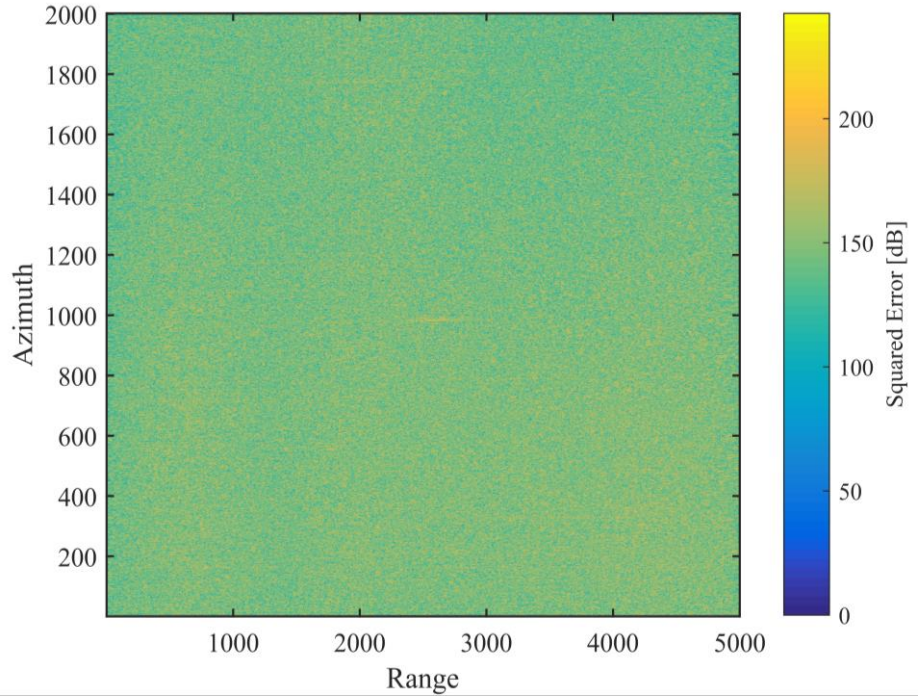

Figure 7.33 Visual representation of the magnitude error between the original image and the image after the BAQ decompression.

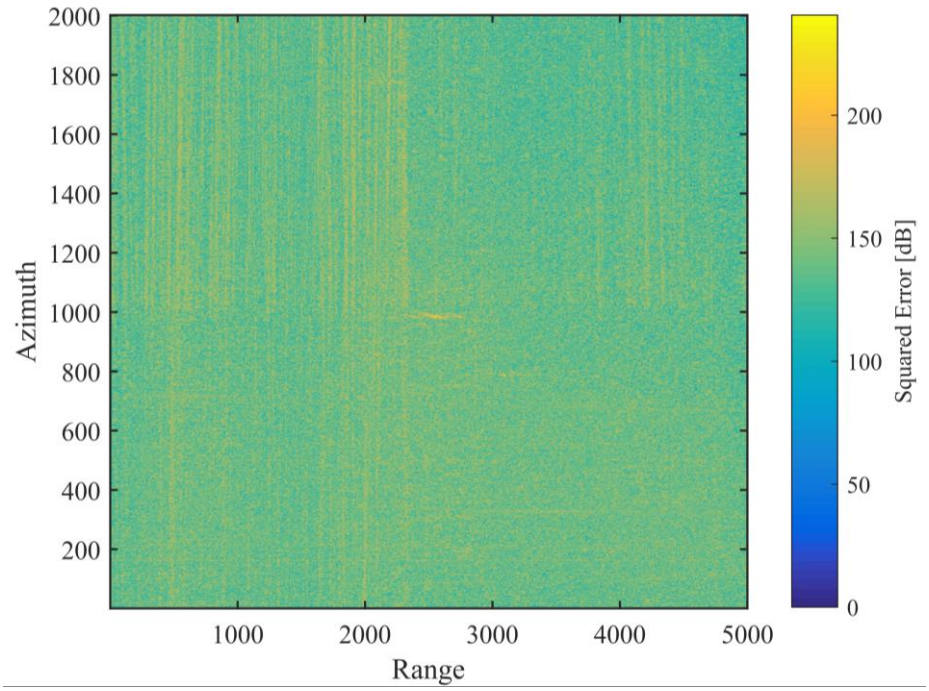

Figure 7. 34 Visual representation of the magnitude error between the original image and the image after the FFT-BAQ decompression.

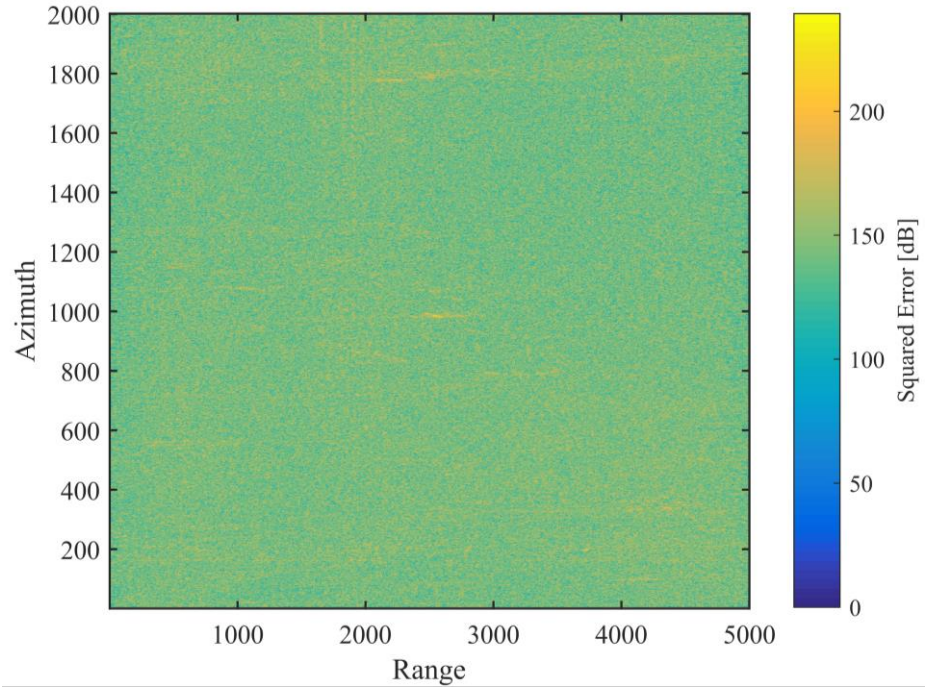

Figure 7.35 Visual representation of the magnitude error between the original image and the image after the FDBAQ decompression.

The MPE was also further investigated to determine whether the error is due to distortion or a bias in the data. This was determined by computing the variance of the phase error (VPE). The results of the Pecanwood scene are summarised in Table 7.23 and are representative of the other two data sets. The VPE shows that the phase errors are due to corruptions caused by the compression algorithms implemented in the data domain, with the FFT-BAQ method causing slightly less corruptions.

Table 7.23 MPE and VPE results for the peri-urban scene.

	BAQ	**FFT-BAQ**	**FDBAQ**
MPE (rad)	0.5779	0.5924	0.5810
VPE (rad)	0.9604	0.7849	0.9332
VPE (degrees)	55.03	44.97	53.47

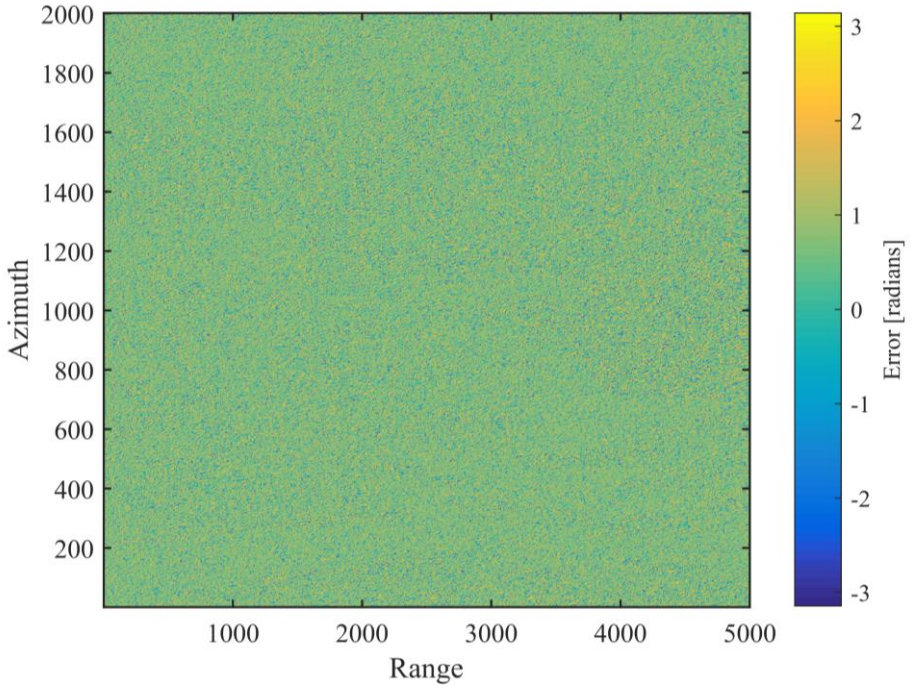

Figure 7.36 Visual representation of the phase error between the original image and the image after the BAQ decompression.

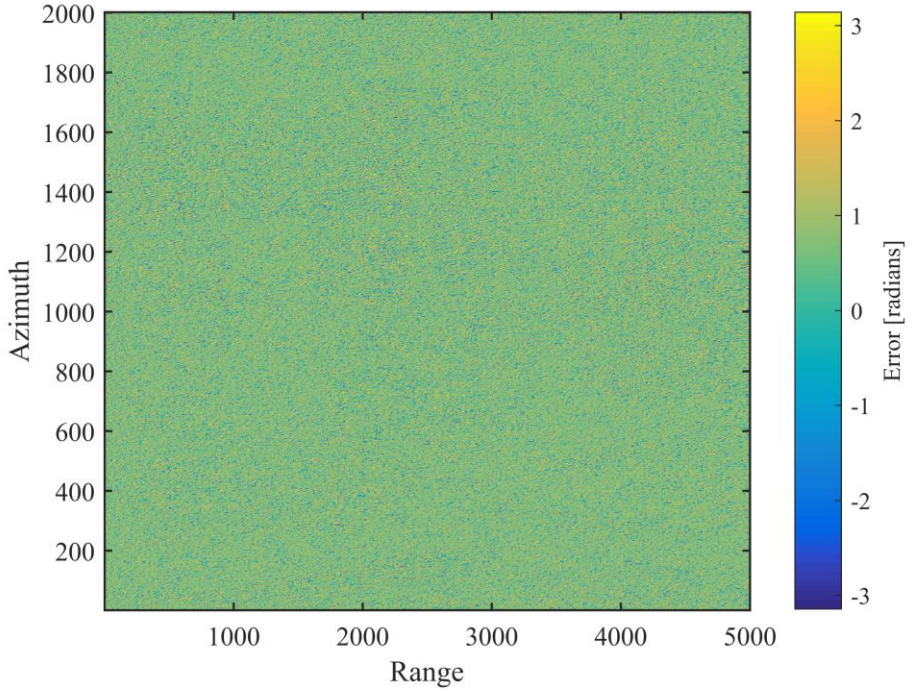

Figure 7. 37 Visual representation of the phase error between the original image and the image after the FFT-BAQ decompression.

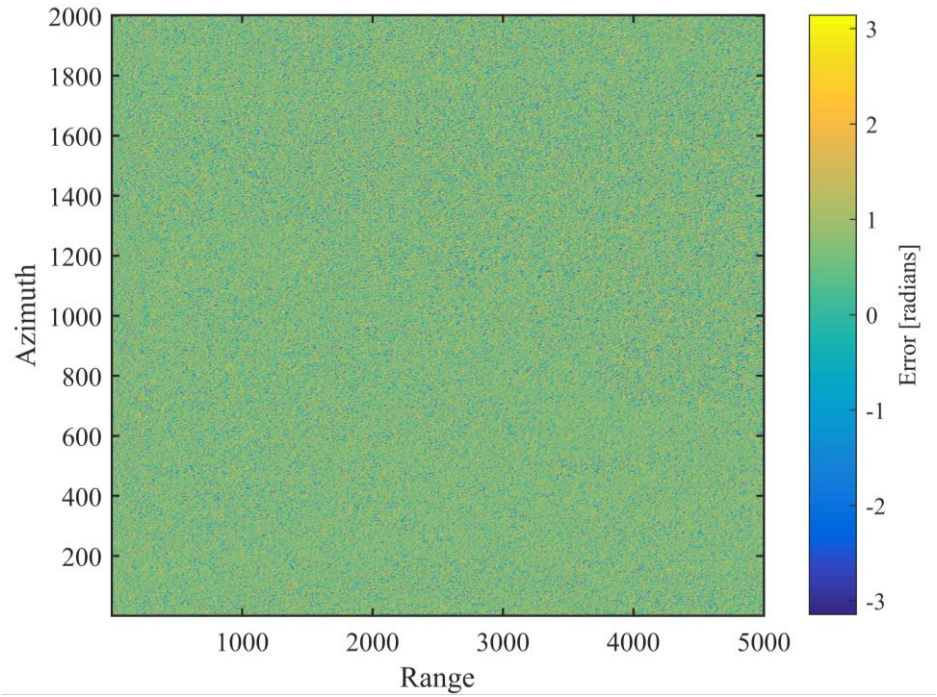

Figure 7.38 Visual representation of the phase error between the original image and the image after the FDBAQ decompression.

To better visualise the distortion that the different compression methods introduce, the error between the phases of the original SAR image and the SAR image from the decompressed data is plotted for each method. The results can be seen in Figure 7.36 to Figure 7.38. The figures show that all three methods perform similar in terms of the corruption of the phase component of the SAR image.

7.4.4.4 Error images

When visually investigating the magnitude error images, Figure 7.26, Figure 7.27, and Figure 7.29, it can be concluded that the BAQ method obtains the best results in all cases. The error images represent the characteristic operation of each algorithm visually. For the BAQ case, errors are present all over the scene, while for the FDBAQ method the errors are confined to the bright scatterers where more bits were used to encode the data, and the spreading of the cyclic errors across the scene due to the FFT computation can be seen for

the FFT-BAQ method. Overall, it seems like the BAQ method has less erroneous samples, or smaller errors, present in the scenes.

After investigating the results in the image domain it is clear that the quality of the SAR images after applying the FFT-BAQ method is better than the quality of the SAR images after applying the BAQ or FDBAQ methods. For all three methods, the characteristic features of the scene can easily be identified, but the images of the different scenes are crisper after applying the FFT-BAQ method. This shows that the error images can only visually represent some of the corruptions that are present in an image.

7.5 DATA-DOMAIN METRICS VS IMAGE-DOMAIN METRICS

The metrics were divided into two domains to evaluate the algorithms at two stages of the SAR system, i.e. before and after SAR processing is performed. Evaluating an algorithm at two stages means one can distinguish between the data volume reduction capability of the algorithm and the image degradation caused by the algorithm.

When considering the results of the data-domain metrics, it was seen that the BAQ and FDBAQ methods had detrimental effects on the phase information since the entropy of the phase component was not preserved. When considering the data histograms of these two algorithms, the change in their probability distributions compared to the original distribution was quite severe. These changes are due to the operation of the algorithms in the time domain where only certain reconstruction values are present. Therefore, it seems like the time-domain methods of compression distorted the original data when considering only the data-domain metrics.

In the data-domain the FFT-BAQ method outperformed the two time-domain methods when considering the statistical parameters like the dynamic range, entropy, skewness, and kurtosis. The entropy of both components of the decompressed FFT-BAQ data compare very well with the entropy of the uncompressed data, indicating that the decompressed data have

a high information content. The data histograms also confirm the that the distributions of the original data components are well preserved. However, the error measures in the data-domain indicated that the FFT-BAQ method introduced the most severe distortions compared to the other two methods.

However, the results of the image-domain metrics show that all three methods performed well. This statement is supported by the IRF, IC and GCF results that compare well with that of the SAR images of the uncompressed data. Where the FFT-BAQ method achieved the lowest SQNR in the data domain, it achieved the highest SDNR in the image domain. It can thus be confirmed that the FFT-BAQ method outperforms the other two methods, but it can be concluded that all three methods are well suited for the compression of raw SAR data.

The outcome of the results confirms that the averaging involved in coherent SAR processing, greatly reduces the effects caused by quantisation in the data domain, so that great differences in the data domain have little effect in the image domain. It therefore remains important to evaluate metrics in both domains, since the data-domain metrics can aid in understanding the operation of an algorithm and the distortion it introduced, while the image-domain metrics aid in evaluating the quality of the SAR image and whether it still contains the necessary information for the specific application.

7.6 3-BIT VS 2-BIT RESULTS

The focus was on the performance of the 2-bit compression case. However, 3-bit compression of the peri-urban scene was also performed to investigate the validity of the proposed evaluation metrics for different scenarios, an output bit rate change in this case.

When decreasing the compression ratio (CR) from 6 (corresponding with an 83 % reduction in the data volume) to 4 (corresponding with a 75 % reduction in the data volume), it is expected that the dynamic range and entropy of the decompressed data will increase for all compression methods, while the distortion errors will decrease, since information is better

preserved. The data-domain results are as expected for the BAQ and FDBAQ methods. For the FFT-BAQ method, however, the dynamic range and entropy remains constant for both the 2-bit and the 3-bit compression results, since all possible values are represented after the FFT-BAQ method has been applied, irrespective of the number of bits used. The error measures also confirm the expected outcome since the MSE and MPE have decreased, while the SQNR has increased in the 3-bit compression case for the time-domain methods. Again, the FFT-BAQ method behaves differently since the SQNR increased by less than a dB, while the SQNR for the two time-domain methods increased by about 5 dB in the 3-bit output bit rate case.

The 3-bit results in the image domain are as expected when decreasing the compression ratio from 6 to 4 since there is an increase in the dynamic range and IC of the SAR images for all compression methods. The error measures also confirm the expected outcome since the MSE and MPE decreased, while the SDNR increased in the 3-bit compression case.

Comparing the 2-bit and 3-bit results confirmed the expected outcome when decreasing the compression ratio since the dynamic range and SNR in both domains increased. An overall observation from this study is that the 3-bit BAQ method outperforms the 2-bit FFT-BAQ method. Therefore, for better performance in terms of data reduction and image quality, but at a lower computational complexity and less overhead data, the 3-bit BAQ method is the suggested solution for the SAR application in this study.

7.7 INVESTIGATION OF THE METRICS OF IMPORTANCE FOR A SINGLE FREQUENCY, SINGLE POLARISATION SAR

In Section 5.4, the SAR technologies and the corresponding metrics that are important to preserve were discussed. Since the data used in this study are from a single frequency, single polarisation SAR, the metrics of importance for this technology were investigated to determine whether the compression algorithms applied in this study are in fact suitable for this SAR technology and do not degrade the performance. If the important metrics were not

well preserved after compressing and decompressing the raw SAR data, it could be concluded that the algorithms are not well suited for this particular SAR technology and its applications. The primary applications of a single frequency, single polarisation SAR system are image classification, detection of man-made targets and change detection.

For image classification, the metrics that need to be preserved are the statistical parameters and the image quality measures like the IC and the GCF. The results showed that the statistical parameters of the SAR images after decompression compare well with the statistical parameters of the original SAR image. The image quality results also showed that the IC and the GCF of the SAR images after decompression compare well with that of the original SAR image, ensuring that a high image contrast is maintained. The BAQ, FFT-BAQ, and the FDBAQ, all achieved high image contrast and would therefore be well-suited for the application of image classification.

The metrics that need to be preserved for the detection of man-made targets are the image quality metrics and the amplitude MSE of the SAR image. The image quality metrics include the impulse response function, i.e. the 3 dB impulse response width (IRW) and the peak-to-side lobe ratio (PSLR), the IC and the GCF. The results showed that the image quality measures of the SAR images after the decompression for all three methods compare well with that of the original SAR image. Since the IRW and PSLR are well maintained after implementing compression as part of the SAR process, this means that high sensitivity to point scatters are maintained. This implies that all three algorithms would be well suited for the application of the detection of man-made targets. However, the FFT-BAQ achieved the highest IC and GCF, and the lowest amplitude MSE, implying that the magnitude component of the data is better preserved, and therefore highly suited for the detection of man-made targets.

For change detection it is important to achieve a high SDNR to ensure that small changes are not masked by noise. The results showed that all three algorithms achieved a SDNR of greater than 11 dB after 2-bit compression. Of the three compression algorithms, the

FFT-BAQ achieved the highest SDNR, and would therefore be well-suited for the application of change detection. Alternatively, the 3-bit BAQ algorithm could be used to achieve a higher SDNR at the price of a slightly higher output data volume.

7.8 CHAPTER SUMMARY

Firstly, the general regions where the flight tests took place were showed to introduce the typical features of each scene type. The SAR image of the specific swath that was imaged in each case was given as a first introduction to how an image of the ground looks, when using a radar as the imaging system. The SAR images, after implementing the three chosen compression algorithms, the BAQ, FFT-BAQ, and FDBAQ, were given and compared to the image when no compression was applied to the raw data.

In Section 7.3 the results of the data-domain metrics were summarised. The results showed that the statistical parameters are representative of the deviation of the distributions after compression from the original distributions without compression. It was seen that the data histograms are an important visual representation of the effects that the different compression algorithms have on the data in the data domain, while the error measures are an indication of the error introduced by quantisation.

In Section 7.4 the results of the image-domain metrics were summarised. The statistical parameters show that the characteristics of the SAR image without compression are largely preserved since the values after compression compare well. Using the image quality metrics, which include the IRF, IC, and GCF, the visual quality of the images with and without compression applied, could be determined. Based on these results, it can be determined whether the compression algorithm caused degradation of the SAR image quality. Another group of metrics evaluated in the image domain, is the image fidelity measures, which are an indication of the exactness with which the SAR image, with compression applied, was reproduced compared to the reference SAR image. These metrics include the MSE, MPE,

and the SDNR, and gives an indication of the errors that propagated into the image domain after quantisation.

In Section 7.5, the results of the data-domain metrics were compared with the results of the image-domain metrics. It was seen that although the data-domain metrics suggested that the BAQ and FDBAQ methods caused information loss due to the low entropy of their phase components and the deviation in the probability distributions, the image-domain metrics suggested that both these methods maintained the quality of the original SAR image. According to the error measures in the data domain, the FFT-BAQ method introduced the most distortion. However, the image fidelity measures in the image domain showed that the FFT-BAQ method outperformed the two time-domain methods. This confirms the importance of evaluating metrics in both domains. The data-domain metrics can aid in understanding the operation of an algorithm and the distortion it introduced, while the image-domain metrics aid in evaluating the quality of the SAR image and determining whether the distortions propagated into the image domain.

In Section 7.6, the 2-bit results and 3-bit results were compared. After taking the data-domain metrics and image-domain metrics into account, it was observed that the 3-bit BAQ method outperforms the 2-bit FFT-BAQ method. The 3-bit BAQ method reduces the data volume by 67 % and achieves better SDNR than the 2-bit FFT-BAQ method. Another advantage is that the BAQ method has lower computational complexity and less overhead data.

The metrics that are important for a single frequency, single polarisation SAR system are investigated in Section 7.7. It was concluded that the compression algorithms that were implemented in this study are all well-suited for the SAR technology. It was seen that all three compression algorithms achieved good results for the image contrast, the impulse response function, and the SDNR. Therefore, these algorithms are suitable for SAR applications like image classification, the detection of man-made targets, and global monitoring or change detection.

CHAPTER 8 CONCLUSION AND FUTURE WORK

8.1 CONCLUSION

An important characteristic of modern spaceborne SAR systems and small unmanned aerial vehicle (UAV) SAR systems is that the acquired data is not processed on the platform, but are transmitted to a ground station for processing or stored on board for post-processing. The main constraints in the design of these SAR systems are the unavailability of a downlink with a high data rate and the immense storage capacity required. In order to address the problem of large data volumes acquired by a SAR system, an efficient compression algorithm had to be investigated and implemented without degrading the SAR image quality and compromising the outcome of the SAR mission. Therefore, the performance and losses caused by these compression algorithms needed to be quantified in order to select the best suited algorithm for the application.

Despite the importance of being able to quantify the performance of SAR data-compression algorithms, it was found that there are no widely-accepted set of metrics available in the literature. Therefore, quantitative performance metrics were established to objectively quantify the performance of SAR data-compression algorithms. These metrics were evaluated for three different SAR-data compression algorithms applied to real airborne SAR data sets.

The main findings of the study are summarised below.

8.1.1 Implemented SAR compression algorithms

An investigation of the results of the data and image domain metrics, shows that all three compression methods chosen for this study, perform well when the objective is to decrease the volume of data while preserving the SAR image quality at the final output. Therefore, these compression algorithms can be said to be well suited for raw SAR data in general since the algorithms performed well for all scenes in this study. From rural to peri-urban scene types, the distinct features could easily be recognised and little degradation of the SAR images occurred. Thus, the BAQ, FFT-BAQ, and FDBAQ algorithms meet the performance and quality requirements for this SAR application, namely a single frequency, single polarisation, basic SAR system.

When comparing the different metrics for the three algorithms, it can be concluded that when only considering the data domain metrics, the time domain methods seem to outperform the FFT-BAQ method. However, when investigating the image domain metrics, it can be concluded with certainty that the FFT-BAQ method actually outperforms the time domain methods, since this method produces a higher SDNR, image contrast and global contrast factor. Therefore, it is concluded that a better quality SAR image is produced after applying the FFT-BAQ algorithm compared to the quality of the SAR images produced after applying the two time-domain methods.

8.1.2 Validity of the proposed metrics

The goal of this work was to determine whether the established metrics can be used to objectively quantify the performance of SAR-data compression algorithms. Metrics were established in two different domains, i.e. before and after SAR processing is performed. The effects of the algorithm on the raw data, as well as on the output of the SAR system, must be quantitatively evaluated to establish whether the algorithm is a viable solution.

It was found that the metrics applied in the two different domains are of tremendous value when determining the effects of compressing the raw SAR data. First, the compression

algorithm metrics can be evaluated to determine the effects of the compression algorithm in the data domain. Important metrics include the CR, the entropy, statistical parameters like the skewness and kurtosis to measure the deviation from the original distributions of the uncompressed data, and the dynamic range. The data histograms are an important visual representation of the effects of the compression algorithm on the data. An important error measure in the data domain is the SQNR and the phase error measures for applications where phase information is an integral part of forming the output of the SAR system.

After the SAR processing, another set of metrics can be evaluated to determine the degradation in the image domain. Here, the emphasis is on the quality of the SAR image that was produced from the data that had undergone the compression on board the SAR platform. Important metrics in the image domain include the dynamic range, the IRF, the image contrast, as well as the error measure, SDNR. In the image domain, the phase error measure, MPE, are important for applications where phase information is required to form the output of the SAR system. The SAR technologies where the phase information is the most important component of the complex SAR image, are InSAR and PolSAR.

It was seen that the metrics could be used to determine the best suited algorithm for each single frequency, single polarisation SAR application, since data from this technology was used to conduct the study. The outcome of the research is thus that the proposed metrics are useful as performance indicators for raw SAR-data compression algorithms, and in turn addresses the lack of standardised, quantitative performance metrics in this field.

8.1.3 Identified trade-offs

For some SAR applications, a certain level of degradation is acceptable and the outcome of the SAR mission will be unaltered. For other applications, much less degradation can be tolerated as it will heavily affect the outcome of the mission. It is also true that for a certain application, one component of the data is more important to preserve than another. Therefore, by evaluating the metrics for different compression algorithms, the data reduction

vs. image degradation can be considered and the best suited algorithm based on the SAR system requirements, can be chosen for onboard implementation.

Although a compression algorithm may have performed better than another in one or both domains, the computational complexity is of importance when practical implementation needs to be considered. Therefore, the computational complexity of each algorithm was determined using big O notation. Due to the SWAP-C limitations of modern SAR platforms, the trade-off between the computational complexity and the performance of the compression algorithm is a very important consideration. Depending on the application of the SAR system, one or the other will be of higher priority.

The metrics proposed in this dissertation can be used during the design phase of a SAR system, when a compression algorithm for implementation on board a platform needs to be chosen. The results of the metrics can be used to conduct a thorough investigation on the performance and complexity of different compression algorithms for raw SAR data.

8.2 SUGGESTED FUTURE WORK

8.2.1 Metrics in the fusion domain

The proposed metrics were shown to be useful when a compression algorithm needs to be selected for onboard implementation, but the metrics are only evaluated in the data and image domains. Since data fusion is an emerging topic and the future of remote sensing systems, establishing metrics to evaluate in the fusion domain could also be beneficial.

8.2.2 Evaluating the metrics for data from multiple SAR systems

In this study, the data from a prototype SAR system were used. The study should be repeated with more data sets from other SAR technologies with different applications. Other types of SAR systems should include FMCW systems, unmanned aerial vehicle (UAV) SAR

systems, spaceborne systems, InSAR, and PolSAR systems to ensure that the metrics still produce valuable information when choosing between various compression algorithms.

8.2.3 Novel SAR compression algorithm and the verification thereof using the proposed metrics

Since three well-known SAR compression algorithms have been implemented in this study, another topic of research could be to build on the successes of each method and design a novel raw SAR-data compression algorithm. The novel algorithm could be optimised for a certain SAR technology and therefore outperform current SAR compression algorithms in that application. Again, the proposed metrics could be used to evaluate the performance of the novel algorithm.

8.2.4 Hardware implementation of the proposed compression algorithms

This study was limited to the implementation of the chosen compression algorithms in software only. Valuable information could be obtained by implementing these algorithms in hardware. The metrics could be evaluated for this implementation and then compared to the outcome of the software implementation. A hardware implementation of the algorithms could also give insights about the real-time performance capabilities, as well as the computational resource requirements of each algorithm. This information could aid in choosing a suitable algorithm for implementation on board a SAR platform

REFERENCES

[1] G. A. Showman, "An overview of radar imaging," in *Principles of Modern Radar, Volume I - Basic Principles* Raleigh, NC: SciTech Publishing, 2010, pp. 835-890.

[2] A. Moreira, "Synthetic Aperture Radar (SAR): Principles and Applications," *4th Advanced Training Course in Land Remote Sensing*, [Online]. pp. 1-62, 2013. Available: https://earth.esa.int/documents/10174/642943/6-LTC2013-SAR-Moreira.pdf.

[3] M. R. Inggs and R. T. Lord, "Applications of satellite imaging radar," in *South African Institute of Electrical Engineers (SAIEE)*, South Africa, 2000, pp. 1-8.

[4] J. McHale. (April). *TRACER synthetic aperture radar from Lockheed Martin completes testing aboard Predator UAV*. Available: http://www.avionics-intelligence.com/articles/2011/04/tracer-synthetic-aperture.html.

[5] P. Guccione, M. Belotti, D. Giudici, A. Monti Guarnieri, I. Navas-Traver, "Sentinel-1A: Analysis of FDBAQ Performance on Real Data," *IEEE Transactions on Geoscience and Remote Sensing*, vol. 53, *(12)*, pp. 6804-6812, Dec., 2015.

[6] S. W. Lasswell, "History of SAR at Lockheed Martin (formerly Goodyear Aerospace)," in *Proc. of the SPIE 5788, Radar Sensor Technology IX*, Orlando, Florida, USA, 2005, pp. 1-12.

[7] A. Moreira, P. Prats-Iraola, M. Younis, G. Krieger, I. Hajnsek, K. P. Papathanassiou, "A Tutorial on Synthetic Aperture Radar," *IEEE Geoscience and Remote Sensing Magazine*, vol. 1, *(1)*, pp. 6-43, Mar. 2013.

[8] S. Nozette, P. Spudis, B. Bussey, R. Jensen, K. Raney, H. Winters, C. L. Lichtenberg, W. Marinelli, J. Crusan, M. Gates, M. Robinson, "The Lunar Reconnaissance Orbiter Miniature Radio Frequency (Mini-RF) Technology Demonstration," *Space Science Reviews*, vol. 150, *(1)*, pp. 285-302, Jan, 2010.

[9] J. N. Koster, A. Buysse, L. Smith, R. J. Huyssen, J. Schneider, J. Hotchkiss, J. Malangoni, "AREND: A sensor aircraft to support wildlife rangers," in *57th AIAA/ASCE/AHS/ASC Structures, Structural Dynamics, and Materials*, San Diego, California, 2016, pp. 1-19.

[10] J. Keller. (2014, October 15). *Army researchers choose IMSAR to develop small radar systems for unmanned aerial vehicles*. Available: http://www.militaryaerospace.com/articles/print/volume-25/issue-10/unmanned-vehicles/army-researchers-choose-imsar-to-develop-small-radar-systems-for-unmanned-aerial-vehicles.html.

[11] *Platforms*. Available: http://www.sandia.gov/RADAR/areas_of_expertise/platforms.html.

[12] (2018, April 4). *Northrop Grumman RQ-4 Global Hawk Unmanned Aerial Vehicle (UAV)/Drone*. Available: https://www.militaryfactory.com/aircraft/detail.asp?aircraft_id=40.

[13] *Deployments*. Available: http://uavsar.jpl.nasa.gov/cgi-bin/deployments.pl.

[14] M. Edrich, "Ultra-lightweight synthetic aperture radar based on a 35 GHz FMCW sensor concept and online raw data transmission," *IEE Proceedings - Radar, Sonar and Navigation*, vol. 153, *(2)*, pp. 129-134, April, 2006.

[15] H. Essen, M. Bräutigam, R. Sommer, A. Wahlen, W. Johannes, J. Wilcke, M. Schlechtweg, A. Tessmann, "SUMATRA, a W-band SAR for UAV application," in *2009 International Radar Conference "Surveillance for a Safer World" (RADAR 2009)*, 2009, pp. 1-4.

[16] H. Essen, W. Johannes , S. Stanko, R. Sommer, A. Wahlen, J. Wilcke, "High resolution W-band UAV SAR," in *2012 IEEE International Geoscience and Remote Sensing Symposium*, 2012, pp. 5033-5036.

[17] E. Zaugg, M. Edwards and A. Margulis, "The SlimSAR: A small, multi-frequency, synthetic aperture radar for UAS operation," in *2010 IEEE Radar Conference*, 2010, pp. 277-282.

[18] P. Kaniewski, C. Lesnik, P. Serafin, M. Labowski, "Chosen results of flight tests of WATSAR system," in *2016 17th International Radar Symposium (IRS)*, 2016, pp. 1-5.

[19] A. S. Belward and J. O. Skøien, "Who launched what, when and why; trends in global land-cover observation capacity from civilian earth observation satellites," *ISPRS*, vol. 103, pp. 115-128, 2015. DOI: https://doi.org/10.1016/j.isprsjprs.2014.03.009.

[20] H. Trigui, "Cost effective, high performance networked ELINT systems for C4ISR missions," in *Tutorial Presented at Int. Conf. EW (EWCI)*, Bangalore, India, 2018.

[21] E. Attema, C. Cafforio, M. Gottwald, P. Guccione, A. Monti-Guarnieri, F. Rocca, P. Snoeij, "Flexible Dynamic Block Adaptive Quantization for Sentinel-1 SAR Missions," *IEEE Geoscience and Remote Sensing Letters*, vol. 7, *(4)*, pp. 766-770, Oct., 2010.

[22] S. Rane, P. T. Boufounos, A. Vetro, Y. Okada, "Low complexity efficient raw SAR data compression," in *Proc. SPIE. 8051, Algorithms for Synthetic Aperture Radar Imagery XVIII*, Orlando, Florida, United States, 2011, pp. 1-11.

[23] S. K. Sharma, S. Chatzinotas and B. Ottersten, "Cognitive radio techniques for satellite communication systems," in *2013 IEEE 78th Vehicular Technology Conference (VTC Fall)*, 2013, pp. 1-5.

[24] C. Zhang and Y. Liu, "OFDM imaging radars spectrum sharing," in *2015 IEEE China Summit and International Conference on Signal and Information Processing (ChinaSIP)*, 2015, pp. 398-402.

[25] J. Liu and Q. Zhou, "SAR raw data compression based on geometric characteristic of Gaussian curve," in *Seventh International Conference on Digital Image Processing*, Los Angeles, 2015, pp. 1-7.

[26] N. Agrawal and K. Venugopalan, "Analysis of complex SAR raw data compression," in *Progress in Electromagnetics Research Symposium (PIERS)*, Cambridge, Massachusetts, 2008, pp. 141-146.

[27] I. H. McLeod and I. G. Cumming, "On-board encoding of the ENVISAT wave mode data," in *International Geoscience and Remote Sensing Symposium (IGARSS), Quantitative Remote Sensing for Science and Applications*, Firenze, Italy, 1995, pp. 1681-1683.

[28] X. Morin, D. Barba and S. El Assad, "Vector quantization of raw polarimetric SAR data by using their statistical properties," in *Proc. SPIE. 3217, Image Processing, Signal Processing, and Synthetic Aperture Radar for Remote Sensing*, London, United Kingdom, 1997, pp. 124-131.

[29] E. Magli and G. Olmo, "Lossy Predictive Coding of SAR Raw Data," *IEEE Trans. Geosci. Remote Sens.*, vol. 41, *(5)*, pp. 977-987, May, 2003.

[30] G. Poggi, A. R. P. Ragozini and L. Verdoliva, "Compression of SAR data through range focusing and variable-rate vector quantization," *IEEE Trans. Geosci. Remote Sens.*, vol. 38, *(3)*, pp. 1282-1289, 2000.

[31] J. C. Curlander and R. N. McDonough, *Synthetic Aperture Radar Systems and Signal Processing.* New York, USA: John Wiley and Sons, 1991.

[32] C. Pieterse, W. P. du Plessis and R. W. Focke, "Metrics to Evaluate Compression Algorithms for Raw SAR Data," *IET Radar, Sonar & Navigation*, accepted 5 October, 2018.

[33] C. A. Wiley, "Synthetic Aperture Radar: A Paradigm for Technology Evolution," *IEEE Transactions on Aerospace and Electronic Systems*, vol. AES-21, *(3)*, pp. 440-443, May, 1985.

[34] L. Blanton, "Space-based SAR for remote sensing," in *Principles of Modern Radar, Volume 3 - Radar Applications*, W. L. Melvin and J. A. Scheer, Eds. Edison, New Jersey: SciTech Publishing, 2014, pp. 431-494.

[35] G. W. Stimson, H. D. Griffiths, C. J Baker, D. Adamy, *Stimson's Introduction to Airborne Radar.* (3rd ed.) Edison, New Jersey: SciTech Publishing, 2014.

[36] A. C. Frery, C. Freitas, S. J. S. Sant'Anna, C. D. Rennó, "Statistical properties of SAR data and their consequences," *Seminars of the United Nations Programme on Space Applications,* vol. 10, pp. 53-68, 1999.

[37] A. Moreira, J. Mittermayer and R. Scheiber, "Extended chirp scaling algorithm for air- and spaceborne SAR data processing in stripmap and ScanSAR imaging modes," *IEEE Trans. Geosci. Remote Sens.,* vol. 34, *(5),* pp. 1123-1136, Sep, 1996.

[38] Y. K. Chan and V. C. Koo, "An introduction to Synthetic Aperture Radar (SAR)," *Progress in Electromagnetics Research B,* vol. 2, pp. 27-60, Jan., 2008.

[39] P. T. Gough and D. W. Hawkins, "Unified Framework for Modern Synthetic Aperture Imaging Algorithms," vol. 8, pp. 343-358, 01, 1997.

[40] P. Lacomme, J. Hardange, J. Marchais, E. Normant, "Synthetic aperture radar specific aspects," in *Air and Spaceborne Radar Systems - an Introduction*, New York, USA: William Andrew Publishing, 2001, pp. 265-328.

[41] A. H. S. Solberg, C. Brekke and P. O. Husoy, "Oil Spill Detection in RADARSAT and Envisat SAR Images," *IEEE Trans. Geosci. Remote Sens.,* vol. 45, *(3),* pp. 746-755, Mar., 2007.

[42] C. Oliver and S. Quegan, *Understanding Synthetic Aperture Radar Images.* Raleigh, North Carolina: SciTech Publishing, 2004.

[43] H. Greidanus, M. Alvarez, T. Cokacar, A. Pesaresi, C. Santamaria, V. Kyovtorov, "Satellite SAR ship detections from PMAR in support of cutlass express," European Union, Luxembourg, Tech. Rep. LB-NA-25140-EN-N, 2011.

[44] C. C. Lin and P. L. Mancini, "A SAR instrument for global monitoring of land surfaces and polar ice," in *International Geoscience and Remote Sensing Symposium (IGARSS)*, Pasadena, California, 1994, pp. 1525-1528.

[45] T. Zwick, W. Wiesbeck, J. Timmermann, G. Adamiuk, *Ultra-Wideband RF System Engineering.* Cambridge, United Kingdom: Cambridge University Press, 2013.

[46] L. Fu-lai, S. Qian, W. Yu-ming, Z. Han-hua, Z. Zhi-min, "Ultra-wideband synthetic aperture radar landmine detection based on landmine-enhanced imaging," in *2013 IEEE International Conference on Ultra-Wideband (ICUWB)*, 2013, pp. 201-204.

[47] M. Naveena, D. K. Singh and H. Singh, "Design of UHF band UWB antenna for foliage penetration application," in *2017 IEEE International Conference on Antenna Innovations Modern Technologies for Ground, Aircraft and Satellite Applications (iAIM)*, 2017, pp. 1-3.

[48] Y. J. Ren, C. P. Lai, P. H. Chen, R. M. Narayanan, "Compact Ultra-wideband UHF Array Antenna for Through-Wall Radar Applications," *IEEE Antennas and Wireless Propagation Letters*, vol. 8, pp. 1302-1305, 2009.

[49] D. Oloumi, M. I. Pettersson, P. Mousavi, K. Rambabu, "Imaging of Oil-Well Perforations Using UWB Synthetic Aperture Radar," *IEEE Trans. Geosci. Remote Sens.*, vol. 53, *(8)*, pp. 4510-4520, Aug, 2015.

[50] D. Oloumi, P. Boulanger, A. Kordzadeh, K. Rambabu, "Breast tumor detection using UWB circular-SAR tomographic microwave imaging," in *2015 37th Annual International Conference of the IEEE Engineering in Medicine and Biology Society (EMBC)*, 2015, pp. 7063-7066.

[51] D. Massonnet and K. L. Feigl, "Radar Interferometry and its Application to Changes in the Earth's Surface," *Rev. Geophys.*, vol. 36, *(4)*, pp. 441-500, Nov., 1998.

[52] J. van Zyl and Y. Kim, *Synthetic Aperture Radar Polarimetry.* Hoboken, New Jersey: John Wiley and Sons, 2011.

[53] C. Pohl and J. L. Van Genderen, "Multi-sensor image fusion in remote sensing: Concepts, methods and applications," *Int. J. Remote Sens.*, vol. 19, *(5),* pp. 823-854, March, 1998.

[54] A. H. Schistad Solberg, A. K. Jain and T. Taxt, "Multisource Classification of Remotely Sensed Data: Fusion of Landsat TM and SAR Images," *IEEE Trans. Geosci. Remote Sens.,* vol. 32, *(4),* pp. 768-778, 1994.

[55] H. Zhang, H. Lin and Y. Li, "Impacts of feature normalization on optical and SAR data fusion for land use/land cover classification," *IEEE Geosci. Remote Sens. Lett.,* vol. 12, *(5),* pp. 1061-1065, 2015.

[56] M. Quartulli and M. Datcu, "Information fusion for scene understanding from interferometric SAR data in urban environment," *IEEE Trans. Geosci. Remote Sens.,* vol. 41, *(9 PART I),* pp. 1976-1985, 2003.

[57] A. Salentinig and P. Gamba, "A General Framework for Urban Area Extraction Exploiting Multiresolution SAR Data Fusion," *IEEE J. Sel. Top. Appl. Earth Obs. Remote Sens.*, vol. 9, *(5),* pp. 2009-2018, 2016.

[58] M. I. Skolnik, *Radar Handbook.* (2nd ed.) Boston, Massachusetts: McGraw-Hill, 1990.

[59] M. P. Zénere, "SAR Image Quality Assessment," 2012.

[60] R. Kwok and W. T. K. Johnson, "Block Adaptive Quantization of Magellan SAR Data," *IEEE Trans. Geosci. Remote Sens.*, vol. 27, *(4),* pp. 375-383, July, 1989.

[61] M. G. Bulmer, *Principles of Statistics.* New York: Dover Publications Incorporated, 1979.

[62] G. Kuduvalli, M. Dutkiewicz and I. Cumming, "Synthetic aperture radar signal data compression using block adaptive quantization," in *Science Information Management and*

Data Compression Workshop, 1994, Available: https://ntrs.nasa.gov/search.jsp?R=19950008176.

[63] I. H. McLeod, I. G. Cumming and M. S. Seymour, "ENVISAT ASAR data reduction: impact on SAR interferometry," vol. 36, pp. 589, 04, 1998.

[64] C. O. Archer, "Some properties of Rayleigh distributed random variables and of their sums and products," Naval Missile Center, Point Mugu, California, Tech. Rep. TM-67-15, April. 1967.

[65] S. M. Parkes and H. L. Clifton, "The compression of raw SAR and SAR image data," *Int. J. Remote Sens.*, vol. 20, *(18)*, pp. 3563-3581, 1999.

[66] D. R. Sheen and L. P. Johnston, "Statistical and Spatial Properties of Forest Clutter Measured with Polarimetric Synthetic Aperture Radar (SAR)," *IEEE Trans. Geosci. Remote Sens.*, vol. 30, *(3)*, pp. 578-588, 1992.

[67] M. W. Long, *Radar Reflectivity of Land and Sea.* (3rd ed.) Boston: Artech House, 2001.

[68] M. S. Greco and F. Gini, "Statistical Analysis of High-Resolution SAR Ground Clutter Data," *IEEE Transactions on Geoscience and Remote Sensing*, vol. 45, *(3)*, pp. 566-575, 2007.

[69] J. Martín-de-Nicolás, M. P. Jarabo-Amores, D. Mata-Moya, N. Del-Rey-Maestre, J. L. Bárcena-Humanes, "Statistical Analysis of SAR Sea Clutter for Classification Purposes," *Remote Sensing*, vol. 6, *(10)*, pp. 9379-9411, 2014.

[70] A. M. Raynal, D. L. Bickel, D. F. Dubbert, T. J. Verge, B. L. Burns, R. Dunkel, A. W. Doerry, "Radar cross section statistics of cultural clutter at Ku-band," in *Proc. SPIE 8361, Radar Sensor Technology XVI*, Baltimore, Maryland, United States, 2012, pp. 195-207.

[71] K. Sayood, *Introduction to Data Compression.* (3rd ed.) 2006Available: https://www-sciencedirect-com.uplib.idm.oclc.org/science/book/9780126208627. DOI: https://doi-org.uplib.idm.oclc.org/10.1016/B978-012620862-7/50001-8.

[72] S. Wolfram, "Processes of perception and analysis," in *A New Kind of Science*, Champaign, IL: Wolfram Media, 2002, pp. 546-1106.

[73] U. Dalal, "Source coding techniques," in *Wireless Communication and Networks*, New Delhi, India: Oxford University Press, 2015, pp. 165-216.

[74] T. M. Cover and J. A. Thomas, *Elements of Information Theory.* New York, New York: John Wiley & Sons, 1991.

[75] B. Pikacz, "An algorithm for a lossless compression of raw radar data," in, Warsaw, Poland, 2014, pp. 1-8.

[76] T. Ma, M. Hempel, D. Peng, H. Sharif, "A Survey of Energy-Efficient Compression and Communication Techniques for Multimedia in Resource Constrained Systems," *IEEE Communications Surveys & Tutorials*, vol. 15, *(3)*, pp. 963-972, Third, 2013.

[77] R. Steinmetz, "Data compression in multimedia computing - standards and systems," *Multimedia Systems*, vol. 1, *(5)*, pp. 187-204, Mar, 1994.

[78] R. M. Gray and D. L. Neuhoff, "Quantization," *IEEE Trans. Inf. Theory*, vol. 44, *(6)*, pp. 2325-2383, Oct, 1998.

[79] H. E. A. Laue, "Demystifying Compressive Sensing [Lecture Notes]," *IEEE Signal Process. Mag.*, vol. 34, *(4)*, pp. 171-176, 2017.

[80] E. J. Candes and M. B. Wakin, "An introduction to compressive sampling: A sensing/sampling paradigm that goes against the common knowledge in data acquisition," *IEEE Signal Process. Mag.*, vol. 25, *(2)*, pp. 21-30, 2008.

[81] A. Massa, P. Rocca and G. Oliveri, "Compressive sensing in electromagnetics - A review," *IEEE Antennas and Propagation Magazine,* vol. 57, *(1),* pp. 224-238, 2015.

[82] J. H. G. Ender, "On compressive sensing applied to radar," *Signal Process,* vol. 90, *(5),* pp. 1402-1414, 2010.

[83] U. Benz, K. Strodl and A. Moreira, "A Comparison of Several Algorithms for SAR Raw Data Compression," *IEEE Transactions on Geoscience and Remote Sensing (TGRS),* vol. 33, *(5),* pp. 1266-1276, Sept., 1995.

[84] V. Pascazio and G. Schirinzi, "SAR raw data compression by sub-band coding," *IEEE Trans. Geosci. Remote Sens.,* vol. 41, *(5 Part 1),* pp. 964-976, May, 2003.

[85] J. M. Moureaux, P. Gauthier, M. Barlaud, P. Bellemain, "Vector quantization of raw SAR data," in *IEEE International Conference on Acoustics, Speech and Signal Processing (ICASSP),* 1994, pp. V189-V192.

[86] J. Max, "Quantizing for minimum distortion," *IRE Transactions on Information Theory,* vol. 6, *(1),* pp. 7-12, Mar., 1960.

[87] S. P. Lloyd, "Least squares quantization in PCM," *IEEE Transactions on Information Theory,* vol. 28, *(2),* pp. 129-137, Mar., 1982.

[88] A. Moreira and F. Blaeser, "Fusion of block adaptive and vector quantizer for efficient SAR data compression," in *International Geoscience and Remote Sensing Symposium (IGARSS),* Tokyo, Japan, 1993, pp. 1583-1585.

[89] H. M. Qi, W. D. Yu, X. Z. Yuan, X. W. Tian, "Performance evaluation of amplitude-phase algorithm for SAR raw data compression," in *International Geoscience and Remote Sensing Symposium (IGARSS),* 2006, pp. 809-812.

[90] T. Algra, "Data compression for operational SAR missions using entropy-constrained block adaptive quantisation," in *International Geoscience and Remote Sensing Symposium (IGARSS)*, 2002, pp. 1135-1139.

[91] T. Algra and L. Bierens, "Advanced on-board SAR data compressor," in *International Geoscience and Remote Sensing Symposium (IGARSS)*, 2006, pp. 3537-3540.

[92] E. Malz, R. Scheiber, J. Mittermayer, P. Snoeij, E. Attema, "Sentinel-1 FDBAQ performance validation using TerraSAR-X data," in *International Geoscience and Remote Sensing Symposium (IGARSS)*, 2012, pp. 1629-1632.

[93] P. Snoeij, E. Attema, A. M. Guarnieri, F. Rocca, "FDBAQ a novel encoding scheme for sentinel-1," in *International Geoscience and Remote Sensing Symposium (IGARSS)*, 2009, pp. I44-I47.

[94] B. L. Huneycutt, "Innovative Operating Modes and Techniques for the Spaceborne Imaging Radar-C Instrument," *IEEE Trans. Geosci. Remote Sens.*, vol. 28, *(4)*, pp. 603-608, 1990.

[95] Z. Guan and Z. Zhou, "Adaptive vector quantization of SAR raw data," in *2009 1st International Conference on Information Science and Engineering, ICISE 2009*, 2009, pp. 103-105.

[96] C. D'Elia, G. Poggi and L. Verdoliva, "Compression of SAR raw data through range focusing and variable-rate trellis-coded quantization," *IEEE Trans. Image Process.*, vol. 10, *(9)*, pp. 1278-1287, 2001.

[97] M. A. Klimesh and B. Moision, "Onboard data compression of synthetic aperture radar data: Status and prospects," in *Proceedings of SPIE - the International Society for Optical Engineering*, 2008.

[98] J. W. Owens, M. W. Marcellin, B. R. Hunt, M. Kleine, "Compression of synthetic aperture radar video phase history data using trellis-coded quantization techniques," *IEEE Trans. Geosci. Remote Sens.,* vol. 37, *(2),* pp. 1080-1085, 1999.

[99] J. Fischer, U. Benz and A. Moreira, "Efficient SAR raw data compression in frequency domain," in *Geoscience and Remote Sensing Symposium,* Hamburg, Germany, 1999, pp. 2261-2263.

[100] V. Pascazio and G. Schirinzi, "Wavelet transform coding for SAR raw data compression," in *International Geoscience and Remote Sensing Symposium (IGARSS),* Hamburg, Germany, 1999, pp. 2251-2253.

[101] A. El-Boustani, K. Brunham and W. Kinsner, "Investigation of wavelets for raw SAR data compression," in *International Geoscience and Remote Sensing Symposium (IGARSS),* 2003, pp. 1814-1816.

[102] K. Brunham, "Development of an FPGA Based Wavelet Transform for the Compression of Raw SAR Data.", University of Manitoba, Manitoba, Canada, 2002.

[103] S. Bhattacharya, T. Blumensath, B. Mulgrew, M. Davies, "Fast encoding of synthetic aperture radar raw data using compressed sensing," in *IEEE Workshop on Statistical Signal Processing Proceedings,* 2007, pp. 448-452.

[104] S. Bhattacharya, T. Blumensath, B. Mulgrew, M. Davies, "Synthetic aperture radar raw data encoding using compressed sensing," in *2008 IEEE Radar Conference,* 2008.

[105] G. Rilling, M. Davies and B. Mulgrew, "Compressed sensing based compression of SAR raw data," in *Signal Processing with Adaptive Sparse Structured Representations (SPARS),* Saint Malo, France, 2009, pp. 1-6.

[106] T. Ikuma, M. Naraghi-Pour and T. Lewis, "Predictive Quantization of Range-Focused SAR Raw Data," *IEEE Trans. Geosci. Remote Sens.,* vol. 50, *(4),* pp. 1340-1348, Apr., 2012.

[107] F. Esser and R. Vliegenthart, "Comparative Research Methods," *The International Encyclopedia of Communication Research Methods*, 08/01; 2018/08, 2017.

[108] M. Dutkiewicz and I. Cumming, "Methods of evaluating the effects of coding on SAR data," in *The Space and Earth Science Data Compression Workshop*, NASA, Goddard Space Flight Center, 1993, pp. 59-72.

[109] M. Soumekh, *Synthetic Aperture Radar Signal Processing with MATLAB Algorithms.* Wiley Interscience, 1999.

[110] Y. Zuo, Y. Zhu, H. Zhao, Q. Fu, "Application of two-dimensional time-domain correlation method to stepped-frequency radar motion compensation," in *2009 Asia-Pacific Conference on Synthetic Aperture Radar (APSAR)*, 2009, pp. 412-416.

[111] A. Ribalta, "Time-domain reconstruction algorithms for FMCW-SAR," *IEEE Geosci. Remote Sens. Lett.*, vol. 8, *(3)*, pp. 396-400, 2011.

[112] *Level-0 Raw Products*. Available: https://earth.esa.int/web/sentinel/technical-guides/sentinel-1-sar/products-algorithms/level-0-products/raw.

[113] (2015, November 30). *Airborne versus Spaceborne Radars*. Available: http://www.nrcan.gc.ca/node/9397.

[114] B. P. Lathi and Z. Ding, *Modern Digital and Analog Communication Systems.* (4th ed.) New York: Oxford University Press Inc., 1992.

[115] M. Naraghi-Pour, R. Cortez and T. Ikuma, "Analysis-by-synthesis compression of range-focused SAR raw data," *IEEE Trans. Aerosp. Electron. Syst.*, vol. 51, *(2)*, pp. 1298-1309, 2015.

[116] R. J. Sullivan, "SAR image quality," in *Radar Foundations for Imaging and Advanced Concepts*, Raleigh, North Carolina: SciTech Publishing, 2004, pp. 209-215.

[117] T. D. Penrod and G. G. Kuperman, "Image quality analysis of compressed synthetic aperture radar imagery," U.S. Air force, Tech. Rep. AL/CF-TR-1993-0156, Jan. 1993.

[118] R. K. Raney, "Theory and Measure of Certain Image Norms in SAR," *IEEE Transactions on Geoscience and Remote Sensing*, vol. GE-23, *(3)*, pp. 343-348, May, 1985.

[119] R. H. Mitchel and S. Marder, "Synthetic Aperture Radar (SAR) Image Quality Considerations," *Optical Engineering*, vol. 21, *(1)*, pp. 048-055, Jan./Feb., 1982.

[120] M. S. Clinard, C. E. Farnung, P. Kopacz, K. S. Miettinen, "Impulse response function (IPR) estimation method using detected synthetic aperture radar (SAR) mission data," in *Proc. SPIE 4727, Algorithms for Synthetic Aperture Radar Imagery IX*, Orlando, Florida, United States, 2002, pp. 178-185.

[121] H. Zhang, Y. Li and Y. Su, "SAR image quality assessment using coherent correlation function," in *5th International Congress on Image and Signal Processing (CISP)*, Chongqing, China, 2012, pp. 1129-1133.

[122] K. Matković, L. Neumann, A. Neumann, T. Psik, W. Purgathofer, "Global contrast factor - a new approach to image contrast," in *Proceedings of the First Euro Graphics Conference on Computational Aesthetics in Graphics, Visualization and Imaging*, Girona, Spain, 2005, pp. 159-167.

[123] J. Yang, Y. Yamaguchi, J. S. Lee, R. Touzi, W. M. Boerner, "Applications of Polarimetric SAR," *Journal of Sensors*, vol. 2015, *(Article ID 316391)*, pp. 1-2, May, 2015.

[124] A. A. Neath and J. E. Cavanaugh, "The Bayesian information criterion: background, derivation, and applications," *WIREs Comp Stat*, vol. 4, *(2)*, pp. 199-203, 03/01; 2018/10, 2012.

[125] G. W. Zeoli, "A lower bound on the data rate for synthetic aperture radar," *IEEE Transactions on Information Theory*, vol. 22, *(6)*, pp. 708-715, November, 1976.

[126] L. Fan, S. Jin, C. K. Wen, H. Zhang, "Uplink achievable rate for massive MIMO systems with low-resolution ADC," *IEEE Commun Lett*, vol. 19, *(12)*, pp. 2186-2189, 2015.

[127] S. Rane, P. Boufounos, A. Vetro, Y. Okada, "Low complexity efficient raw SAR data compression," in *Proc. SPIE 8051, Algorithms for Synthetic Aperture Radar Imagery XVIII, 80510W*, 2011.

[128] A. Martinez and J. Marchand, "SAR Image Quality Assessment," *Spanish Journal of Remote Sensing (RAET)*, vol. 2, pp. 1-7, 1993.